University of Alberta

Experimental Study of Commercial PAI for Integrated Optics

by

Mahmoud S. Abbas

A thesis submitted to the Faculty of Graduate Studies and Research
in partial fulfillment of the requirements for the degree of

Master of Science

Department of Electrical and Computer Engineering

Edmonton, Alberta
Fall 2007

Library and Archives Canada

Published Heritage Branch

395 Wellington Street
Ottawa ON K1A 0N4
Canada

Bibliothèque et Archives Canada

Direction du Patrimoine de l'édition

395, rue Wellington
Ottawa ON K1A 0N4
Canada

Your file Votre référence
ISBN: 978-0-494-33186-6
Our file Notre référence
ISBN: 978-0-494-33186-6

NOTICE:
The author has granted a non-exclusive license allowing Library and Archives Canada to reproduce, publish, archive, preserve, conserve, communicate to the public by telecommunication or on the Internet, loan, distribute and sell theses worldwide, for commercial or non-commercial purposes, in microform, paper, electronic and/or any other formats.

The author retains copyright ownership and moral rights in this thesis. Neither the thesis nor substantial extracts from it may be printed or otherwise reproduced without the author's permission.

AVIS:
L'auteur a accordé une licence non exclusive permettant à la Bibliothèque et Archives Canada de reproduire, publier, archiver, sauvegarder, conserver, transmettre au public par télécommunication ou par l'Internet, prêter, distribuer et vendre des thèses partout dans le monde, à des fins commerciales ou autres, sur support microforme, papier, électronique et/ou autres formats.

L'auteur conserve la propriété du droit d'auteur et des droits moraux qui protège cette thèse. Ni la thèse ni des extraits substantiels de celle-ci ne doivent être imprimés ou autrement reproduits sans son autorisation.

In compliance with the Canadian Privacy Act some supporting forms may have been removed from this thesis.

While these forms may be included in the document page count, their removal does not represent any loss of content from the thesis.

Conformément à la loi canadienne sur la protection de la vie privée, quelques formulaires secondaires ont été enlevés de cette thèse.

Bien que ces formulaires aient inclus dans la pagination, il n'y aura aucun contenu manquant.

Canada

To my loving parents: ***Sayed Abbas*** & ***Magda El Sayed***,

my caring sisters: ***Yasmeen*** & ***Nisreen***,

and my thoughtful brother ***Mohammed***

Abstract

This work is an investigation of embossing and waveguiding using a high-performance commercial thermoplastic known as polyamide-imide. Polyamide-imides possess many superior properties that make them attractive for integrated optics, including excellent thermal, chemical, and mechanical stability. In this study, polyamide-imide was investigated as a core material for polymer-based, high-index contrast waveguides. A spectral analysis of material loss was completed and the absorption peaks were correlated with well-known overtones of C-H, N-H, and O-H bonds. Using polyamide-imide waveguides fabricated by reactive ion etching, it was shown that the sidewall roughness can be reduced by a thermal reflow technique. Subsequently, the fabrication of waveguides using hot embossing lithography was investigated. Embossing was attempted on fully cured and soft-baked films, using both a home-made and a commercial embossing machine. Embossing of fully cured films proved challenging due to their high glass transition temperature. Better results were obtained by embossing partially cured films.

Acknowledgements

Firstly, I would like express my sincere gratitude to Dr. Ray DeCorby for supervising my work. I would like to thank him for providing me with this opportunity and for all the help he gave me. I found his researching experience and patience a valuable resource throughout my studies.

A big thanks goes to my colleague Nakeeran Ponnampalam for all his helpful discussions, insightful comments, and for always being around when needed. I am also grateful to TRLabs Edmonton for this opportunity, and would like to thank all its members for all the different support they provided and for always having a smile on their face. I would like to specifically mention David Clegg, the lab manager at TRLabs Edmonton. His sharp eye for details and superb experimental skills has been instrumental in completing this work.

Many thanks go to Hue Nguyen for all the training she gave me at the NanoFab, and for always taking the time to respond to my questions. I would to give a special thanks to Ahmed Allam, Thomas Clement, Trevor Allen, and Mahesh Pai for all their help as well as Ahmed Zaky and Florian Lenz for their helpful comments.

I would like to thank George Braybrook for taking the SEM images, and for all the interesting stories he shared. I also want to acknowledge Herbert Dexel, from the Machine shop at the U of A, for his help with the embossing machine and Javed Ally for taking the time to help me with some schematics.

My sincere thanks goes to all my previous professors and teachers, as well as to everyone that helped or supported me in any way, but I have forgotten to mention.

Finally, I would like to express my deepest gratitude to my family for their patience, love and understanding during the past years, and for being a constant source of motivation for me.

Table of Contents

Chapter 1 Introduction 1
1.1 History of Telecommunication 1
1.2 Polymers in Integrated Optics 2
1.3 Polyimides in Integrated Optics 5
1.4 Polyamide-imides 5
1.5 Outline 7

Chapter 2 Background & Theory 9
2.1 Waveguiding by total internal reflection 9
2.2 Propagation Losses in Polymer Waveguides 10
2.2.1 Absorption Loss 11
2.2.2 Scattering Loss 14
2.3 Hot Embossing Lithography 14
2.3.1 Process Description 15
2.3.2 Typical Polymers Used 18
2.3.3 Stamps (Molds) 19
2.3.4 Embossing Conditions & Parameters 21
2.3.5 Process Flow 32
2.3.6 Challenges 37
2.3.7 Commercial Embossers 42
2.3.8 Designing an Embossing System 43

Chapter 3 Results for etched PAI waveguides 53
3.1 PAI Waveguide Fabrication 53
3.2 Loss Measurements 58
3.3 Transmission Spectrum and Absorption Peaks 60
3.4 Thermal Reflow 65

Chapter 4 Embossing of PAI 68
4.1 Interest in Embossing PAI 68
4.2 Fabrication of Si Stamp 68
4.3 Preliminary Embossing Tests 75
4.4 Design and Fabrication of a custom Embossing Station 85
4.5 Results obtained by placing the home-made embossing unit in an oven 101
4.6 Embossing using a Commercial Embosser 107

Chapter 5 Conclusion & Future Work 114
5.1 Polyamide-imide waveguides 114
5.2 Embossing 115
5.2.1 Viscosity and other thermal properties 115
5.2.2 Embossing above Tg and Process Control 116
5.2.3 Reflow and using PAI as a mold 117

5.2.4 Variation of the embossing tool 119
5.2.5 Simulations 119
5.2.6 Uses for the embossing station built 119

Bibliography 121

Appendix A: HEX01 Macros 129
A.1 Standard Preparation Macro 129
A.2 Silicone Adhesion Macro 130
A.3 Typical Embossing Macro 131

List of Tables

Table 1.1: Properties of key integrated optic materials at 1550 nm [9] 3
Table 1.2: Glass transition temperature of different thermoplastics [34] 6

Table 2.1: Wavelengths and intensities of important vibrational overtones 12
Table 2.2: Experimental conditions required to fill a 20 μm square cavity with PMMA samples with different molecular weights [46] 36
Table 2.3: Classification of the different defect classes [56] 51
Table 2.4: Quality assessment of structures with different molecular weight produced with and without vacuum [56] 51

Table 3.1: PAI cut-back method loss summary 59

Table 4.1: Structure depth and height vs. reactive ion etching time 69
Table 4.2: Difference between the actual and displayed temperature in the embossing station. 97
Table 4.3: Embossing of SB Torlon at 360°C for 200 min. T_{read} refers to the temperature read in the poling station's software interface, while T_{TC} gives the temperature measured with the thermometer. 98
Table 4.4: Summary of the embossing parameters. 99

List of Figures

Figure 2.1: Total Internal Reflection [1] 9
Figure 2.2: Typical optical waveguide structures [38] 10
Figure 2.3: Overtone positions for different CX-vibrations [40] 13
Figure 2.4: Hot embossing of micro-channels (left), and SEM 16
Figure 2.5: SEM micrograph of very simple replication of PMMA micro pyramid [49]. 17
Figure 2.6: Si mold with 0.8 μm wide ridges (left), and the replicated pattern structure with 0.8 μm wide channels (right) [50]. 17
Figure 2.7: SEM of stamp made from SiO_2 used for fabricating a microring 20
Figure 2.8: Molds fabricated with different methods [47] 21
Figure 2.9: Optical images of the step by step filling of a square cavity (from a to h) [46] 23
Figure 2.10: Three-dimensional AFM images of three different stages of fill of a square cavity [46] 24
Figure 2.11: Schematic showing forces acting as cavity fills [46] 25
Figure 2.12: Mound formation during squeezed flow into a cavity [60] 25
Figure 2.13: Polymer flow for different stamp geometries [46] 26
Figure 2.14: Two-dimensional model for determining time required to fill a cavity [46] 29
Figure 2.15: Viscous Fingering [60] 30
Figure 2.16: Patterns imprinted with and without an ASL [62] 31
Figure 2.17: Different temperature and pressure stages [59] 33
Figure 2.18: Typical Embossing process flow diagram [61] 34
Figure 2.19: Microscope images of embossing trials on mr-I 8030 with parameters used to produce them [57] 35
Figure 2.20: SEM of polymer shearing during cool down due to difference in TEC [55] 37
Figure 2.21: Uniformity test involving the comparison of SEM images of similar features embossed at different locations [64]. 39
Figure 2.22: Stamp and the embossed polymer structure after being stretched 40
Figure 2.23: Viscous fingering around structured regions [60] 41
Figure 2.24: Different stages of dewetting [60] 41
Figure 2.25: EVG520HE (left) [61], and HEX03 (right) [47] 42
Figure 2.26: Setup of the stack to be loaded into the EV520HE [56] 43
Figure 2.27: Schematic diagram of compact imprint system [62] 44
Figure 2.28: Close-up of the compact imprint system [53] 44
Figure 2.29: Schematic of hot embossing equipment [44] 45
Figure 2.30: Lab-scale embossing setup at MIT [43] 46
Figure 2.31: Embossing machine with force frame [50] 46
Figure 2.32: Typical blocks needed in an embossing machine [59] 47
Figure 2.33: A copper lower platen [42] 47
Figure 2.34: Different embossing control blocks [43] 49
Figure 2.35: LISA-like defects (left), micrograph of flow borders and 3 different types of defects (right) [56] 50

Figure 3.1: SEM of PAI film on BCB cured at 325°C in N_2 environment 54

Figure 3.2: Variation of Tensile Stress, Birefringence, and Thickness of PAI film with curing temperatures 55
Figure 3.3: Fabrication Process for PAI buried channel waveguides 57
Figure 3.4: SEM of PAI waveguides (a), and end-view after cleaving (b) 58
Figure 3.5: End and Top view of 980 nm (left), and 1550 nm (right) light coupled into PAI waveguides [38] 59
Figure 3.6: Molecular structure of PAI polymer [70] 60
Figure 3.7: Extracted absorption spectra for PAI 61
Figure 3.8: Absorption spectrum of ten-10μm film stack 61
Figure 3.9: Spectral Characterization of PAI waveguide 62
Figure 3.10: Transmission Spectrum of 3 μm waveguide using Super Continuum Laser 63
Figure 3.11: Relative absorption spectrum of both 10 μm and 3 μm waveguides in dB/cm. 64
Figure 3.12: Transmission spectrum of PAI waveguide in the 1550 nm range 65
Figure 3.13: SEM images showing the sidewall of a PAI waveguide before (left) and after annealing for 1-hour at 300°C (right) 66
Figure 3.14: PAI waveguides thermally reflowed at 270°C for 2hrs (left), and 4hrs (right) 67
Figure 3.15: PAI waveguides thermally reflowed at 280°C for 2hrs (left), and 4hrs (right) 67
Figure 3.16: PAI waveguides thermally reflowed at 290°C for 2hrs (left), and 4hrs (right) 67

Figure 4.1: Diagram illustrating processing steps used in the fabrication of silicon ribs (left), and silicon trenches (right) 70
Figure 4.2: 4.2 μm (left) and 6.2 μm (right) wide silicon trenches ~1.8 μm deep (50 s ICP) 71
Figure 4.3: 1.8 μm (left) and 2.4 μm (right) wide silicon trenches ~1.8 μm deep (50 s ICP) 71
Figure 4.4: Sidewalls of 50 s ICP silicon trenches 1.5 μm (left) and 4.4 μm (right) 72
Figure 4.5: Hook-like shape of top edge of 50 s ICP silicon trench 73
Figure 4.6: 2 μm (left) and 3.9 μm (right) wide silicon rib-like structure ~0.9 μm high (40 s ICP) 73
Figure 4.7: 5 μm (left) and 5.5 μm (right) wide silicon rib-like structure 0.9 μm high (40 s ICP) 74
Figure 4.8: Sidewalls of 40 s ICP silicon rib-like structure 74
Figure 4.9: Poling Station Controller Interface 76
Figure 4.10: Optical Microscope images of embossed Torlon trenches 77
Figure 4.11: Incomplete Torlon trenches embossed at 360°C, 200 kPa for 4 hours 78
Figure 4.12: Incomplete Torlon trenches embossed at 360°C, 200 kPa for 12 hours 78
Figure 4.13: SEM of embossed Torlon waveguides (360°C for 4 hours) 79
Figure 4.14: Side-view of Torlon embossed waveguides (360°C for 4 hours) 80
Figure 4.15: Side-view of trench-like distortion on embossed Torlon (360°C for 4 hours) 81
Figure 4.16: Torlon trench embossed by binder-clip based setup 82
Figure 4.17: Broken pieces from silicon waveguide mold, stuck in Torlon trench 83

Figure 4.18: Silicon mold broken even in locations with minimum penetration..... 83
Figure 4.19: SEM of silicon rib mold with parts broken (left), zoomed picture of broken silicon ribs (right)..... 84
Figure 4.20: 3-dimensional schematic of embossing unit 86
Figure 4.21: Exploded-view of embossing unit schematic..... 87
Figure 4.22: Front view schematic of embosser unit..... 89
Figure 4.23: Photograph of embosser force applying unit..... 89
Figure 4.24: Close Up of Embossing Machine..... 90
Figure 4.25: Another view of the springs 91
Figure 4.26: Poling station where the embossing device was mounted 91
Figure 4.27: Device mounted on Poling Station..... 92
Figure 4.28: Extended part of force-applying plate before force is applied 92
Figure 4.29: Top knob applying force fully..... 93
Figure 4.30: Compression springs in the fully compressed state, such that the applied force is maximum 93
Figure 4.31: Extended part of force applying plate with highest force applied..... 94
Figure 4.32: The complete embossing setup including: the force applying unit, the poling station, and the cover 94
Figure 4.33: Silicon mold attached to embosser plate using Silicone adhesive 96
Figure 4.34: Poling Station Profile for Embossing Torlon trenches for 200min..... 99
Figure 4.35: Optical microscope view of PAI embossed trenches 100
Figure 4.36: PAI embossed trenches. 100
Figure 4.37: Overview of the oven. 101
Figure 4.38: Control Switches 102
Figure 4.39: Temperature Reading (left), Switch and Temperature Control (right) 102
Figure 4.40: Inside of the Oven 103
Figure 4.41: Embossing Machine placed in the oven..... 103
Figure 4.42: Probe connected to embossing machine..... 104
Figure 4.43: Probe opening covered with insulation to avoid heat escape..... 104
Figure 4.44: Thermocouple (left), Oven turned on (right)..... 105
Figure 4.45: Embossed trenches in a PAI film that was cured at 200°C for 2 hours. The embossing pressure, temperature, and time were 2.6 MPa, 328°C, and 5 hours, respectively. 105
Figure 4.46: Part of a silicon waveguide mold broken and attached to the PAI trench.. 106
Figure 4.47: SB PAI trenches embossed at 200°C for 4 hours. 107
Figure 4.48: Jenoptik HEX01 hot embosser..... 108
Figure 4.49: Overview of embossed PAI waveguide (top), with close-up view at different locations along the guide (bottom) 110
Figure 4.50: Embossed PAI trenches at 3001N and 180°C..... 111
Figure 4.51: Embossed numerical and circular markers on PAI film..... 112

List of Symbols

AFM	Atomic Force Microscope
ASL	Anti-sticking Layer
BCB	Benzocyclobutene
CTE	Coefficients of Thermal Expansion
DMAC	Dimethyl-acetamide
DMF	Dimethyl Formamide
FAP	Force-Applying-Plate
GaAs	Gallium Arsenide
HEL	Hot Embossing Lithography
HSQ	Hydrogen Silsequioxane
IC	Integrated Circuits
ICPRIE	Inductively Coupled Plasma Reactive Ion Etching
InP	Indium Phosphide
$LiNbO_3$	Lithium Niobate
MEM	Micro-Electro-Mechanical Systems
MOEMS	Micro-Opto-Electro-Mechanical Systems
Mw	Molecular Weight
OSA	Optical spectrum analyzer
PAI	Polyamide-imides
PC	Polycarbonate
PCB	Printed Circuit Board
PI	Polyimides
PMMA	Polymethyl-Methacrylate
PR	Photoresist
PS	Polystyrene
PVB	Polyvinyl Butyral
RIE	Reactive Ion Etching
RT-NIL	Room Temperature Nanoimprint Lithography
SB	Soft baked
SEM	Scanning Electron Microscope
SOG	Silicon-on-glass
Tg	Glass Transition Temperature
TIR	Total Internal Reflection
VOA	Variable Optical Attenuators

Chapter 1 Introduction

In this chapter a brief background on the use of polymers in telecommunications is given, along with a discussion of the factors motivating the use of polyamide-imides in these applications. An outline of the thesis is also provided.

1.1 History of Telecommunication

After the invention of the transistor, the processing and transmission of information has been largely based on semiconductors. Continued advancements in electronics have revolutionized computing and telecommunications. However, demand for bandwidth has exceeded the performance of electronics in many applications [1]. To overcome these barriers, computing and communication systems were in many cases supplemented or totally replaced by optical components, and photons started to replace electrons as the information carriers. An obvious example is the dominance of optical fiber as a long haul transmission medium.

Advances in computing systems have caused the speed and complexity of integrated circuits (IC), as well as the number of components per chip and the number of chips per board, to increase. This has created a bottleneck for the use of electrical interconnects, and different solutions are being sought to solve the speed, packaging, and power dissipation problems that are arising [1]. Furthermore, the cost of chip fabrication is rising; lithography alone can amount to 35% of the total chip cost [2]. As for the telecommunications industry, the increased demand for bandwidth is outgrowing the capacity of electronic systems [1]. This has resulted in an urgent need to develop new methods that permit the control and processing of huge amounts of data transfer. Similarly, the movement into higher clock frequencies has led to an increase in the impedance of the electrical conductors on chips and boards, making propagation characteristics less favorable. Overall, there is an increasing drive to move from electronic to optical (photonic) communication systems, even for short haul interconnects. Photonic systems bring many advantages including larger bandwidth and information carrying capacity, very low transmission losses and heat generation, immunity to crosstalk, and reduced weight and size compared to their electronic counterparts.

Several materials have been studied as platforms for optical devices and integrated optical systems, each having advantages and disadvantages. Lithium Niobate, for example, is a very promising material used extensively in the fabrication of many functional devices [3-5]. Glass-based devices have demonstrated low optical loss, which along with low material cost make them very attractive. However, they typically do not possess properties useful for the active control of light, and this has restricted their applications mainly to passive devices [6, 7]. Indium Phosphide (InP) and Gallium Arsenide (GaAs) are seen by some as the materials of the future since they offer the possibility of monolithic integration of passive and active devices. Problems with these materials, however, include the high material cost as well as the difficulty in integrating crystalline materials on electronics platforms [8]. Silicon-based optical devices capitalize on the huge technological infrastructure that has already been set by the IC industry [9-11]. However, silicon has limited light-emitting capabilities and cannot typically form the basis of ultra fast modulators and switches. Thus, for the foreseeable future, integrated photonics is likely to require a diverse set of materials.

1.2 Polymers in Integrated Optics

Polymers have been widely studied (but only sparingly implemented) as enabling materials for integrated optics [1, 12], where the main applications have traditionally been in fiber optic systems. Polymeric materials, however, are gaining more attention [13], and are expected to play a key role in the rapidly growing fields of telecommunications, computing, and integrated optics in general. They demonstrate excellent performance in many applications, and have a greater potential for integration on electronics platforms when compared to most other materials. Several polymers show excellent mechanical properties. Their optical properties, such as the refractive index [14, 15], can be easily tuned by doping them with different materials, or through chemically modifying their monomers. Control of the polymer/solvent ratio as well as the spin casting speed can yield a wide range of film thickness. Many polymers have been shown to exhibit very low optical loss in the 1300 nm and 1550 nm wavelength bands, as well as low birefringence when formed as a thin film. The fabrication of optical waveguides using polymeric materials is very attractive due to the associated low costs [16],

especially when compared to other commonly used materials such as InP and $LiNbO_3$. Many polymers show non-linear effects, or can be doped with materials to introduce needed effects [17]. Several polymers, for example, possess a high thermo-optic coefficient which allows for the design of low power optical switches [16, 18]. Also the electro-optic effect of dye-doped polymers has been used and a modulation up to 110 GHz has been reported [16]. Table 1.1, compares several properties of polymers with other materials [9] (these quantities are described in more detail in the cited source).

Table 1.1: Properties of key integrated optic materials at 1550 nm [9]

	Propagation Loss (dB/cm)	Pigtail Loss (dB/chip)	Refractive Index (n)	Index Contrast Range in Waveguide (Δn)	Birefringence ($n_{TE} - n_{TM}$)	T/O Coef. dn/dT (K^{-1})	Maximum Modulation Frequency	Passive / Active
Silica [SiO_2]	0.1	0.5	1.5	0-1.5% (Channel)	10^{-4}-10^{-2}	10^{-5}	1 kHz (T/O)	Y/Y
Silicon [Si]	0.1	1.0	3.5	70% [range=0] (Silicon on Insulator Rib)	10^{-4}-10^{-2}	1.8×10^{-4}	1 kHz (T/O)	Y/N
Silicon Oxynitride [SiO_xN_y]	0.1	1.0	SiO_2:1.5 Si_3N_4:2.0	0-30% [30%: Si_3N_4 core] (Channel, SiO_2 clad)	10^{-3}-5×10^{-8}	10^{-5}	1 kHz (T/O)	Y/N
Sol-Gels	0.1	0.5	1.2-1.5	0-1.5% (Channel)	10^{-4}-10^{-2}	10^{-5}	1 kHz (T/O)	Y/Y
Polymers	0.1	0.5	1.3-1.7	0-35% (Channel)	10^{-6}-10^{-2}	$-1\rightarrow-4\times10^{-4}$	>100 GHz (E/O) 1 kHz (T/O)	Y/Y
Lithium Niobate [$LiNbO_3$]	0.5	2.0	2.2	0-0.5% (Channel)	10^{-2}-10^{-1}	10^{-5}	40 GHz (E/O)	Y/Y
Indium Phosphide [InP]	3	10	3.1	0-3% (Channel)	10^{-3}	0.8×10^{-4}	40 GHz (E/O)	Y/Y
Gallium Arsenide [GaAs]	0.5	2.0	3.4	0-14% [14%: AlAs clad] (Rib)	10^{-3}	2.5×10^{-4}	20 GHz (E/O)	Y/Y

The processing flexibility of polymers has allowed different optical devices to be fabricated using several conventional and unconventional techniques. These techniques include: reactive ion etching, wet etching, electron-beam lithography, ultraviolet embossing, hot embossing [2], soft lithography [12, 19], photo-bleaching [1], ion implantation [16], and microcontact printing [19, 20].

Extensive work has already been done on polymers and several devices have already been demonstrated. Some of these include splitters [1], microring resonators [12, 13, 21], Mach-Zehnder interferometers [13], directional couplers [14], thermo-optical switches [14, 18, 22], electro-optic modulators [23], micro-electro-mechanical systems (MEMS), micro-opto-electro-mechanical systems (MOEMS) [23], variable optical attenuators (VOA) [1, 22-24], arrayed waveguide gratings [1, 14, 22, 25], tunable filters [1], as well

as DNA-sensitive micro-devices [26]. Polymers have also been used as optical interconnects for computing systems [1].

While polymers have made some inroads for active and passive devices in fiber systems, several requirements are imposed on the materials to be used in optical communications. These include, low losses, low birefringence, as well as thermal and environmental stability [22]. Traditionally, however, polymers that have shown excellent transparency around the telecommunication wavelength do not possess the needed thermal stability [14, 27]. PMMA, for example, is limited to temperatures below ~80°C, because its glass transition temperatures (T_g) are ~100°C [16]. Use of polymers in several computing and telecommunication systems requires the polymer to have high thermal stability, and good adhesion with electronic substrates [28] to provide compatibility with electronic device fabrication [29]. Many commercially available polymers, especially fluorinated polymers, do not exhibit good adhesion.

High optical losses in polymers, due mostly to the strong absorption by their C-H bonds in the telecommunication wavelength range, can be significantly reduced through fluorination (replacing the C-H bonds with C-F bonds, which have a lower absorption in that range). As a result, great emphasis has been placed on developing fluorinated polymers having ultra-low absorption in the near infrared [13]. Several techniques have also been successfully employed to reduce birefringence [22]. One of the major reliability concerns arises from the effects of moisture and other environmental issues. This can be addressed through the use of proper packaging to completely seal the polymer devices.

In solving these problems, there are often associated tradeoffs with respect to the optical properties (transparency, etc.) of the polymers. Also the intrinsic glassy nature of many polymers can create some reliability concerns, due to effects such as molecular relaxation. This had led to performance deterioration in many polymeric devices, and causes the refractive index to change over time [22]. These effects are enhanced when operating at a temperature close to the polymer's glass transition temperature. For this reason, polymers with high glass transition temperatures are required for certain applications. For example, it has been reported that for use in a thermo-optic based variable optical attenuator, the polymer's glass transition temperature needs to exceed 200°C [22]. This rules out many polymers for use in this and many other telecommunication applications.

1.3 Polyimides in Integrated Optics

Although many polymers have demonstrated attractive properties for integrated optics, most do not possess the needed thermal stability for on-chip or printed circuit board (PCB) interconnect applications. Polyimide (PI) is a high temperature polymer which has been effectively used in several microelectronics applications. Their high thermal and chemical stability, dielectric properties, and high breakdown voltage [30] make them excellent candidates for use in communication as well as computing systems. Polyimides can be used for creating highly complex integrated optical devices and interconnects on a planar substrate [31], and their optical properties can easily be tailored. Polyimides have been used in the fabrication of optical switches [31], as well as in several other optical applications [27]. They are also proven to be biocompatible [30].

Polyimides have traditionally faced several problems such as high water absorption, birefringence, high scattering loss due to ordered molecular domains, and high polarization dependent loss [1]. While fluorinated polyimides have been shown to address some of these issues [29, 31], they tend to suffer from poor adhesion and insolubility in common solvents, which limits their processing options.

1.4 Polyamide-imides

Polyamide-imides (PAI) are an important class of high performance polymers, and they recently have been studied as optical material. PAI has better processability and superior mechanical properties when compared to polyimides [32], but by having a similar chemical structure retains many of the attractive properties of polyimides. PAI is a tough thermoplastic that offers high thermal stability, good chemical resistance, excellent mechanical properties, and a wide range of processing methods such as spin-coating and injection molding [33].

PAI polymers possess a glass transition temperature greater than 270°C, which is the highest among true thermoplastics (see Table 1.2). They have decomposition temperatures greater than 400°C [33], meaning they can survive excursions to very elevated temperatures that would destroy most thermoplastics. They exhibit outstanding chemical durability, resistance to most organic solvents and acids, and an excellent

resistance to radiation. Furthermore, they possess high impact resistance and high creep resistance as well as several others outstanding mechanical properties.

Polymers can generally be divided into two groups: thermosetting and thermoplastics. Thermosetting polymers are polymers that when cured are hardened into a permanent shape. Thermoplastics, on the other hand, can repeatedly be transferred into a softened state when heated, and hardens when cooled. Being a thermoplastic, PAI can be easily processed by a variety of different methods such as injection molding, extrusion and compression molding, which allows parts and devices to be fabricated using different techniques.

Table 1.2: Glass transition temperature of different thermoplastics [34]

Polymer	T_g, °C
Polyamideimide (PAI)	295
Polyethersulfone (PES)	230
Polyarylsulfone (PAS)	220
Polyetherimide (PEI)	218
Polyarylate (PAR)	198
Polysulfone (PSU)	190
Polyphenylcarbonate (PPC)	180
Polyamide, amorphous (PA)	155
Polycarbonate (PC)	145
PPO-IPS-1	143
PPO-IPS-2	124
Styrene maleic anhydride (SMA)	122
Chlorinated PVC (CPVC)	107
PMMA	105
SAN	104
PS	100
ABS	100
PETG	81
PVC	65

All these attractive properties have created a great interest in PAI polymers. While not yet widely explored as a waveguiding material, PAI has found application in several fields that require strength and durability at very high temperatures. For example, PAI has been used to make automotive parts, aircraft and space shuttle parts (including those for military aircrafts), hydraulic parts, seal rings, washers and bushings, protective coatings, as well as high temperature adhesives [32, 35, 36].

Torlon AI-10, a commercial aromatic polyamide-imide (PAI) polymer available in powder form from Solvay Advanced Polymers, was evaluated as a waveguiding material in a previous study [32, 37]. It was verified that Torlon PAI exhibited high adhesion to a variety of materials, and that its solubility in standard solvents opens the doors to several fabrication techniques. Preliminary tests showed that Torlon adhered well to substrates such as Si, SiO_2 coated Si, quartz, as well as various metals and other polymers [32]. Low optical propagation loss of 0.2 dB/cm at 830 nm was obtained [32] for multimode waveguides fabricated from Torlon PAI. This thesis builds on previous work, and investigates the suitability of Torlon PAI for microfabrication of micro-devices using hot embossing lithography.

1.5 Outline

As was mentioned, several limitations and challenges face the future development of polymer-based integrated optics. One challenge is the inadequate thermal stability of most polymers that exhibit low optical loss at telecommunication wavelengths. A second challenge is the need for a high throughput fabrication method that can assist mass production in the future. Torlon PAI, with its outstanding stability and processability has potential to address these challenges.

This work focuses on addressing these two issues. Further studies were done to characterize the optical properties of PAI. This was followed by attempts to fabricate waveguides on Torlon PAI using hot embossing lithography.

Chapter 2 starts by providing relevant background and theory important to this work, as well as an overview of the principles of the hot embossing process. Chapter 3 starts by giving an overview of the work that has been previously completed by this group on characterizing the optical properties of PAI film, and describes the characterization of

PAI waveguides fabricated by conventional means (reactive ion etching, RIE). This work starts by continuing the examination of PAI waveguides fabricated by RIE. This is followed by exploring the use of thermal reflow for reducing the sidewall roughness of polyamide-imide waveguides. Chapter 4 then discusses the steps taken in this study for the fabrication of waveguides and trenches on polyamide-imide using hot embossing lithography. This chapter explores and discusses the difficulties that were faced and the important observations that were made. Finally, Chapter 5 gives a summary of the observations and conclusions that were made throughout this work. Several suggestions are made for future work.

Chapter 2 Background & Theory

This chapter provides relevant theory and background in the field of optics related to the work to be discussed in future chapters. The chapter also gives an overview of the principles of the hot embossing process along with its important principles and parameters.

2.1 Waveguiding by total internal reflection

The confinement of light by total internal reflection (TIR) is the basic phenomenon by which most optical systems work; a material that posses a certain refractive index is surrounded by a material with a lower refractive index. TIR confines light within the high refractive index medium and is used to create optical waveguides that direct light from one point to another, as shown Figure 2.1.

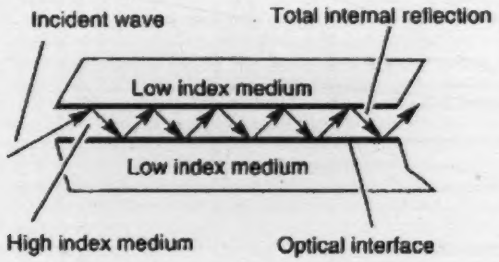

Figure 2.1: Total Internal Reflection [1]

The medium with the higher refractive index is called the core, while the one with the lower refractive index is called the cladding. Different structures that use this principle have been developed, including slab waveguides, strip waveguides, embedded strip waveguides, rib waveguides, and optical fibers, some of which are shown in Figure 2.2. The slab waveguide provides light confinement in one direction only, while the rest offer confinement in two dimensions. Optical fibers are used for long-haul transmission of light signals. The choice of a suitable two dimensionally confining waveguide depends mostly on the application.

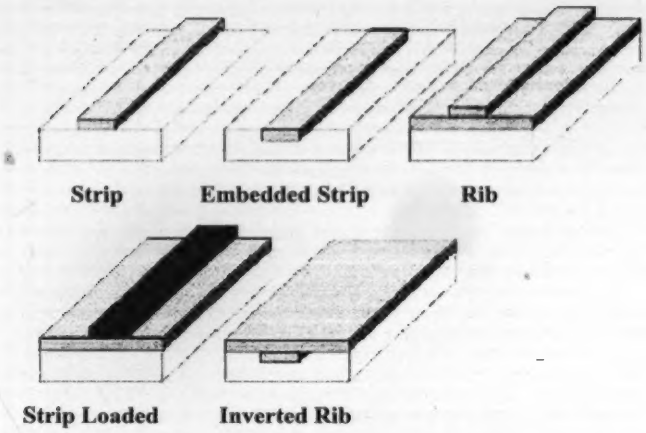

Figure 2.2: Typical optical waveguide structures [38]

Apart from the structure, the core and cladding materials should also be chosen properly. The appropriate materials depend on the application and operational conditions, as well as on their transparency at the wavelength of operation. Optical loss is usually given by the following relationship:

$$I_1(z) = I_o e^{-\alpha . z} \quad , \tag{2.1}$$

where I_0 is the input intensity, I_1 is the output intensity, z is the propagation length, and α is the loss coefficient. The following section discusses the main sources of optical loss in polymer waveguides.

2.2 Propagation Losses in Polymer Waveguides

One of the major concerns when designing optical waveguide devices is ensuring that they have low optical loss in the wavelength range of operation. Optical losses are caused by many factors, but can be divided into two types: intrinsic losses and extrinsic losses. Intrinsic losses are due to the nature of the material and can be affected by the processing conditions (which might lead to internal stresses). Extrinsic losses are due to the nature of the structure, and can be caused by the problems resulting from the processing methods and conditions. The sources of loss include absorption, scattering, fiber coupling, and bending.

2.2.1 Absorption Loss

In absorption processes, energy from the propagating wave is converted to a different form of energy (typically heat). One form of absorption loss is electronic absorption, which is related to the direct excitation of electrons. In polymers, electronic absorption features tend to be in the near ultraviolet range (200 nm – 400 nm) for polymers with a significant number of aromatic molecular structures, and in the deep ultraviolet range (less than 200 nm) for polymers with predominantly aliphatic molecular structures [1]. Electrons in molecules with aromatic structures, such as benzene, are free to cycle around circular arrangements of atoms. Polymers with aromatic molecular structures typically display enhanced chemical and thermal stability, compared to non-aromatic polymers containing mainly aliphatic C-H bonds. In any case, electronic transitions in polymers do not contribute significantly to optical losses in the major telecommunication windows [1]. The other cause of intrinsic material loss is vibrational absorption, where some of the energy of the propagating electromagnetic wave is coupled into the lattice vibrations of the material, and dissipated as heat. This loss mechanism peaks as the frequency of the traveling wave approaches the natural lattice vibrational frequencies of the material [39]. Knowledge of the positions and intensities of the overtones of the fundamental molecular vibration is often important in understanding the resulting absorption.

Table 2.1 gives a rough estimation of relative overtone intensities along with the positions of various vibrational overtones that have been identified in organic polymers [40]. The strength of each overtone is expected to differ slightly between polymers. The relative intensity of a vibrational overtone is listed with respect to the intensity of the fundamental vibration of that overtone. Figure 2.3 gives the overtone positions and the normalized integral band strength (E, measured in cm/mol), normalized relative to the fundamental vibration of the C-H bond.

Besides the molecular vibrations mentioned in the table, other vibrational absorptions can occur in polymers, such as those related to C=C or C-C bonds. However, there is less information in the literature about their corresponding overtone wavelength and intensity. Another source of absorption is the presence of water, which may be introduced by atmospheric humidity or during the preparation of the polymer.

Table 2.1: Wavelengths and intensities of important vibrational overtones

Bond	Overtone order	Wavelength [nm]	Relative Intensity
C-H	1	3390	1
C-H	2	1729	7.7×10^{-2}
C-H	3	1176	6.8×10^{-3}
C-H	4	901	7.2×10^{-4}
C-D	1	4484	1
C-D	2	2276	6.0×10^{-2}
C-D	3	1541	4.1×10^{-3}
C-D	4	1174	3.3×10^{-4}
C-D	5	954	3.2×10^{-5}
C-F	1	8000	1
C-F	2	4016	1.6×10^{-2}
C-F	3	2688	2.9×10^{-4}
C-F	4	2024	6.3×10^{-6}
C-F	5	1626	1.6×10^{-7}
C-F	6	1361	4.7×10^{-9}
C-F	7	1171	1.6×10^{-10}
C-F	8	1029	5.9×10^{-12}
C-F	9	919	2.5×10^{-13}
C=O	1	5417	1
C=O	2	2727	2.6×10^{-2}
C=O	3	1830	7.7×10^{-4}
C=O	4	1382	2.7×10^{-5}
C=O	5	1113	1.1×10^{-6}
C=O	6	934	5.5×10^{-8}
O-H	1	2818	1
O-H	2	1438	8.0×10^{-2}
O-H	3	979	7.3×10^{-3}

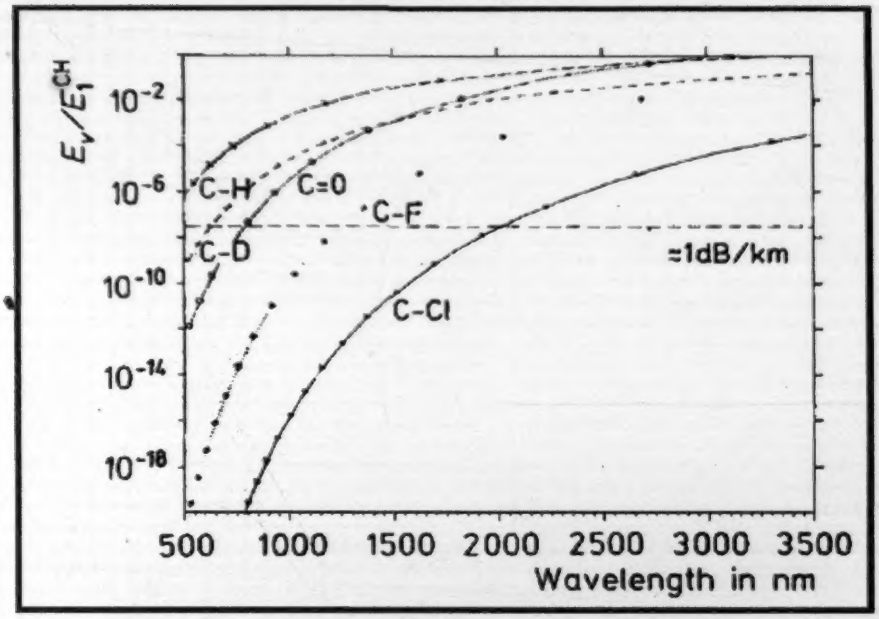

Figure 2.3: Overtone positions for different CX-vibrations [40]

C-H and O-H overtones typically make the dominant contribution to absorption in the telecommunication windows, while C-F overtones show extremely low absorption in the telecommunication windows. This is why fluorine atoms have been incorporated into several polymers to replace the hydrogen atoms and thus reduce the losses caused by absorption. Examples of fluorinated polymers reported in the literature include, fluorinated acrylates, perfluorocyclobutanes, cross-linkable fluorinated dendrimers, fluorinated polyimides, as well as several others [28]. However, fluorination is not always desirable, since the incorporation of fluorine will result in a reduction of the refractive index of the polymer due to the greater volume of fluorine compared to that of hydrogen [1]. Several studies have been made to study the effect of the fluorine content on the refractive index [31]. Another major drawback of fluorination is that fluorinated polymers tend to become more difficult to process and suffer from solubility issues as well as poor adhesion. This difficulty in processing is clear when examining polymers such as Teflon [24].

2.2.2 Scattering Loss

Scattering losses can be both intrinsic and extrinsic, but generally imply that a portion of the traveling electromagnetic wave is diverted away from the original direction of propagation. Intrinsic scattering losses are caused by refractive index inhomogeneity in the medium. This can be due to intrinsic stresses, created during the preparation of the polymer waveguide. In most cases however, polymer films are very homogeneous and these losses are negligible at telecommunication wavelengths. Extrinsic scattering losses can be caused by the presence of particles, bubbles, cracks, etc. in the waveguiding film. Generally, however the dominant source of extrinsic scattering losses is waveguide sidewall roughness. This roughness arises from imperfections during lithography, uneven etching, or some other fabrication step. Several models have been used to approximate the propagation loss caused by sidewall scattering. Some of the factors that are expected to increase scattering include: higher amplitude of the sidewall roughness, a high core-cladding index contrast given by $(n_{WG}^2 - n_C^2)$ were n_{WG} and n_C are the refractive indices of the waveguide core and the cladding respectively [17], and a reduced width of the waveguide core.

Extrinsic scattering losses can be reduced through modifying the etching conditions or through the use of high resolution fabrication methods that minimize sidewall roughness.

2.3 *Hot Embossing Lithography*

As structure sizes continue to decrease, further advancements become limited by the lack of a low-cost, high throughput fabrication technology [41]. As pattern sizes decrease, optical lithography becomes increasingly complicated and techniques such as electron beam lithography suffer from low throughput. Thus, alternative approaches are needed [42]. One possible solution is the new non-conventional lithographic method called hot embossing lithography (HEL). The key advantage of this technique is its ability to pattern sub-10 nm structures over a large area with a high-throughput and low-cost [41].

Several characteristics of HEL provide it with these advantages. First, HEL is a physical process, rather than a chemical process, and does not use any energetic beam. Thus, the resolution is not limited by any chemical effects (arising from etching and chemical

interactions), or the effects of wave diffraction, scattering and interference in the resist, and backscattering from the substrate [41]. Furthermore, the minimum feature size that can be imprinted is limited mainly by the minimum feature size on the mold (or stamp). This means that if the polymer has sufficient mechanical strength, imprint lithography should be able to produce sub-10 nm feature size in polymers [41]. Another advantage of HEL is that it is a single step process for forming components that might otherwise require multiple processing steps [43]. This is made clear when comparing it to more traditional processes such as reactive ion etching. While the fabrication of structures on a polymer layer using RIE would require a sequence of photoresist (PR) deposition, patterning, and etching, an embossing process could produce the needed structure with a single step process (once the appropriate mold is available). This makes HEL a high-throughput process. It is even envisioned that embossing could be transferred into a mass production process by machining the molds onto a roller that transfers patterns to polymeric sheets as they are pulled through the roller [44].

All these advantages and characteristics give embossing a great potential as a candidate for the next generation lithography [45]. It is conceivable that in the future, the mold can be made using a high-resolution, but low-throughput process, and then HEL can be used for low-cost mass production of nanostructures [41].

2.3.1 Process Description

A typical HEL process is as follows. First, a thin polymer (usually a thermoplastic) film is spin coated onto the substrate (or undercladding). The film is made to have a thickness of at least that of the required structure height [46] (mostly, however, the polymer thickness is made thicker then the mold intrusion (the part of the mold that is supposed to penetrate the polymer) in order to prevent the mold from touching the substrate [41]). The thermoplastic-coated substrate is then inserted into the embossing machine. Next, a micro-structured tool, known as the mold or stamp, is pressed (embossed) with high force into the film after it has been heated above its softening temperature (glass transition temperature, T_g). The mold is then filled by the plastic material, which replicates the microstructures in detail. Finally, after an adequate embossing time (holding time) the setup is cooled down below its glass transition temperature and the mold insert is

withdrawn from the plastic (de-embossing) [47]. The residual layer that might remain in some cases (outside the intended features) can be removed by dry etching [41]. Compared to similar methods, such as injection molding, the polymer only has to flow a short distance. This results in low stress and reduces the frictional forces acting on the polymer structures during demolding, making HEL more suitable for the fabrication of optical components, and for building delicate structures with higher aspect ratio [47].

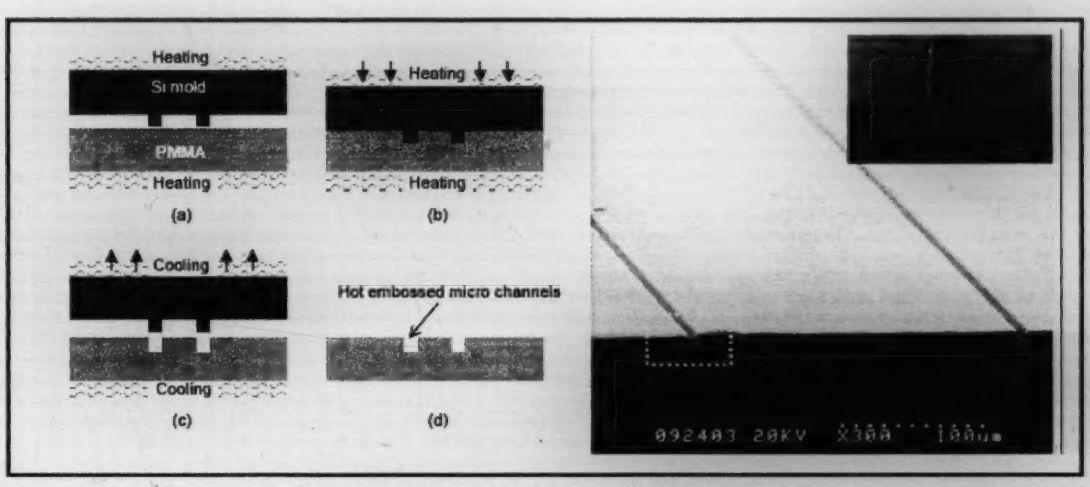

Figure 2.4: Hot embossing of micro-channels (left), and SEM of the hot embossed waveguide channels (right) [23]

This process has been used to fabricate different devices and structures on different kinds of polymers. Structures as simple as channels (Figure 2.4), and as complex as pyramids (Figure 2.5) or micro-lenses [48] can be easily fabricated by providing a suitable mold and by using proper embossing conditions.

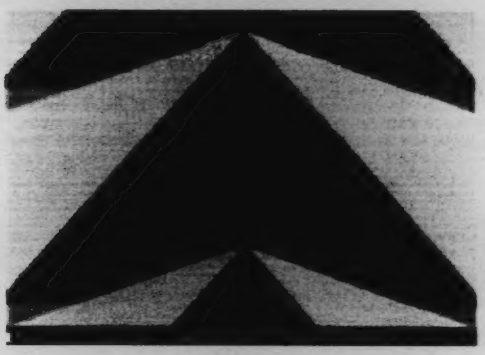

Figure 2.5: SEM micrograph of very simple replication of PMMA micro pyramid [49].

Figure 2.6 shows several channels, 0.8 μm wide, that were produced by a hot embossing process using a silicon mold; the mold was fabricated by an advanced silicon etch process [50]. Once the mold is fabricated, it can potentially be re-used many times permitting the required pattern to be produced by a single step process (embossing), where it would otherwise require multiple processing steps for the production of each subsequent pattern using more traditional fabrication techniques.

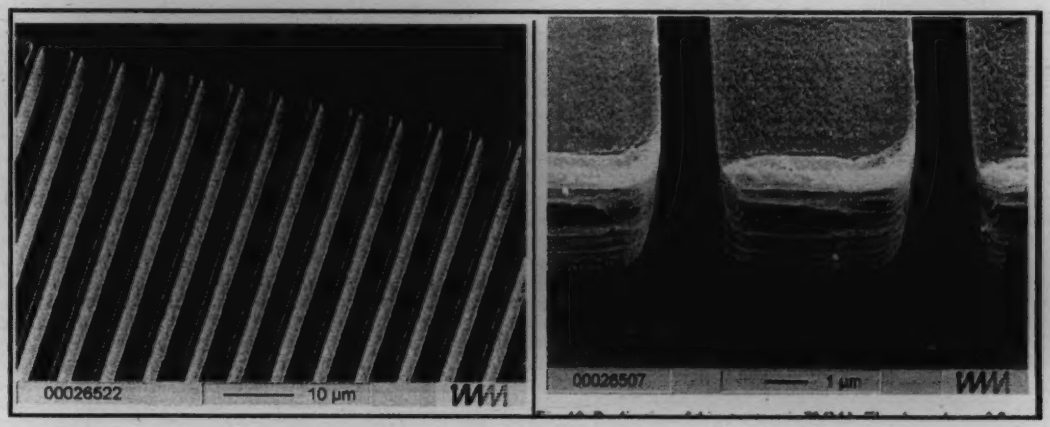

Figure 2.6: Si mold with 0.8 μm wide ridges (left), and the replicated pattern structure with 0.8 μm wide channels (right) [50].

2.3.2 Typical Polymers Used

Different types of polymers have been used successfully in fabricating structures by hot embossing. Due to the different properties of these polymers, they required different embossing conditions. Examples of polymers used are polyvinyl butyral (PVB) [51], which is a rubbery polymer at room temperature with $T_g = 15°C$ and a molecular weight of 143,000 g/mol, polystyrene (PS) [52], with $T_g = 92°C$ and a molecular weight of 181,000 g/mol, and polycarbonate (PC) [17, 51, 52], with $T_g = 145°C$, a molecular weight of 18,000 to 37,000 g/mol, and a refractive index of 1.6.

The most commonly used polymer, however, has been polymethyl-methacrylate (PMMA). It has several properties that make it an attractive option when choosing a suitable material for hot embossing. First, it can be directly patterned with fine resolution using electron beams [16]. This allows for correction of flaws that might remain after the embossing step. It can also be obtained in a variety of molecular weights such as 15,000 [17], 25,000, 75,000, and 350,000 [46] g/mol. PMMA has a small pressure shrinkage coefficient [41], a relatively low glass transition temperature of around 105°C [41, 46], a refractive index of 1.48 at 1550 nm [23], good optical transparency in the visible and near-IR regions, and a birefringence less then 5.5×10^{-6} [24]. These properties along with its ease of processing have made PMMA the most widely used polymer in embossing.

Materials such as silicon-on-glass (SOG) and hydrogen silsequioxane (HSQ) have been used in a process known as room temperature nanoimprint lithography (RT-NIL), where the embossing process is carried out at room temperature [53]. The interest in these materials arose due to their superiority to PMMA for use as a mask in dry etching, and due to added advantages of embossing at room temperature.

The fabrication of molds required in hot embossing processes is both time consuming and expensive. These molds are subjected to high temperatures and pressures and may suffer damage or degradation. Thus it was proposed in some papers to move from silicon molds to thermosetting replicas [54]. These thermosetting molds can then be used in embossing thermoplastic polymers [55]. Some of the polymers that have been used for molds include mr-L 6000 [55], and mr-L 8000 [56] (with a molecular weight of 99,000 or 350,000 g/mol, respectively).

2.3.3 Stamps (Molds)

One of the most important components of a successful embossing process is the use of a proper stamp; the stamp is also known as the mold, mold insert, or master. This mold will be heated to a temperature above the glass transition temperature of the polymer to be embossed, and then cooled again during demolding. This makes it desirable to choose a mold with a thermal expansion coefficient (TEC) that is reasonably well matched to that of the polymer (in order to avoid distortion of the structures during the hot embossing process) [55].

In spite of this, *silicon* (with a TEC of 2.6 x 10^{-6}/°C, more than one order of magnitude lower than is typical for a polymer) has been the most widely used mold material [23, 46, 49, 55, 56]. Silicon molds are very attractive due to their excellent surface quality and easy mold release (low adhesion to the polymer). SiO_2 molds have also been used as a stamp in several processes [17, 57]. Other materials that have been used include *ceramics* and *metals* due to their high mechanical and thermal strength. Two commonly used metals are *stainless steel* [44] and *nickel* [58]. Some papers reported using stamps made from *thermosetting polymers* [54]. Thermosetting polymers are seen as an attractive option since there is a smaller difference between the TEC of the thermosetting mold and the polymer to be embossed, when compared to using silicon molds. Embossing trials can be done using different molds, in order to determine which mold produces the best structure.

In order to emboss a pattern on polymer, the negative of this pattern has to be fabricated on the mold. An example of the mold used to fabricate a microring resonator is shown in Figure 2.7. The suitability of the stamp fabrication method depends on the mold material, resolution needed, surface roughness tolerated, sidewall angle, aspect ratio, along with other factors. For example, to achieve high aspect ratio, the sidewalls must be as smooth as possible (to minimize friction force), and a suitable fabrication technique has to be chosen accordingly. In many cases in order to ease this constraint the sidewalls could be fabricated with a small angle of inclination (draft angle) [50, 59].

Figure 2.7: SEM of stamp made from SiO_2 used for fabricating a microring resonator [17].

With respect to feature definition on the molds, electron-beam lithography is the most popular method when fabricating structures smaller than 1 μm [12, 17, 46]. It utilizes the fact that some materials (such as SU-8 [13], and PMMA [16]) will undergo chemical changes when exposed to a beam of energetic electrons. Using electron-beam lithography, structures in the nm-range can easily be fabricated.

For structures greater than 1 μm, it is more common that standard photolithography followed by reactive ion etching is used. This approach has been successfully used for fabricating high aspect ratio masters [23, 42]. RIE is also the technique of choice for removing any residual layer that might remain after the embossing process.

There are several other methods that can be used to fabricate a master including: CNC-machining, mechanical micromachining, excimer or fs laser-based process, and LIGA-like methods. LIGA [58], or Lithographie (lithography) Galvanoformung (electroplating) Abformung (molding), a technology based on X-ray deep-etch lithography, is characterized by extremely high structural heights and small lateral dimensions. More relaxed mold requirements are met by using UV lithography instead of the complex X-ray technology [47, 49, 59].

CNC (computerized numerically controlled) machining can also be used to fabricate molds. However, it typically does not provide a smooth surface finish, a high aspect ratio, or good dimensional control [58]. Mechanical micromachining techniques such as

turning, drilling or milling were used in some cases in fabricating the master, often with diamond tools [47, 59].

A new technology that offers good potential in terms of aspect ratios and minimum structural dimensions is laser patterning. An advantage of this technology is it allows processing of new materials, such as stainless steel or tungsten carbide [46, 47], thus allowing exploration of these new materials for use as molds. Figure 2.8 shows several molds that were fabricated using different technologies.

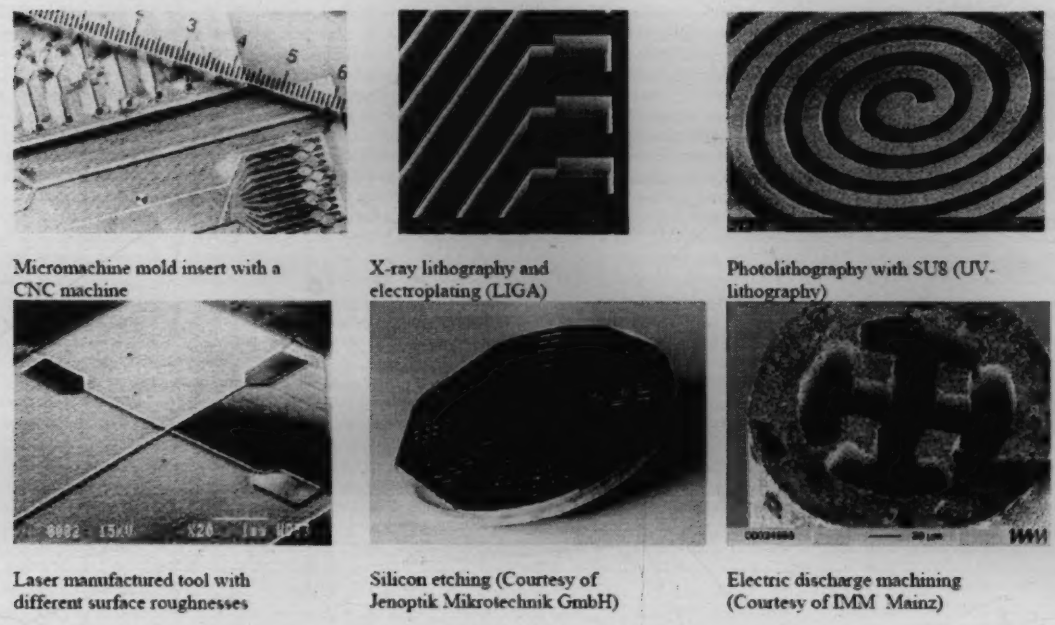
Micromachine mold insert with a CNC machine
X-ray lithography and electroplating (LIGA)
Photolithography with SU8 (UV-lithography)
Laser manufactured tool with different surface roughnesses
Silicon etching (Courtesy of Jenoptik Mikrotechnik GmbH)
Electric discharge machining (Courtesy of IMM Mainz)

Figure 2.8: Molds fabricated with different methods [47].

2.3.4 Embossing Conditions & Parameters

Several conditions must be carefully considered in order to perform a successful embossing process. These conditions include: the embossing and de-embossing temperature, the pressure or force that would be applied, the time needed to complete the embossing process, the need for vacuum, and the use of an anti-stick layer (ASL). Another important and usually neglected variable is the embossing speed (speed at which

pressure is applied) [42, 51]. Finally, it was found advantageous in some cases to aid the pattern transfer by leaving traces of solvent in the polymer layer [56]. This effectively reduces the glass transition temperature of the polymer; the residual solvent can be removed (and the polymer hardened) in a post-embossing anneal step.

Nevertheless, the success of the hot embossing procedure depends mostly on three variables: pressure, temperature, and time [44]. It was identified that temperature and hold time are the most important parameters to achieve full stamp cavity filling, and that pressure needs to be above a certain threshold, but is the least sensitive variable of the three [43, 57]. In most cases, trials are performed with two variable kept constant while one variable is varied to find the optimal embossing conditions [48].

For every design of a microstructure, the process conditions vary slightly with the properties of the design, such as the distribution of large and small structures over the wafer area, total processed wafer area, and the geometry of the structures [50]. Following is a detailed discussion of some important parameters.

2.3.4.1 Filling and Flow Characteristics:

It is important to have a good understanding of the flow characteristics of the polymer in order to fully understand the embossing process.

As the polymer is heated above its glass transition temperature, its viscosity or resistance to flow starts to decrease [52]. When a stamp is applied to the softened polymer, the polymer starts to flow. Three forces may be present during embossing. The first is the applied force, which helps the polymer flow into the mold insert. The other two are the interface frictional force (between the polymer and the mold insert) and surface tension [49].

In order to study the fill characteristics experimentally, the embossing temperature can be lowered and embossing time shortened so that the polymer is hardened and demolded when the cavity is only partially filled [46].

As seen in Figures 2.9 and 2.10 below, the filling starts from the edges (a). The polymer, PMMA in this example, then flows further at the corners due to the combination of pressure from two edges, which results in the formation of the square-shaped hole (b, c). As the cavity continues to fill, the original cavity shape no longer dictates the shape of the hole. The surface tension is now more important and the hole becomes circular to minimize the surface energy until it disappears (d-g). It is likely that the air cannot escape here and is just compressed to very small fraction of its original volume (h) [46]. Figure 2.10, then gives a three dimensional AFM image of the cavity as it is being filled.

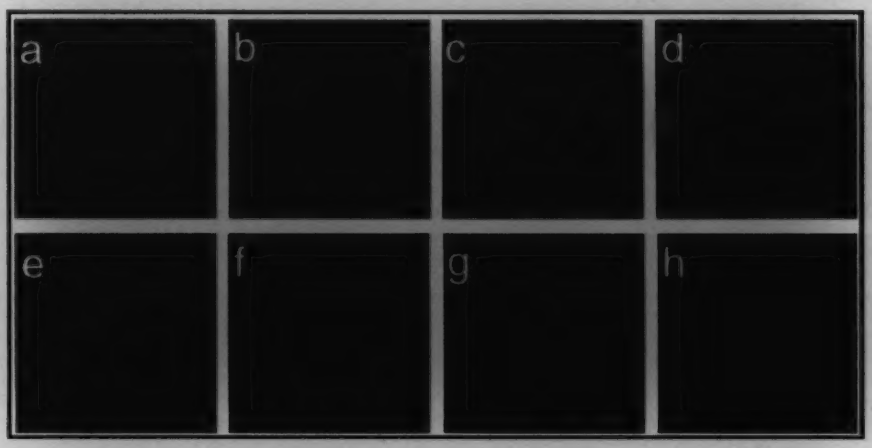

Figure 2.9: Optical images of the step by step filling of a square cavity (from a to h) [46]

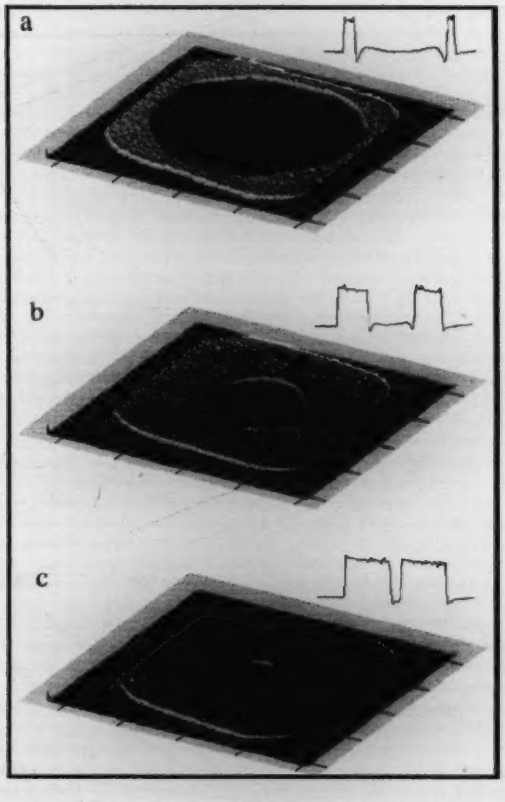

Figure 2.10: Three-dimensional AFM images of three different stages of fill of a square cavity [46]

The material tends to fill first at the edges since the material gradient is greater there, and progresses to the center with time [43]. A height profile of a partially filled stamp cavity is shown in Figure 2.11. Here it can be seen that both capillary effects, causing the polymer to flow up the cavity walls, and compressive effects, seen as a bowing of the central region, are present [46]. The polymer melt is squeezed into the cavity, flows up the walls of the cavity and compresses the polymer film in the centre of the cavity. As a result of lateral compressions, the surface wave-like features are intensified causing buckling of the polymer film [60], as shown in Figures 2.11 and 2.12.

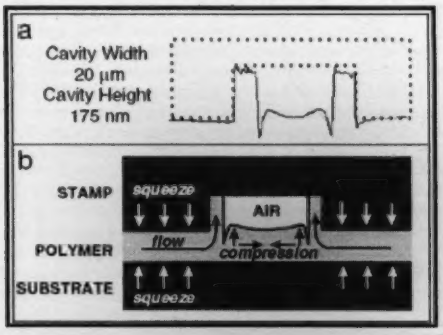

Figure 2.11: Schematic showing forces acting as cavity fills [46]

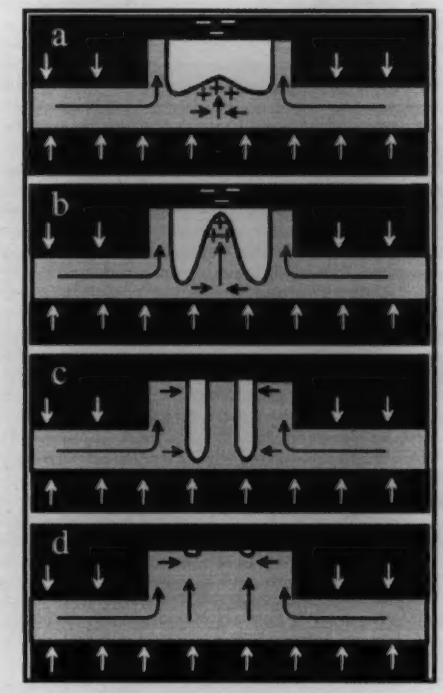

Figure 2.12: Mound formation during squeezed flow into a cavity [60]

Another important factor that determines the final configuration of plastic structures in a hot embossing process is the geometrical shape of the mold inserts [48]. It was determined, for example, that for small feature sizes the pattern transfer poses no particular difficulty [57], while more demanding conditions are needed when filling structures with wider feature sizes.

Two possible stamps are shown in Figure 2.13 [46]. In Figure 2.13a, a large area of periodic structures (such as a grating) is shown. The distance between the cavities is given by S_1. This limits the specific area that contributes to the filling of a single cavity. The local flow of the polymer is indicated by the arrows in the figure and results in simultaneous filling of the cavities. In the case shown in Figure 2.13b (with the large unstructured area), the majority of material flows from the borders. This results in sequential filling of the cavities. For this case, the squeeze flow in the intercavity regions can be neglected and the effective stamp area is then the area between the edge of the structured region and the stamp border, indicated by the stamp width S_2. This results in the polymer flow shown by the arrows.

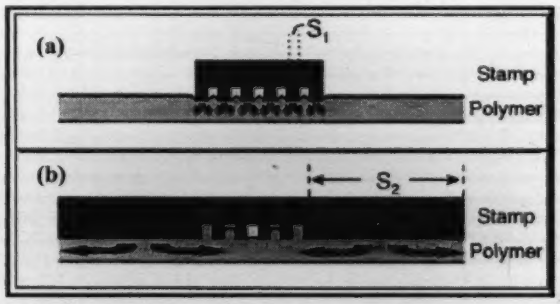

Figure 2.13: Polymer flow for different stamp geometries [46]

2.3.4.2 Pressure (force applied)

Pressure has been found to be less critical than the other two important parameters (time and temperature), and needs only to be above a critical value. A relationship has been found between the applied pressure, the surface tension force on top of the polymer layer, and the interfacial shear force. A simplified model was used to determine the critical pressure needed to overcome surface tension in order for the polymer to flow [48]. This critical pressure is given by:

$$P_{cr} = \frac{4 f_s}{D}, \qquad (2.2)$$

where f_s is the surface tension at the processing temperature, and D is the diameter of the cavity. For example, the surface tension of polycarbonate (PC) is 0.046 N/m at 250°C; therefore, the critical pressure for defining holes with 100 μm diameter in PC is 1840 Pa. Typically, however, the embossing pressure should be around 0.5 (5 MPa) to 2 (20 MPa) kN/cm^2 [59] in order to ensure well-defined features.

Generally, the most suitable pressure depends on the other parameters used, and is determined by experimental trials. When embossing PMMA, for example, the pressure that was used ranged from 0.35 MPa [23] to 13 MPa [41]. In practice, this pressure also depends on the capabilities of the embossing machine.

2.3.4.3 Embossing Temperature

Embossing temperature is the most important and most critical embossing parameter. The material is first heated to a temperature above the glass transition temperature, but below the decomposition temperature of the polymer [43]. It has been reported [61], that the temperature-time relationship that describes the polymer flow, the time is excepted to have a linear effect, while the impact of temperature is exponential. This makes increasing the temperature more effective then increasing time. As a general rule, a drop in temperature of approximately 20°C from the optimum temperature could require an increase in embossing time by approximately 5 times [46]. Another observation recorded is that doubling the embossing force enabled a reduction by approximately 20°C in the required embossing temperature [46].

Studies on shear deformation in several polymers including PMMA showed that there is a sharp change in viscosity at 1.05 T_g [43]. The higher the temperature, the lower the viscosity, thus allowing easier polymer displacement and a faster fill [59]. The polymer film thickness was also found to have an effect on the required temperature. Decreasing the polymer thickness was found to give a significant increase in the required temperature. The increase is likely due to adhesion of the polymer at the substrate and stamp surface, which hinders the movement of the polymer [46].

There are a lot of things to consider when deciding on a suitable thermal cycle for the embossing process. One factor is the rate of heating the polymer. Although no effect was reported on varying the rate of heating the polymer, it might be an important parameter to

consider. The process can be carried out isothermally or non-isothermally [59]; i.e., where the polymer and the mold are kept at the same temperature (above T_g) or varied differently.

The de-embossing temperature should also be considered when deciding on the embossing parameters. One can cool the whole device to room temperature before de-embossing, or on the other hand one can cool it down to a temperature just below the glass transition temperature. In most cases a compromise is needed between structure quality and processing time [58]. The difference between embossing and de-embossing temperatures is usually set between 25°C – 40°C, in order to reduce thermally induced stress (although this is not always the case) [59].

As an example, the embossing temperatures chosen for PMMA (with $T_g \sim 105$°C) range from 120°C [62] to ~200°C, when embossing features with sizes up to 100 μm into a polymer of about 300,000 g/mol molecular weight [57]. A high embossing temperature is sometimes necessary for complete filling to occur. However, when the embossing temperature is increased above a certain limit, the embossed material can become brittle [44]. The de-embossing temperature, in general, varies from 15°C below T_g [59] to room temperature.

2.3.4.4 Time

The hold time is a function of both material temperature and forming force [43]. It is difficult to predict the exact time needed for the embossing process to be complete. Real time observation is useful [46], and can be realized using transparent molds. Embossing time can also be optimized using experimental trials or by using a suitable model.

A simple 2D squeeze flow theory can be used to determine the time required to fill a cavity in the stamp [43, 46]. This is done by calculating the time required to displace a given amount of polymer of height $h(t)$ with a stamp of width S. The effective stamp width was discussed earlier in Section 2.4.4.1, and as was shown in Figure 2.13 only half that stamp width displaces the polymer into the cavity, while the other half displaces the polymer to the borders. Taking all this into consideration, and assuming that the liquid is

purely viscous, the polymer melt is incompressible, and that $S >> h(t)$, the fill time can be given as:

$$t_f = \frac{\eta_0 S^2}{2p}\left(\frac{1}{h_f^2} - \frac{1}{h_0^2}\right), \tag{2.3}$$

where h_0 is the initial height of polymer, h_f is the final height of the polymer, n_0 is the polymer viscosity and p is the embossing pressure. The final height of the polymer after the cavity has been filled is given by:

$$h_f = h_0 - WD/S, \tag{2.4}$$

where W and D are the width and depth of the cavity, as is shown in Figure 2.14.

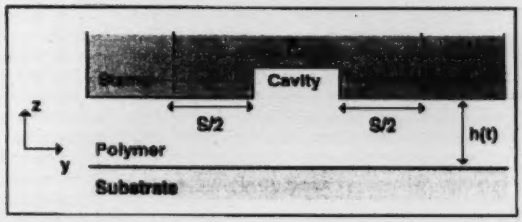

Figure 2.14: Two-dimensional model for determining time required to fill a cavity [46]

From the above formula we can see that in order to decrease time, the polymer viscosity should be decreased (by increasing the temperature) and the embossing pressure increased. Also, increasing the film thickness or decreasing the ratio of cavity volume to stamp width will reduce the time to fill a cavity [46, 63]. The time needed to emboss a pattern could range from a few minutes to a few hours.

2.3.4.5 Vacuum

From various studies [43, 46, 56], it was found that embossing is more uniform and exhibits fewer defects if performed in vacuum. This was found to be dependent on the molecular weight of the material, where materials with lower molecular weight being more sensitive to entrapped air [43, 56]. Embossing in vacuum was not necessary in many applications [46], but crucial in others [56].

When using polymers with low molecular weight, it is beneficial if contact is facilitated by the evacuation of the space between the stamp and the polymer layer. This ensures that no air is trapped between the two layers, thus enhancing the large area uniformity of the imprint [41, 56, 61]. It is found that high-temperature induced defects (such as those caused by overheating trapped air) are also substantially reduced under vacuum [56].

It has been reported that if the embossing pressure is applied rapidly or the embossing pressure is released before cooling features known as viscous fingerings are formed. Viscous fingering is a phenomenon that occurs due to overheating of compressed gas (trapped during hot embossing) leading to the formation of finger-like patterns.

Some examples are shown in Figure 2.15, were the spot in the middle is the location of air at high pressure before expansion [60]. This effect can substantially be reduced if a vacuum is used.

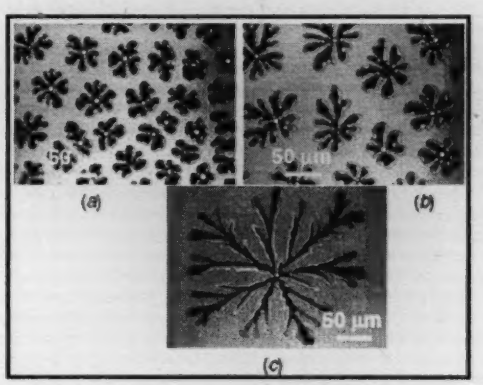

Figure 2.15: Viscous Fingering [60]

When dealing with a new material, several trials could be run to determine the importance of vacuum in embossing such material. It is important to note, however, that earlier investigations revealed an increased mechanical stress on the stamp and sample when performing a hot embossing experiment under vacuum condition, which often causes damage to one or both of the wafers. A possible cause of this phenomenon is a vertical temperature gradient, resulting in an abrupt thermal expansion when the wafers are brought into contact. In combination with the external force hindering free movement, the thermal expansion mismatch in many cases led to damage to one or both of the wafers

through mechanical stress. In this case, a process flow can be devised to overcome this limitation [56].

2.3.4.6 Anti-stick layer

Adhesion between the mold mask and the polymer layer is frequently observed. This causes damage to the mold and subsequent replications suffer degradation, as seen in Figure 2.16. To avoid the sticking problem between the mold and the polymer, an anti-sticking layer (ASL) can be used to reduce the polymer's adhesion to the mold [41, 62]. The use of an anti-stick coating allows the mold to be used repeatedly without loss in quality.

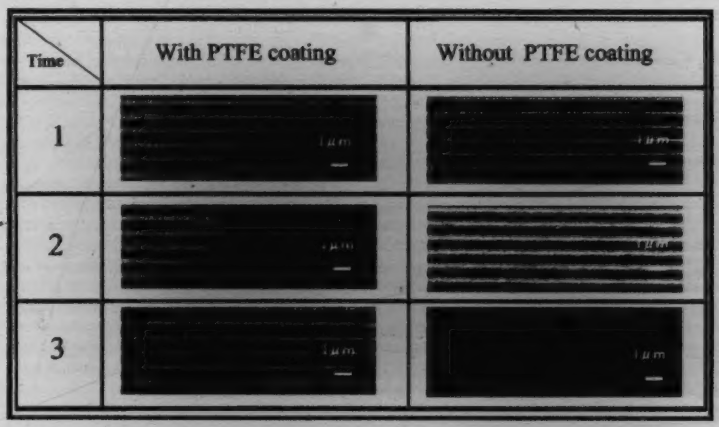

Figure 2.16: Patterns imprinted with and without an ASL [62]

In some applications, such as in the fabrication of biochemical or biomedical devices, a mold release agent is not desirable since it might lead to contamination of the fabricated device [59].

Several anti-adhesion layers have been reported and used in different applications. One widely used ASL is *1H, 1H, 2H, 2H-perfluorooctyl-trichlorosilane, or F6, (Fluorochem, Ltd.)*, typically employed on silicon molds. Evaporation of F6 onto Si results in a self-assembled monolayer on the mold surface [55-57, 59], which prevents sticking between the mold and the embossed polymer material during the hot embossing process. Stamps

coated with F6 could be separated from the polymer using only weak forces. F6 was also found to be superior to other ASL for embossing of nanometer-scale features.

Synthetic grease Mobil-1® was also used as an ASL in some experiments [44]. The ASL was applied to the material to be embossed. After the embossing process, however, big portions of grease were found and had to be removed using absorbent paper. A suitable solvent (Castrol Super Clean®) and a toothbrush were used for degreasing. Then, the material was rinsed with water and inspected until it looked completely degreased. Finally, the excess water was removed using air pressure and an air heater was used to dry the wafer [44].

An alternative to the above methods is the development of a *Teflon-like ASL* from the gas phase, usually done by sputtering or plasma deposition. Teflon-like ASL can be deposited on any stamp material. However, it was found that this layer suffered from mechanical wear, and some of the ASL was transferred to the imprinted surface. In some cases however, the wear was found desirable since it facilitated separation of the stamp and sample [54, 55].

Other *Fluorinated alkylsilanes* [55], as well as other chemicals such as *Octadecyltrichlorosilane* (OTS) [57], have also been successfully used with Si and SiO_2 molds.

2.3.5 Process Flow

In a hot embossing process, it is important to select an appropriate temperature and pressure profile to ensure complete feature formation. Figure 2.17 shows different possible stages of heating, cooling, and pressure application [59]. These stages can be varied in an effort to devise the most suitable embossing conditions.

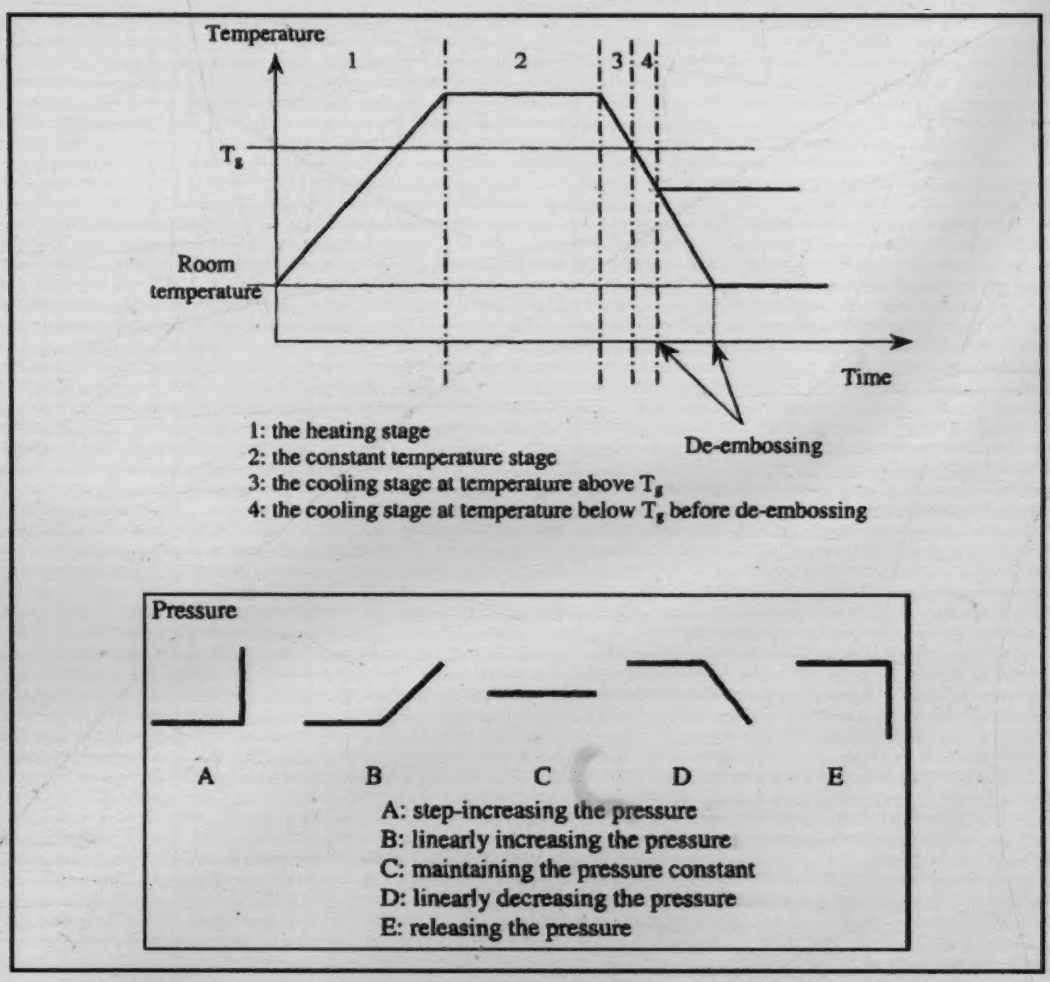

Figure 2.17: Different temperature and pressure stages [59]

One of the major goals with embossing is to increase the throughput as much as possible (by reducing overall processing time). However, the required temperature determines the processing time, and the higher the process temperature, the longer the overall processing time [61]. The glass transition temperature (T_g) and molecular weight (M_w) of the polymer are the key parameters that determines a suitable processing temperature. In order to ease this processing temperature restriction, the embossing system can be held at an elevated temperature (T_e) below T_g during loading and unloading, so that effective heating and cooling times in between T_e and the processing temperature (T_p) are minimized (see Figure 2.18).

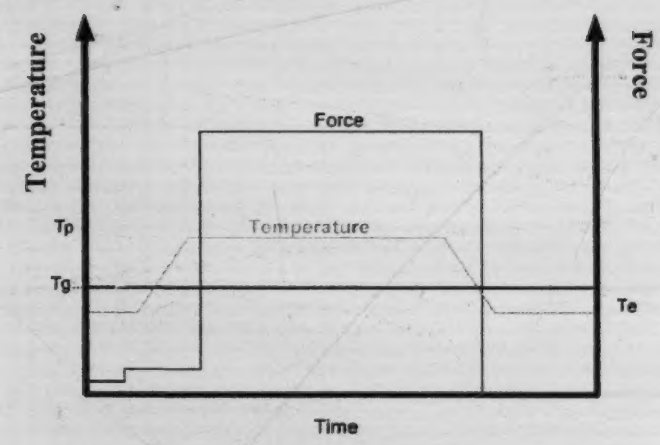

Figure 2.18: Typical Embossing process flow diagram [61]

Because of the interrelated process variables (time, temperature, pressure, etc.), it is often a challenge to decide between different embossing conditions. This can be done experimentally using several trial experiments. Figure 2.19 shows different embossing results on mr-I 8030 polymer along with the different embossing parameters used to produce them [57]. The top and bottom heating chucks were heated to their respective temperatures T_{top} and T_{bot} typically within 15 minutes. Temperatures used were between 110°C and 225°C for the top chuck and between 200°C and 225°C for the bottom chuck. When both chucks had reached their set points they were brought into contact and pressure was applied. Forces between 7 kN and 40 kN were used corresponding to external pressures from 1 MPa to 5.5 MPa when considering a circular contact area of 4 inch diameter. After a holding time between 5 and 15 minutes, cool down was initiated. The pressure was sustained until the temperature of both chucks fell below T_g of the polymer [57].

Samples a-d were initially 390 nm thick, while sample e was 445 nm thick. It can be seen that case (b) provided the best result for samples with 390 nm polymer layers. Case (e) produced the best imprint of the whole series. However, that might be because flow properties in thicker layers are more favorable.

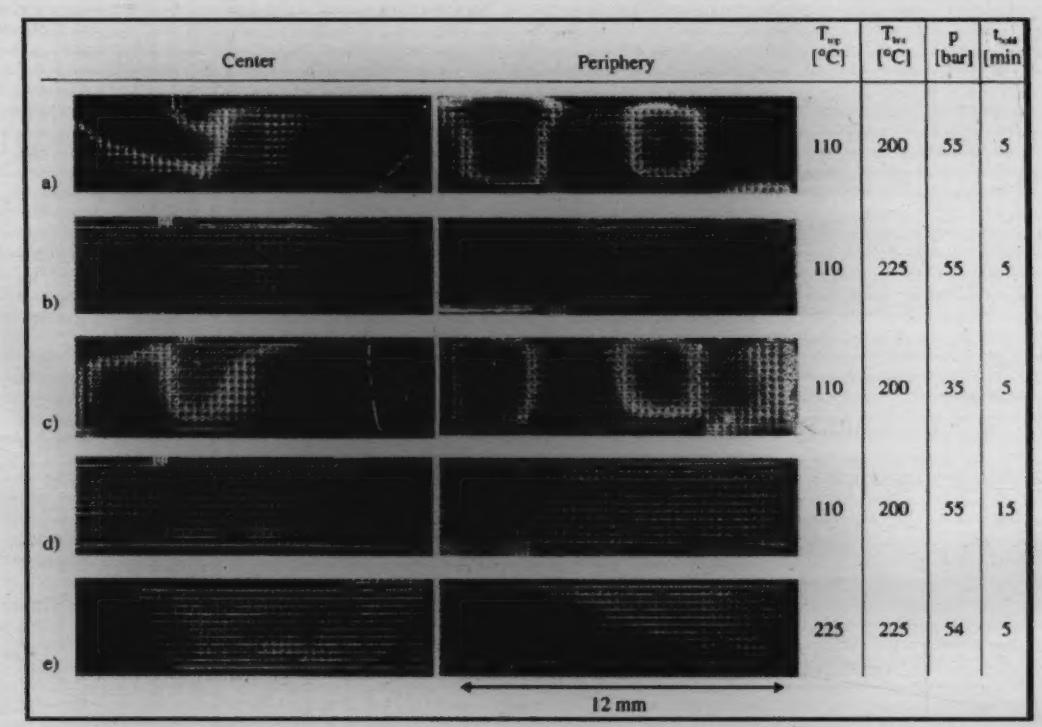

Figure 2.19: Microscope images of embossing trials on mr-I 8030 with parameters used to produce them [57]

Another example of trials performed to determine the most suitable embossing conditions is shown in Table 2.2. The first step was to find the temperature required for the polymer to completely fill the stamp cavities in a time of 2 min (Trial 1-3). Note, the PMMA polymer with a molecular weight of 350,000 g/mol required a temperature of 290°C. In Trial 4, the temperature for case 3 was reduced to 270°C, which resulted in complete fill occurring in 10 min. Additional results were obtained using lower temperature, increased pressure, and a thicker film, as shown in Trials 5 – 8 [46].

Table 2.2: Experimental conditions required to fill a 20 μm square cavity with PMMA samples with different molecular weights [46]

Trial no.	Mol. wt. M_w (kg/mol)	PMMA thickness (nm)	Force (kN)	Cavity depth (nm)	Temp. (°C)	Zero shear viscosity (Pa s)	Time of embossing (min)	Cooling time (min)
1	25	200	15	175	230	363	2	12.0
2	75	200	15	175	250	2648	2	12.5
3	350	200	15	175	290	–	2	14.0
4	350	200	15	175	270	–	10	14.5
5	25	100	15	70	200	3244	10	12.0
6	75	100	15	70	230	7915	10	13.5
7	75	385	15	70	200	70 717	2	12.0
8	350	100	30	70	250	–	10	12.5

Several variations to hot embossing exist and have been reported. For example, some papers reported applying the stamp to a spin-coated uncured polymer layer, which is then cured with the stamp in place (by UV exposure or heating). This is essentially a form of RT-NIL. For conventional embossing, the resist has to be heated above its T_g which can cause problems in pattern accuracy (due to thermal expansion mismatches, etc.). RT-NIL was thus proposed to overcome this problem [62]. The RT-NIL process is also faster, since no heating and cooling is required [53].

Another variation is where the mold separation is performed at the process temperature (above T_g). In some cases, it was found that the imprint quality was not affected [61]. This may be due to the fact that, without pressure applied, the driving force for deformation of the imprinted pattern is gravity only. Furthermore, since removal of the imprint from the system and from the bottom chuck takes no longer than half a minute, the time the polymer remains at elevated temperature is too short for significant flow [61].

2.3.6 Challenges

2.3.6.1 Thermal Expansion Mismatch

Several challenges arise when developing an embossing process. One of the most common challenges is the difference in the thermal expansion coefficient between the stamp and the polymer material. This effect leads to structural distortion and cracks in many cases [54]. To avoid this problem, it is beneficial to choose a mold whose TEC is matched to that of the polymer. If the mold and polymer possessed varying TEC then it is useful to separate the mold and the polymer sample at a high temperature in order to avoid shearing of the embossed features during cool down [55], shown in Figure 2.20.

Figure 2.20: SEM of polymer shearing during cool down due to difference in TEC [55]

Other proposed solutions include making the thermal cycle as small as possible (~30°C) [50], or moving towards RT-NIL [53] (discussed earlier). An important factor that is yet to be fully studied is the effect of this thermal expansion mismatch on resolution [41].

2.3.6.2 Alignment between multiple layers

Alignment is a major issue when dealing with multilayer embossing processes, and one of the challenges is the realization of a fully automated process. Methods developed for conventional lithography can be used, and an accuracy better then 1 μm is achievable without major effort (using optical alignment marks). In the case of a non-transparent

stamp, alignment marks can be placed at the backside, or several other techniques can be used [61].

2.3.6.3 Uniformity over large areas

Some important issues that are yet to be studied in detail are the uniformity over a large area and the variation in the patterns produced. To test for uniformity, in one experiment [64] arrays with 30 nm wide strips and a 150 nm pitch were fabricated at the four corners and the center of a mold that had a size of 15 mm by 18 mm (as shown in Figure 2.21). After embossing, a lift-off process left 30 nm wide metal lines with a 150 nm pitch on the substrate. The structures were found to be uniform over a significantly large area. It is expected that good uniformity over a much larger imprint area can be achieved [64], although further studies must be done in order to ensure proper uniformity.

In another study [42], to test for the variation in the patterns produced, several test wafers were embossed using the same mold. It was found that standard deviations of widths at the 3-4 μm scale were on the order of 0.5 μm leading to a coefficient of variation as high as 13 %. Thus it is important (before the transition from testing to manufacturing) to fully understand the causes of this variation and devise control methods to minimize its magnitude over all parts. Presently, the cause behind these variations is not clear, but could be different for different cases. Some of the possible causes include: the variability in different embossing cycles inherent to the embossing machine, variability in the polymer used for embossing, and the variations in the environment (temperature, humidity, etc.) [42].

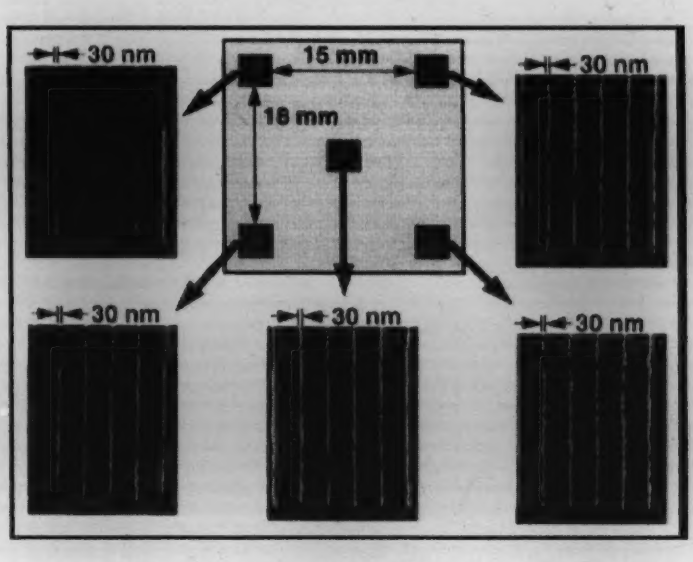

Figure 2.21: Uniformity test involving the comparison of SEM images of similar features embossed at different locations [64].

2.3.6.4 Other Challenges

Distortion or damaging of the mold during de-embossing can occur as a result of different effects such as adhesion at the surface, friction due to surface roughness and trapping of the polymer due to negative slopes of cavity sidewalls [46]. For separation, it is important to note that, when using a hard stamp, vertical separation is required in order to avoid excess strain. Separation forces are reduced for stamps with low surface roughness, high quality anti-sticking layers, and for 'non-sticky' polymers [61].

A separation challenge is also encountered when separating the polymer from a mold with curved structures (such as a ring resonator). It was found that the polymer could easily be torn apart from the substrate at the curve [17]. To avoid this problem, the surface of the mold and polymer should be kept parallel during separation. It is also beneficial to use polymers that posses tough mechanical properties [17].

Mold and polymer interlocking is another challenge that frequently arises. Figure 2.22 shows a burr located on the sidewall of the stamp grooves (see arrows), which interlocks the polymer during demolding. This has little effect on large polymer structures (greater than 1 μm wide), but as the features on the stamp become smaller, the polymer can undergo a plastic deformation as the stamp is removed. The stretching is significant at

linewidth below 300 nm, and might cause the polymer structure to break. In some cases, this stretching effect might be useful since it can enhance the aspect ratio of nanostructures. It can assist also in processes such as lift-off, and providing narrow gaps for electronic applications [46].

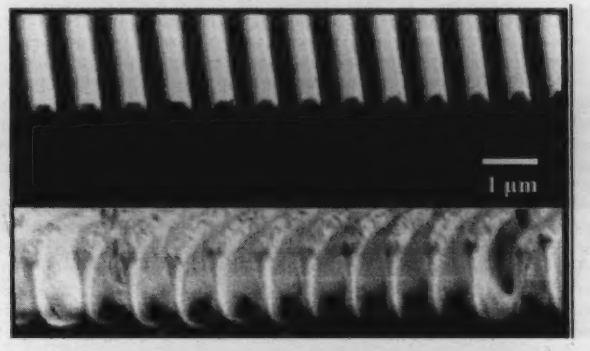

Figure 2.22: Stamp and the embossed polymer structure after being stretched during demolding [46].

Some other challenges that can occur (and should be avoided) during hot embossing are: the occurrence of viscous fingering (discussed in Section 2.4.4.5 and shown in Figure 2.23), and dewetting (shown in Figure 2.24). Dewetting is a case of thin film breakage, where holes form in the polymer film during hot embossing. The cause behind this breakage is not fully understood, but it seems to occur when the pressure is unevenly distributed over the substrate. In order to avoid these two effects, the polymer should be sufficiently cooled before demolding to avoid the formation of viscous fingering patterns, or the embossing process should be done under vacuum. Care should also be taken to ensure a uniform distribution of the embossing pressure to avoid the dewetting behavior of the polymer [60]. Also, the embossing time must be long enough to achieve a complete fill of the master cavities [60].

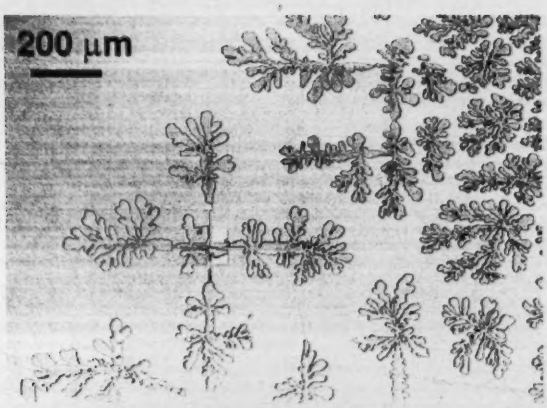

Figure 2.23: Viscous fingering around structured regions [60]

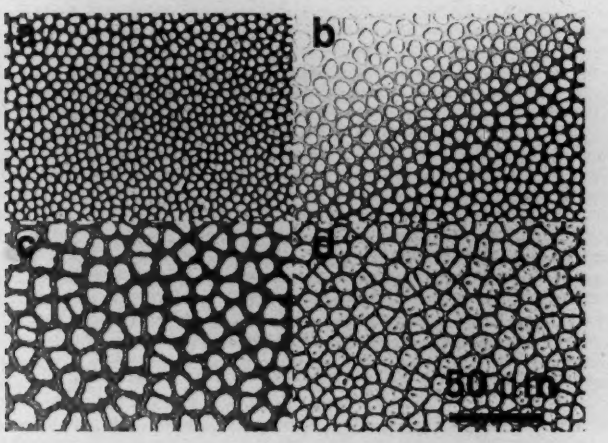

Figure 2.24: Different stages of dewetting [60]

Finally, other factors that must be carefully considered are the stamp durability, surface sticking, and choice of the proper molding conditions. A better understanding of the embossing process will surely result in solving many of the challenges discussed above [41].

2.3.7 Commercial Embossers

Several embossing machines are commercially available. For most machines, the typical parameters that are under operator control include force trajectory, velocity trajectory, temperature, hold time, and the cooling rate [43]. The key parameters determining good quality imprints are the uniformity of contact force, temperature uniformity, and a fully automated de-embossing process [61]. The two most commonly used embossing machines are the EVG520HE (EV Group, Austria) [56, 57, 61], followed by the HEX Series embossing machine (Jenoptik Microtechnik, Jena, Germany) [47], see Figure 2.25.

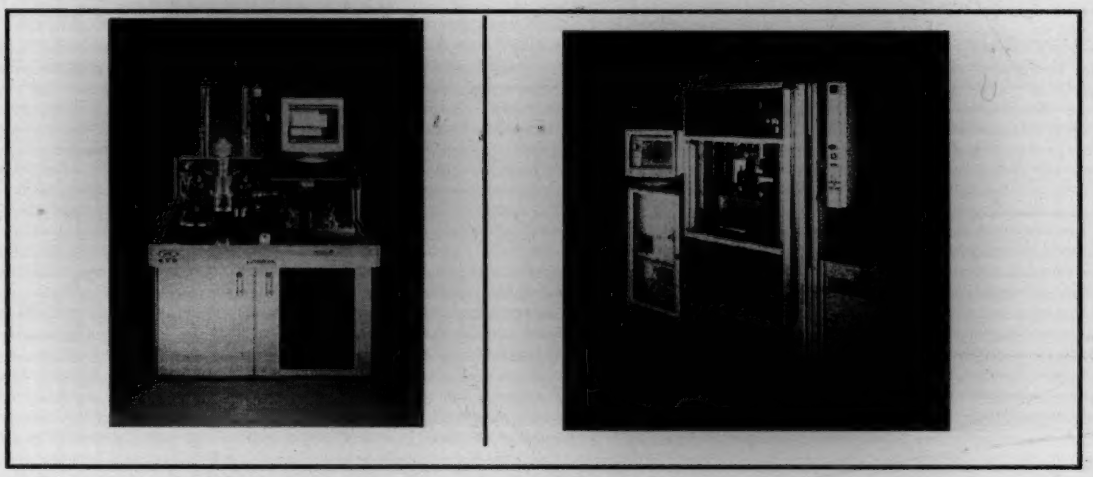

Figure 2.25: EVG520HE (left) [61], and HEX03 (right) [47]

The EVG520HE has several attractive characteristics:

- Capable of hot embossing substrates of up to 150 mm (~6 inch) in diameter.
- Suitable for imprinting features from sub-100 nm up to μm range.
- Supports computer controlled process flow.
- An upper temperature limit of 550°C, which covers the whole range of polymers that are suitable for hot embossing.
- Evacuation of the chamber to a pressure of 10^{-3} mbar (0.1 Pa, 0.00075 Torr), and pressurization up to 2 bar (200,000 Pa, 1500 Torr) is feasible. The overpressure fills the chamber with an inert gas (argon or nitrogen) to avoid oxidation of the polymer at the elevated temperature.
- For automatic de-embossing, the system features vacuum chucks that fix the sample to the bottom tool, and the stamp to the top one.
- Independent top and bottom heating, which helps to minimize thermal stress between stamp and substrate.
- A contact force of up to 40-kN.

- A maximum pressure of 55 bar (5.5 MPa) for a circular area of 4inch diameter.
- An integrated compliant layer that guarantees good uniformity of pressure and temperature within +/- 1%.

A typical experimental setup is shown below [56]:

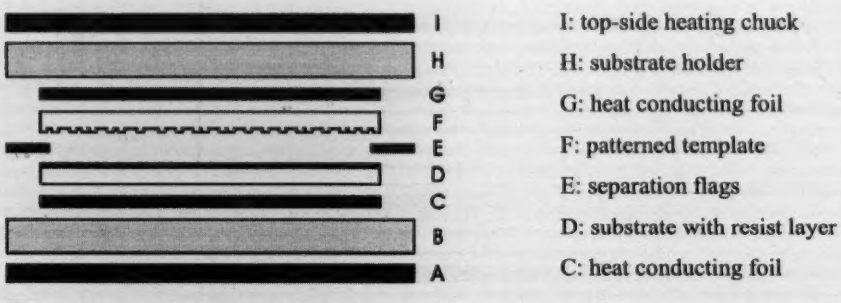

Figure 2.26: Setup of the stack to be loaded into the EV520HE [56]

The HEX embosser has also several attractive characteristics, but the most interesting one is that it allows more precise alignment between layers. The alignment unit allows a multitude of possibilities such as double-sided replication with two molding tools, or the possibility to mold on top of a pre-structured substrate [47].

2.3.8 Designing an Embossing System

Although commercial embossing machines are available, a home-made embossing machine has certain advantages. Aside from the lower cost, a home-built system can allow better understanding of process dynamics, flexibility in designing its control system, and the possibility to meet requirements that might not be met by any commercially available embossing system [42].

Before designing an embossing machine, it is important to understand the challenges (section 2.3.6) and the features that are already present in commercial systems (section 2.3.7). Things like lateral movement during demolding, position control, and uniform pressure must all be considered.

2.3.8.1 Home-made Embossing Systems

Several embossing systems that were either developed or modified are discussed below. The first example is shown in Figure 2.27 and Figure 2.28, where a compact imprint system was designed. The system is 17 cm in width and 30 cm in height, and has a 10 mm x 10 mm mold-mask holder and a 5 cm (2 in.) wafer stage. The z-positioning accuracy using a stepping motor was 2 μm. A heater is buried in the wafer stage to heat resist coated on a wafer to above the T_g. A 5 cm wafer could be imprinted by an x – y step and repeat stage. All stepping stages were connected to stepping motors controlled by signals from a computer. A piezoelectric component was used [53, 62] to measure the pressure.

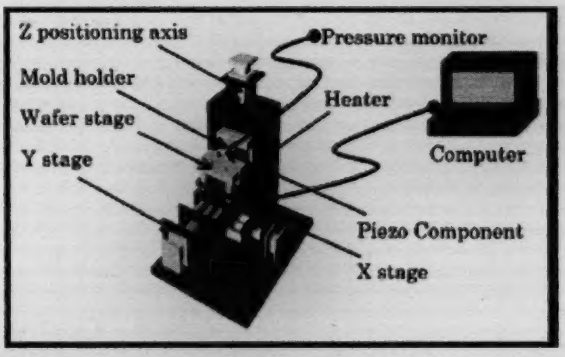

Figure 2.27: Schematic diagram of compact imprint system [62]

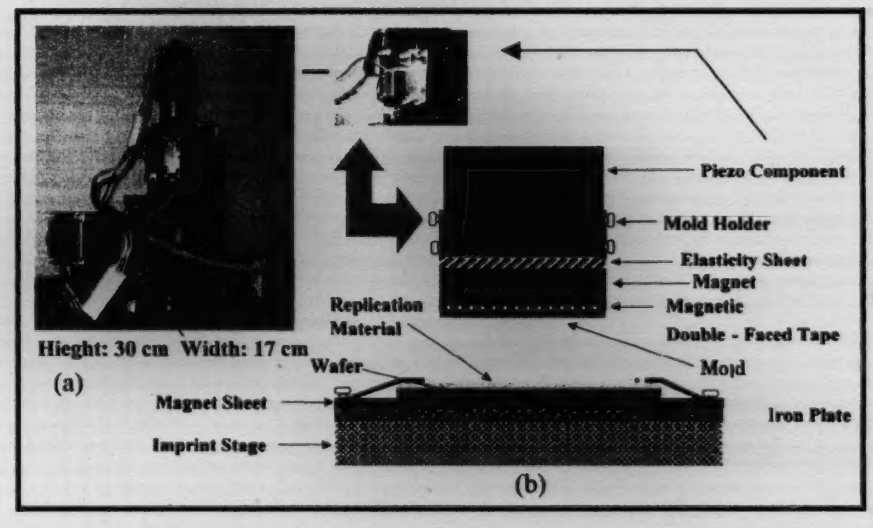

Figure 2.28: Close-up of the compact imprint system [53]

A schematic of another embossing machine is shown in Figure 2.29. The machine was composed from the following parts:

- A: An adjustable auto-alignment single ball bearing, used to compensate for misalignment between the die (D) and receiver (E).
- B and C: Fixtures used to apply force to the die.
- D: Die, connected to components B and C through four bolts and fastened using standard nuts and washers.
- E: Receiver: a flat plate (28.7 cm x 28.7 cm x 25 cm), made from ASTM 1020 Cold Rolled Carbon Steel.

This setup was able to apply a uniform pressure of 1.72 MPa acting over an area of 625 cm^2 (25 cm x 25 cm) [44].

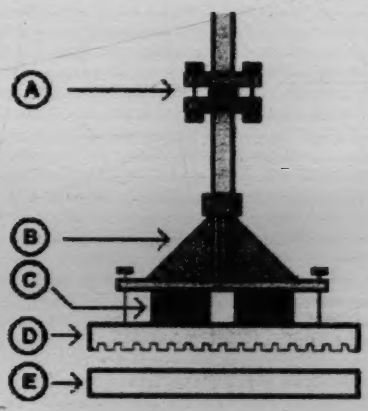

Figure 2.29: Schematic of hot embossing equipment [44]

Figure 2.30 shows a lab set-up for an embosser developed at Massachusetts Institute of Technology (MIT) [42, 43]. This setup included heated platens, tool and workpiece holders, and a single axis actuator for applying a well controlled forming force. To apply the embossing force a commercial material testing machine (Instron Model 5869) was chosen. This machine is described in greater detail in Section 2.4.8.4.

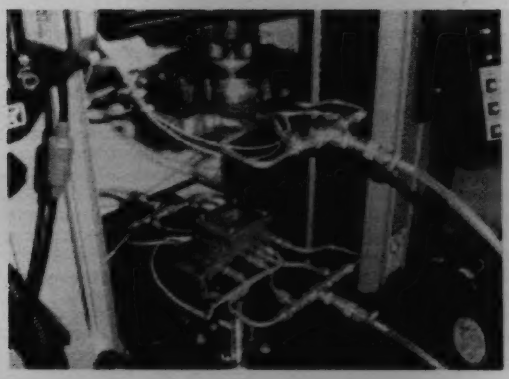

Figure 2.30: Lab-scale embossing setup at MIT [43]

Finally, an embossing machine constructed around a force frame is shown in Figure 2.31. The force frame delivers the embossing force via a spindle and a T-bar. The embossing tool and the planar polymer substrate are mounted on heating plates, which contain also cooling channels. In these channels, high heat capacity oil is circulated in the cooling phase, which allows active cooling with cooling times equivalent to heating times at about 1 minute between upper and lower cycle temperatures. This configuration allows an isothermal heating and cooling of both tool and substrate [50].

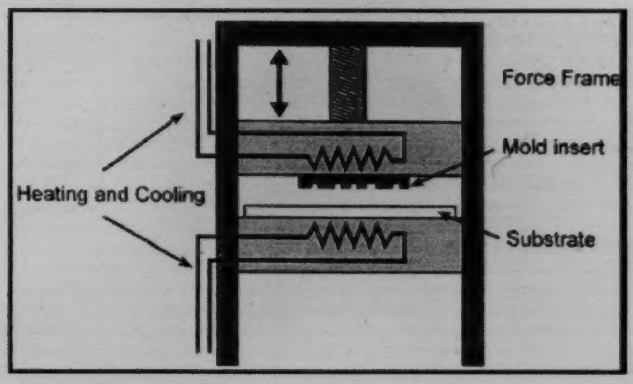

Figure 2.31: Embossing machine with force frame [50]

The typical parts of a general embossing system are shown in Figure 2.32. The next sub-sections will discuss parts that can be used for heating, cooling, applying pressure, etc.

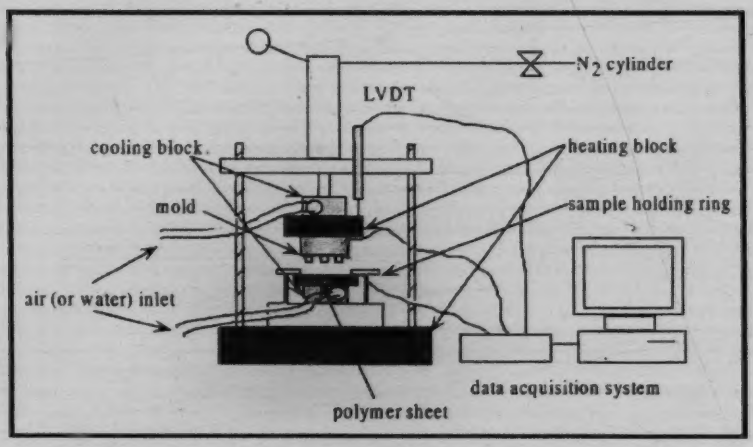

Figure 2.32: Typical blocks needed in an embossing machine [59]

2.3.8.2 Heating

Several methods have been used to heat the mold and polymer during embossing. Perhaps the simplest method is to place the entire assembly into an oven [44]. Other heating methods include using cartridge heaters, with the tips placed ~ 2 mm from the mold surface [59], or using heating platens [42]. In some other cases the heater was buried in the wafer stage [53]. Using platens has become very attractive since it helps hold and maintain the orientation of the work piece and the tool, supply and evenly distribute heat, as well as cools the work piece and the tool. A copper lower platen is shown in Figure 2.33. For measuring the temperature, a digital thermometer [53, 62] or a thermal couple can be used [48].

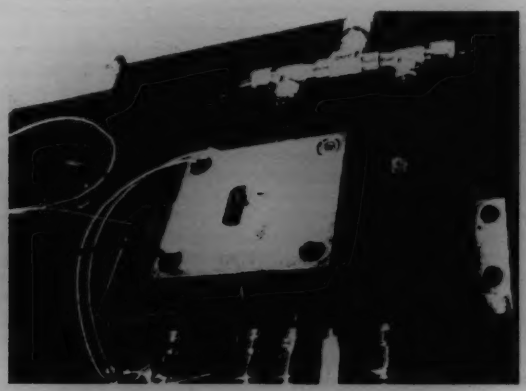

Figure 2.33: A copper lower platen [42]

2.3.8.3 Cooling

Several cooling methods have been used, including cooling water [44, 59], natural air cooling [44, 48, 59], or the platens described above [42]. The platens were capable of cooling a setup from 150°C to 50°C in 5 minutes.

2.3.8.4 Force

Various techniques have been used for applying the force between the mold and the polymer. A pneumatic cylinder pump, used in one setup, provided a constant compression force during embossing [59]. Other methods used include a commercial hydraulic press [62] or a stepping motor [62]. The stepping motor offers the advantage of making the system smaller in size, and lowering the cost compared to the setup with the hydraulic press. In the setup shown in Figure 2.31, a force frame delivered an embossing force via a spindle and a T-bar [50]. The embosser system developed by MIT used an Instron 5869, which is a table-mounted materials-testing system with a maximum applied force of 50 kN. It has a test speed range of 1 μm/min to 500 mm/min with a 50 kN load cell. It can deliver a load accuracy of +/- 0.4 N and position control accuracy of 0.063 μm. The 5869 also provides a closed loop control of force or displacements of the platens with control algorithms written in LabView allowing the flexibility of programming specific trajectories [42].

To measure the applied pressure, piezo-components can be placed in the z-axis of the mold holder. By connecting a pressure monitor to the piezo-element, the pressure can be measured [53, 62].

2.3.8.5 Holding the stamp and substrate in place

In order to hold the wafer in place, many methods such as using clamps or vacuum chucks (such as the ones used in the EVG520HE) can be used to hold the mold and wafer in place. When using metal molds, an alternative method is to use magnets. A magnet is inserted between the mold holder and the mold mask (similar to Figure 2.28). Similarly, a magnetic sheet and an iron plate are inserted between an imprint stage and the wafer.

This can also assist in making a parallel and hard contact between mold mask and the wafer [53].

2.3.8.6 Control

System control is one of the most important things to consider when designing an embossing system. Control is usually a feedback-oriented problem. The various loops that can be controlled are shown in Figure 2.34 [43]. Experimental parameters (position, temperature, force, etc.) can be recorded by using a data acquisition system. For example, a linear variable differential transformer (LVDT) can be mounted on the top plate to monitor the displacement of the mold during embossing [59]. Three stepping motors, controlled by pulses from a computer, control the x-axis, y-axis, and z-axis wafer stages [53].

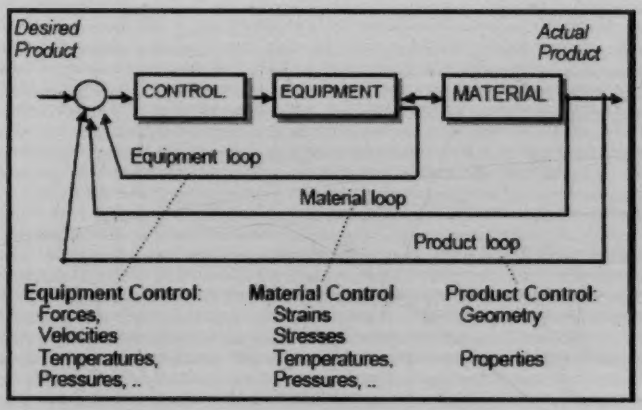

Figure 2.34: Different embossing control blocks [43]

2.3.8.7 Characterization and Quality Assessment

Many methods are currently being used to assess the quality of the structures produced. These methods can be divided into two categories: the first is based on examining defects and other structural changes, and the second is based on comparing features sizes.

Roos created a set of quality criteria that allows the study of the effect of experimental changes [43, 56]. This work establishes a measurable set of attributes that can be used for statistical studies, by looking at the following:

- *Width of the flow borders* (in μm): this refers to the range of lateral polymer transport.
- *LISA-like defects* (self assembled trenches at the surface): these are self-assembled structures forming when only a small gap exists between polymer surface and the stamps. They are usually trenches that go down to the wafer surface as shown in Figure 2.35.
- *Viscous fingering* (% of features present): this refers to defects that are assumed to result from overheated compressed gas.
- *Visual uniformity* (e.g., % degree of filling): this refers to the overall visual impression of the imprint. It combines the evenness of the color of the sample and the overall homogeneity.

These parameters are illustrated in Figure 2.35 [56].

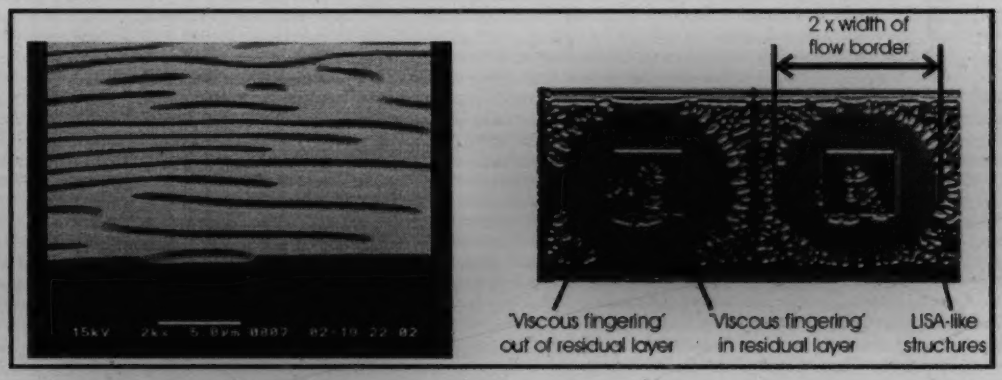
2 x width of flow border
'Viscous fingering' out of residual layer
'Viscous fingering' in residual layer
LISA-like structures

Figure 2.35: LISA-like defects (left), micrograph of flow borders and 3 different types of defects (right) [56]

Defects can be divided into the following categories:

- Defects that are not usually related to the embossing process e.g. inclusion of particles.
- Defects that will lead to holes in the embossed material where it should remain intact and which are therefore 'critical'.
- Defects in the residual layer to be removed after embossing. They are regarded non-critical.
- Viscous fingering; these are non critical as long as they occur only in the residual layer.
- LISA-like defects that always go down to the substrate surface and occur only in regions that must remain intact.

Table 2.3 below shows how these attributes can be used to characterize the embossing process [56]. Table 2.4 shows an example where this technique was used to compare the effect of vacuum on materials with different molecular weights.

Table 2.3: Classification of the different defect classes [56]

Attribute \ class	0	+	++	+++
width of flow borders	<< 50 µm	< 50 µm	< 100 µm	complete filling
area of LISA-like critical defects	100 % of unfilled recessed regions	> 50 % of unfilled recessed regions	< 50 % of unfilled recessed regions	none
'viscous fingering'	in > 10 % of pads	in 5 – 10 % of pads	in < 5 % of pads	none
visual uniformity	non-uniformity > 20 % of wafer area	non-uniformity < 20 % of wafer area	non-uniformity < 10 % of wafer area	no discernable inhomogeneities across the wafer area

Table 2.4: Quality assessment of structures with different molecular weight produced with and without vacuum [56]

Polymer	Imprint recipe	Category	Results based on Table 2.3 classifications	Characteristic micrograph
mr-I 8000 99 kg/mol	no vacuum	flow borders	++	
		LISA-like defects	0	
		'viscous fingering'	0	
		visual uniformity	0	
mr-I 8000 99 kg/mol	vacuum	flow borders	+++	
		LISA-like defects	+++	
		'viscous fingering'	+++	
		visual uniformity	+	
mr-I 8000 350 kg/mol	no vacuum	flow borders	+	
		LISA-like defects	0	
		'viscous fingering'	+	
		visual uniformity	++	
mr-I 8000 350 kg/mol	vacuum	flow borders	+	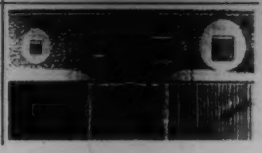
		LISA-like defects	0	
		'viscous fingering'	++	
		visual uniformity	+++	

The second category of methods by which quality can be assessed involves using different measurement techniques to compare the quality of structures produced. For example, microring resonators were used to evaluate the quality of the replication, because of their sensitivity to small fabrication errors [12, 13]. In other cases, SEM [23, 55], AFM [46, 49], and confocal laser microscopes [55] were used to characterize and compare devices and feature sizes. These measurement techniques have been use to measure dimensions of different structures and compare them in order to evaluate the quality and repeatability of the process [42, 65].

Chapter 3 Results for etched PAI waveguides

This chapter describes previous work done by this group on waveguide fabrication using Torlon PAI [38], and builds on that work. Further characterization of the high index contrast, etched polymer waveguides from [38] was conducted, and those results are presented.

A polyamide-imide (PAI) polymer, Torlon AI-10 (from Solvay Advanced Polymers) was used as the core material to fabricate buried channel waveguides, with a commercial benzocyclobutene (BCB) polymer (Cyclotene 3022-63, Dow Chemical) being used as the cladding material. These polymers are stable up to very high temperatures (> 300°C), exhibit good mutual adhesion and chemical compatibility, and provide a refractive index offset greater than 0.1. Single and multimode waveguides were fabricated by photolithography and reactive ion etching, and propagation losses were measured. The losses are reported, and the sources of these losses are studied along with techniques by which these losses can be reduced.

3.1 PAI Waveguide Fabrication

Before the fabrication of PAI waveguides, the silicon substrate was cleaned in a piranha solution (with a 2:1 sulphuric acid to hydrogen peroxide ratio). The wafer was then rinsed with water and dried.

A commercial polymer, benzocyclobutene (BCB) (Cyclotene 3022-63, Dow Chemical), was used as an undercladding material in this study. BCB has shown chemical, thermal, and mechanical compatibility with PAI, and has a low moisture uptake [18] which makes it very suitable for use as a cladding and encapsulating material. One very important attribute of BCB as a cladding material is its good adhesion to PAI, especially upon cleaving. Finally, the coefficients of thermal expansion (CTE) of the two polymers are reasonably well matched, which helps to avoid film cracking during heating and cooling cycles. The CTE of PAI and BCB are 30×10^{-6} and 52×10^{-6} C^{-1}, respectively [66].

An adhesion promoter (AP3000, Dow Chemical) was spun on the cleaned silicon wafer, and then a BCB undercladding layer was spun coated to a thickness of about 10 μm.

Wafers were then baked at 250°C for 1 hour in an oven under nitrogen environment, and left to cool.

Torlon PAI solution was prepared by dissolving the PAI powder in a standard solvent [67]. The PAI powder to solvent ratio is a very important factor in determining the thickness of the polymer film. In the past, relatively thick films were spun when using N,N-dimethyl formamide (DMF) as a solvent [32], but for films on the order of 1 μm thick or less, the best and most consistent results are obtained using Dimethyl-acetamide (DMAC) as a solvent. Typically, 25 g of PAI powder is dissolved in 100 ml of DMAC by stirring for 2 hours. Residual particulates are then removed by passing the solution through a double layer of a 1-micron filter (VWR Grade 410, 1 μm particle retention). After the solution has been filtered, it is spun onto the BCB layer. Along with the solution ratio, the spin speed plays an important role in determining the final thickness of the PAI film. While high quality films as thin as 280 nm have been realized, this work concentrates on films that are about 1 μm thick, suitable for the fabrication of channel waveguides. Spinning at a speed of 2500 rpm gave a thickness of around 1.5 μm. Immediately after spinning, PAI films are soft-cured for 3-5 minutes at a temperature between 70-90°C on an open-air hot plate. They are subsequently fully cured in a vacuum oven at temperatures up to 325°C, under nitrogen. This step helps the PAI film achieve its desired properties, and drives out any solvent or micro-voids that might remain in the film. Figure 3.1 shows an SEM image of a PAI film, processed in the manner described above. Good adhesion between the PAI and BCB layers can be seen in the SEM, and good quality cleaved facets are typical for this material combination.

Figure 3.1: SEM of PAI film on BCB cured at 325°C in N_2 environment

The cure schedule was varied in an effort to optimize PAI film properties. This was done by measuring the film stress, refractive index, and thickness at different curing temperatures; results are shown in Figure 3.2[1]. In these experiments, the wafer was cured in air to a certain temperature for 4 hours and then the stress, birefringence, and thickness were measured. After obtaining the needed measurements, the same sample was cured further. Thus, these measurements represent the residual values of stress and birefringence after multiple steps.

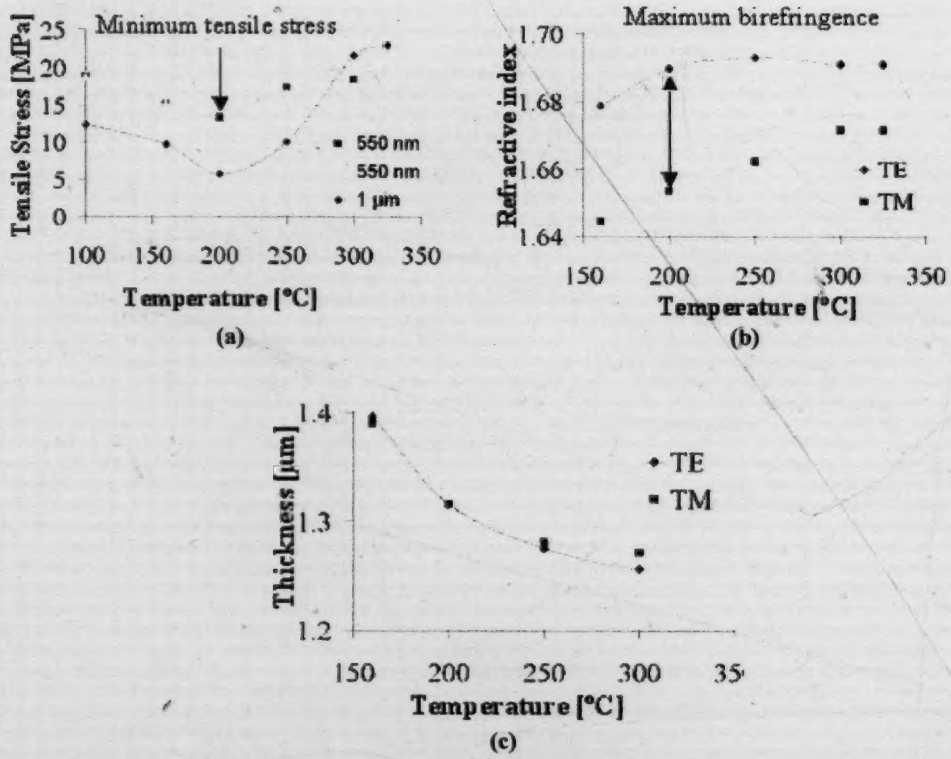

Figure 3.2: Variation of Tensile Stress, Birefringence, and Thickness of PAI film with curing temperatures

Minimizing the film stress is very important for the fabrication of various waveguide devices. Polymer shrinkage, unmatched thermal expansion coefficient, and molecular ordering can all contribute to high stress values [15, 31, 68]. The tensile stress

[1] Measurements were made by Nakeeran Ponnampalam

measurements were repeated on films with different thicknesses (550 nm and 1 μm) and the trends were found to be similar, as can be seen in Figure 3.2 (a). The stress was found to be a minimum when PAI films were cured to a temperature of 200°C, with an increase in stress for higher temperature cures. A possible reason for the initial reduction of stress is the relaxation of the PAI molecules that were aligned during spinning. The increase in stress for higher temperature might be due to shrinkage in the PAI film as residual solvent evaporates.

Figure 3.2 (b) shows the dependence of the refractive index on the curing temperature. The refractive index was measured at 630 nm using the prism coupling technique. Both the transverse electric (TE) and transverse magnetic (TM) fields were measured separately to assess the birefringence. It can be seen that the maximum birefringence also occurs at 200°C. High birefringence is often undesirable and is usually associated with molecular orientation and polymer stress [22]. From Figure 3.2 (a) it can be seen that the maximum birefringence occurs when the stress value is minimum. This suggests that the molecular orientation is the dominant contributor to the birefringence. Different techniques have been used in order to reduce the birefringence caused by molecular orientation [22]. A careful control of spin coating conditions, solvent evaporation, and a proper understanding of polymer cross-linking during film heating and cooling processes might produce PAI films with lower birefringence values [15].

In Figure 3.2 (c), the film thickness was measured at different curing temperatures, and was found to decrease with temperature due to solvent evaporation. The graph shows that the film shrinkage saturates above ~250°C, suggesting most of the solvent has evaporated. Some of the other relevant properties of polyamide-imide films were previously studied and reported elsewhere [32]. The refractive index of PAI at 1.55 μm was found to be about 1.65, in agreement with manufacturer supplied data [67]. Since the refractive index of BCB is around 1.54, the refractive index offset of PAI/BCB waveguides is greater than 0.1. This contrast should allow for tight mode confinement for PAI strip waveguides, and also allow for very low bend radii (~ 100 μm) without significant bending losses.

The process steps used to fabricate Torlon PAI channel waveguides by dry etching are shown in Figure 3.3. A 70 nm gold layer was sputtered on the PAI film, and photoresist (PR) was then patterned on the gold to define the waveguide structures. The gold was

selectively etched with a standard KI/I_2 solution. Waveguides were then etched in PAI using reactive ion etching (RIE) or inductively coupled plasma reactive ion etching (ICPRIE). Both techniques provided good results; however, it was found that the ICPRIE resulted in lower sidewall roughness and surface damage, while achieving higher etch rates. After the etching was completed, the gold layer was removed and a BCB upper-cladding layer was deposited on the PAI waveguides. Further details can be found in reference [38].

Figure 3.4 shows SEM images of PAI waveguides before the deposition of the upper-cladding. Figure 3.4 (a) shows the relatively low sidewall roughness and good verticality that can be obtained with the ICPRIE process. This early work demonstrated the great potential of polyamide-imide for the fabrication of high quality microdevices. Figure 3.4 (b) shows the end view of a 1.1 μm x 1.2 μm cleaved PAI waveguide. Other waveguides with varying dimensions were also fabricated successfully.

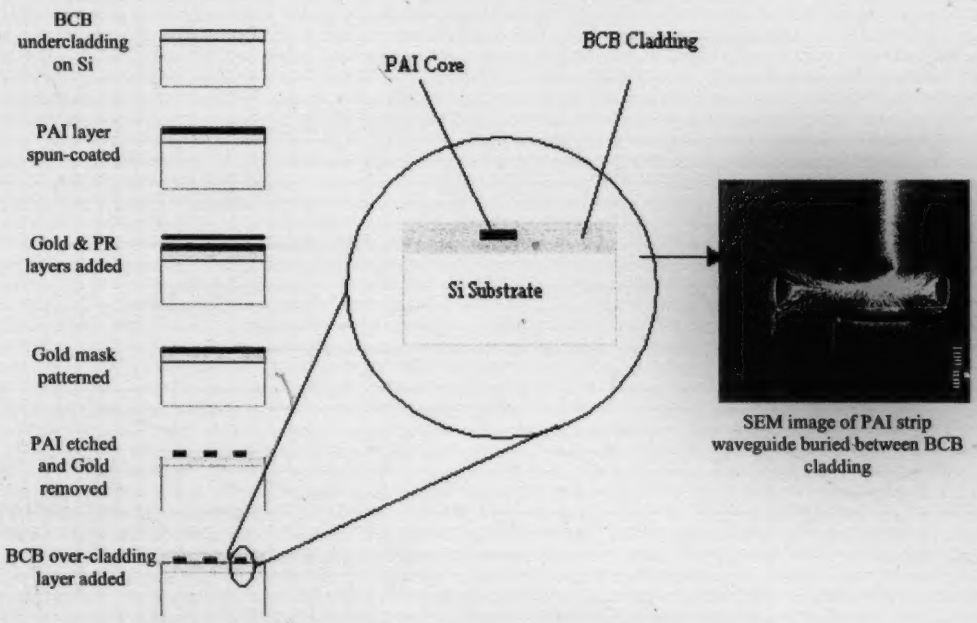
BCB undercladding on Si
PAI layer spun-coated
Gold & PR layers added
Gold mask patterned
PAI etched and Gold removed
BCB over-cladding layer added
PAI Core
BCB Cladding
Si Substrate
SEM image of PAI strip waveguide buried between BCB cladding

Figure 3.3: Fabrication Process for PAI buried channel waveguides

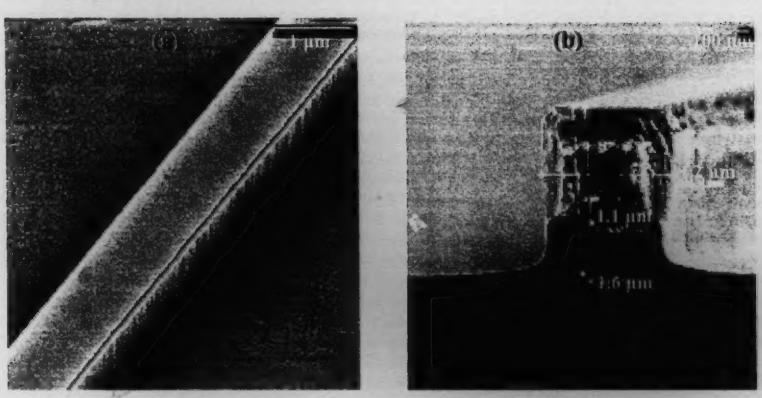

Figure 3.4: SEM of PAI waveguides (a), and end-view after cleaving (b)

3.2 Loss Measurements

The different types of losses that can be present in an optical media were discussed in Section 2.2. The presence of contaminants, dust particles, micro-voids, and surface roughness, which lead to high extrinsic scattering loss, can generally be minimized by using proper processing conditions. Low film stress is associated with low intrinsic scattering loss [31, 68]. Thus, optical propagation losses in polymer waveguides is usually dominated by etch-induced roughness or the intrinsic absorption loss features of the polymer.

Waveguides were fabricated as discussed in Section 3.1, and loss measurements were performed at both 980 nm and 1550 nm [38]. The end and top views of light coupled into the waveguide are shown in Figure 3.5.

Figure 3.5: End and Top view of 980 nm (left), and 1550 nm (right) light coupled into PAI waveguides [38]

The propagation loss was estimated by a cut-back method for both 3 μm and 10 μm wide waveguides. The loss measurements for both transverse electric (TE) and transverse magnetic (TM) waves are summarized in Table 3.1 [97].

Table 3.1: PAI cut-back method loss summary

	980 nm losses (dB/cm)		1550 nm losses (dB/cm)	
	TE	TM	TE	TM
3 μm	4.8	3.2	4.2	3.0
10 μm	3.1	2.7	3.2	2.7

It was observed that TE modes suffered higher propagation losses than the TM modes. This can be explained by the fact that TE modes are less confined than the TM modes in the lateral direction, and thus are more affected by the sidewall roughness [69].

While the results obtained were very promising, the loss is higher than is generally considered optimal for integrated optical waveguides (<1 dB/cm is a typical target). Loss can be reduced through the modification of the fabrication conditions, the use of non-traditional fabrication methods which produce lower sidewall roughness, or the use of

sidewall roughness reduction techniques such as thermal reflow, which can reduce the surface roughness of the PAI waveguide. These goals were the main subject of the present work, and results are described in the remainder of the thesis.

3.3 Transmission Spectrum and Absorption Peaks

Most polymers have high optical losses in the infrared region due to the presence of C-H vibrational absorption overtones.

The molecular structure of Torlon PAI can enable prediction of the vibrational overtones that will contribute to the near-IR loss. From Figure 3.6, it can be seen that the C-H bonds in Torlon (which is highly aromatic) are present in the benzene rings. Other bonds that are present include N-H, C=O, C-C, and C=C.

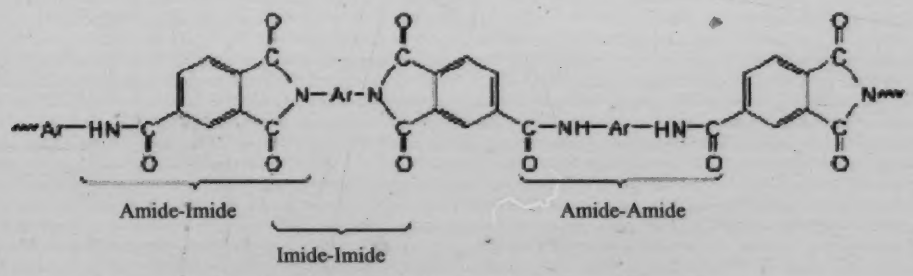

Figure 3.6: Molecular structure of PAI polymer [70]

In previous work[1], the absorption spectrum of Torlon PAI was estimated using a Perkin Elmer Lambda 900 spectrophotometer by two different methods. In the first case, the absorption spectrum of PAI was extracted from the measured absorption data of pure DMAC and PAI in DMAC solution [71]. The derived PAI absorption spectrum is shown in Figure 3.7. It is clear from Figure 3.7 that PAI is highly absorbing in the UV and has residual absorption in the visible region. This is consistent with the yellow color of bulk Torlon parts.

[1] Measurements by N. Ponnampalan & T. J. Clement

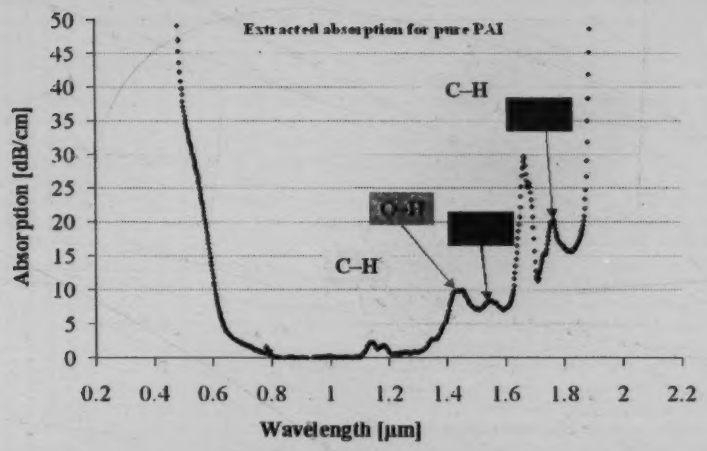

Figure 3.7: Extracted absorption spectra for PAI

The absorption peaks were assigned to coinciding vibrational overtones of C-H, O-H, N-H, and C=O bonds, as reported in the literature [24, 40, 72].

In the second method, a 10 μm PAI film was prepared by spin-casting on a silicon wafer and cured to 160°C. It was then pealed from the wafer and cut into ten pieces. These ten pieces were stacked, and then this stack was used to measure the absorption spectrum of PAI with a spectrophotometer. The spectrum can be seen in Figure 3.8. The spectra of Figure 3.7 and Figure 3.8 are quite similar, but the peaks caused by the O-H and N-H overtones were found to be relatively weak in the second method. This is attributed to water evaporation from the partially cured PAI film, and it is expected that lower absorption could be attained with a fully cured film. It is well known that Torlon PAI polymers liberate water on curing [67].

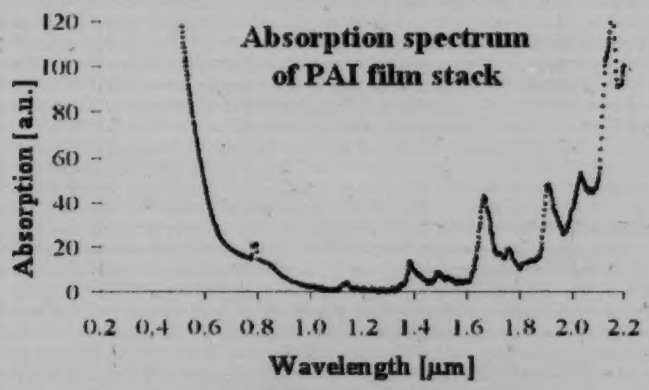

Figure 3.8: Absorption spectrum of ten-10μm film stack

In the present work, the absorption spectrum was determined through measurements on the etched PAI waveguides described in Section 3.1. The PAI films in that case are much thinner (≈ 1 μm) and were extensively cured. Thus, it was of interest to see whether the PAI exhibited a further reduction of its O-H and N-H absorption features. Furthermore, waveguides can in principle allow very sensitive determination of absorption, since light is confined to the film over long propagation distances. Broadband spectral characterization of the waveguides was done using the setup shown in Figure 3.9. A Koheras Super Continuum laser (SuperK SCB-Red 100-PC, S/N: KOH1817) was used as a source. Due to the high absorption of PAI in the UV and visible regions, a silicon wafer was used to filter out the short wavelength light so as not to cause damage to the PAI waveguide. Thus, broadband light in approximately the 1-2 μm range was launched into Torlon PAI waveguides through a single mode optical fiber, with index matching fluid being used between the fiber and the Torlon PAI waveguides in order to reduce coupling losses. The output spectrum was then monitored using a MS9710C Anritsu optical spectrum analyzer (OSA).

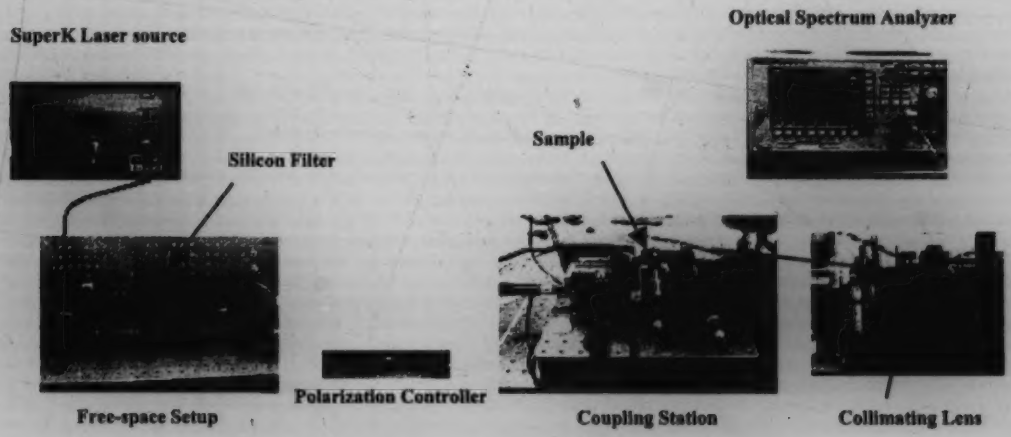

Figure 3.9: Spectral Characterization of PAI waveguide

The transmission spectrum of the optical waveguide was measured in the range from 600 nm to 1750 nm (with the lower wavelengths blocked by the Si filter). Figure 3.10 shows a typical transmission spectrum obtained (using waveguides 0.8 cm long and 3 μm wide).

The lower wavelengths (below 1100 nm) filtered out using the silicon filter are not shown in the plot.

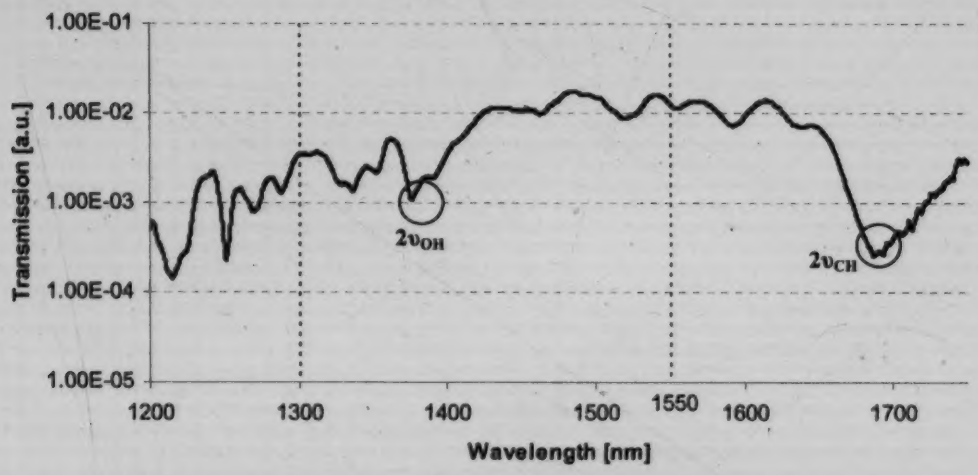

Figure 3.10: Transmission Spectrum of 3 μm waveguide using Super Continuum Laser

From Figure 3.10, it can be seen that regions of transparency exist near 1.3 μm and 1.55 μm, which are the wavelengths of interest in telecommunications. Two of the major peaks occurring around the 1.55 μm window (as is highlighted above) were compared to data available in the literature (see Section 2.2.1), and (given the molecular structure of Torlon PAI) are expected to be caused by the second harmonic of the vibrational C-H bond ($2\upsilon_{CH}$, 1695 nm) and the second harmonic of the O-H bond ($2\upsilon_{OH}$, 1378 nm). The lower transmission in the 1.3 μm range may be partly attributed to the loss of power arising from the use of polarizers and fibers that were designed for the 1.55 μm wavelength range. The smaller absorption peaks in the spectrum could have resulted from impurities (including additional water peaks [73]), imperfections in the waveguide, or absorption caused by the cladding polymer. However, it is quite likely that some of the ripple arises from unintended experimental artifacts. For example, Fresnel reflection at waveguide facets can cause Fabry-Perot effects.

The same experiment was repeated using 10 μm wide waveguides of the same length, and the results were compared to those obtained with the 3 μm waveguides. A plot that shows the relative absorption in both waveguides (relative to the minimum absorption in that waveguide) is shown in Figure 3.11. The absorption peak in the 1690 nm range is apparent in both waveguides; however excess fluctuations apparent because of the low power that was coupled into the OSA makes it difficult to identify the other peaks.

It can be seen that the absorption increases as the wavelength decreases. This is more prevalent in the 3 μm waveguide, and can probably be attributed to scattering by waveguide sidewall roughness [1, 69].

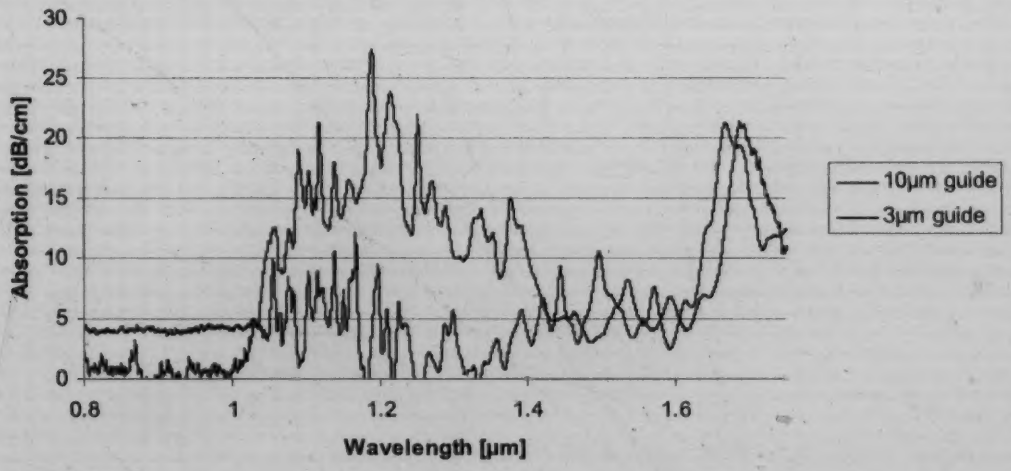

Figure 3.11: Relative absorption spectrum of both 10 μm and 3 μm waveguides in dB/cm.

A spectral transmission scan was also obtained using a Santec Tunable LD Light Source (TSL-320), with the transmitted power measured using an optical power meter. As shown in Figure 3.12, there was no evidence of absorption peaks in the 1520 nm – 1620 nm range, which is consistent with the results described above. The absorption increase at the higher wavelength end of the scan can be attributed to the C-H overtone at 1690 nm.

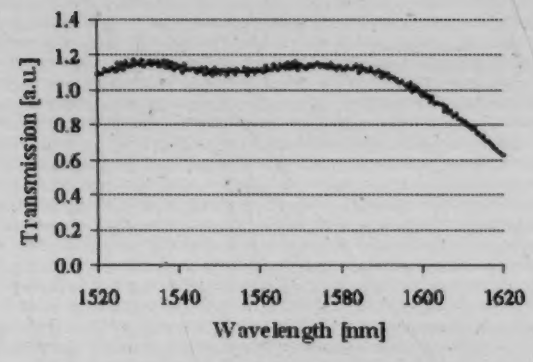

Figure 3.12: Transmission spectrum of PAI waveguide in the 1550 nm range

These experiments demonstrated the potential for low-loss waveguiding in Torlon PAI at telecommunication wavelengths.

3.4 Thermal Reflow

Since the PAI waveguides discussed above were fabricated using reactive ion etching, the sidewalls of the waveguide will have roughness derived from the lithography and etching process. This roughness causes optical loss due to scattering, as discussed in Section 2.2.2. For glassy materials (such as PAI), it has been shown that this roughness can be reduced using a thermal reflow technique [21, 74, 75]. In the thermal reflow process, the polymer sample is heated close to its glass transition temperature for some time and surface tension forces cause smoothening of the sidewalls.

To assess the reflow capabilities of Torlon PAI and as a precursor to the embossing work discussed in Chapter 4, etched PAI waveguides were heated to 300°C for one hour under nitrogen. This heating process reduces the viscosity of the polymer, allowing the polymer molecules to move freely. SEM images showed that the surface roughness of the PAI waveguides was significantly reduced after this process. An SEM of the waveguide before and after reflow is shown in Figure 3.13.

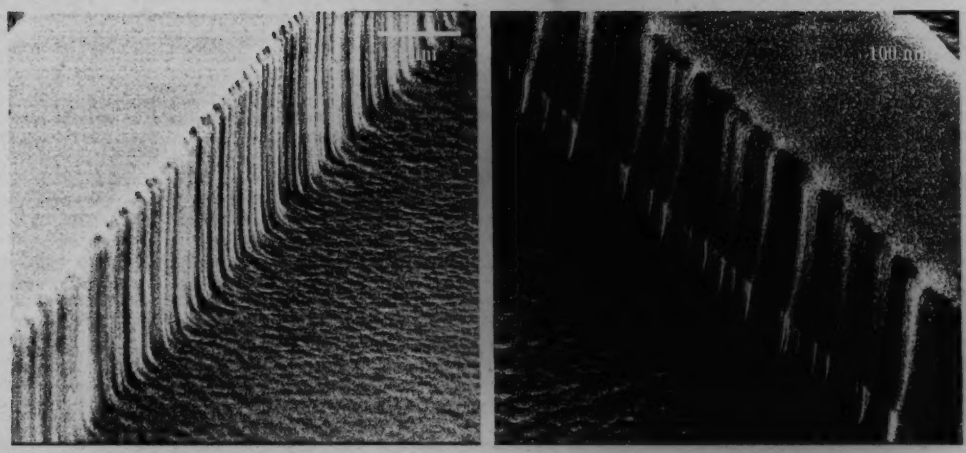

Figure 3.13: SEM images showing the sidewall of a PAI waveguide before (left) and after annealing for 1-hour at 300°C (right)

It was expected that higher temperatures and longer heating times would result in smoother surfaces. It is important, however, not to use very high temperatures or very long times since they might lead to excessive deformation of the waveguide structure and eventual degradation of the polymer material.

Different samples were heated to ≈ 270°C, ≈ 280°C, and ≈ 290°C for two and four hours. SEM images of these reflowed samples are shown in Figure 3.14, Figure 3.15, and Figure 3.16. Nitrogen was passed through the system for 30 minutes in order to drive out air. It is clear from the images that the reflow process helped reduce the sidewall roughness of the PAI waveguides. It can also be seen that the surface roughness was lower for longer reflow time, and that it was most reduced when higher reflow temperatures were used. It is expected that this reduction in surface roughness would significantly reduce the optical loss, but due to the limited size and availability of the etched waveguide samples, verification is left for future work.

Some damage (pinholes near the top surface) can be seen in the waveguides cured at 280°C and 290°C. This might have been caused by shutting the Nitrogen flow during the reflow process, causing air to leak back into the system. The use of a sufficient amount of Nitrogen is expected to solve this problem, and will be tested in the future.

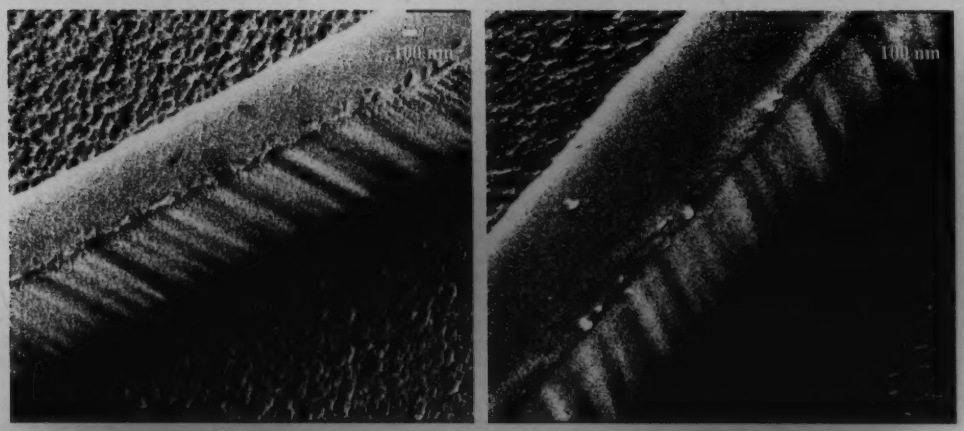

Figure 3.14: PAI waveguides thermally reflowed at 270°C for 2hrs (left), and 4hrs (right)

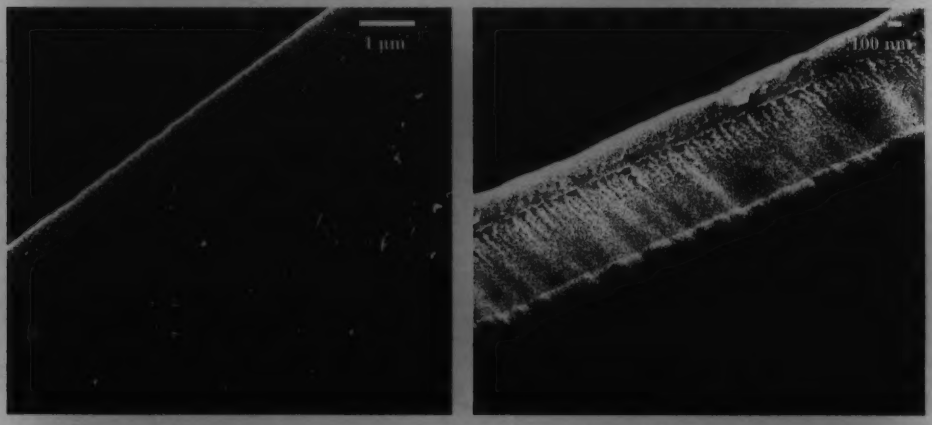

Figure 3.15: PAI waveguides thermally reflowed at 280°C for 2hrs (left), and 4hrs (right)

Figure 3.16: PAI waveguides thermally reflowed at 290°C for 2hrs (left), and 4hrs (right)

Chapter 4 Embossing of PAI

In this chapter, the fabrication of waveguides on Torlon using hot embossing lithography completed in this study is discussed.

4.1 Interest in Embossing PAI

The thermal reflow process discussed in Section 3.4 demonstrated the ability of Torlon PAI to flow when heated to a temperature close to its glass transition temperature. This raised interest in using hot embossing lithography to fabricate structures in Torlon PAI. As a thermoplastic, Torlon PAI softens when heated, and can be deformed and molded through the application of a force [35]. The successful fabrication of waveguides on Torlon PAI would allow us to combine the advantages of the embossing process with the attractive properties of PAI.

The surface roughness of embossed PAI waveguides might also be significantly reduced (compared to the dry-etched waveguide described in Chapter 3) by embossing using a mold fabricated with a high resolution technique. This would allow us to not only produce high performance, low loss waveguides, but also to reduce the fabrication cost and increase the fabrication throughput.

Most of the polymer embossing work reported in the literature used polymers with a T_g much lower then that of PAI. For this reason, unique challenges were expected in the development of an embossing process for PAI.

4.2 Fabrication of Si Stamp

Silicon was chosen as the material for the mold to be used in the hot embossing trials. In our study we used both silicon trenches, for the fabrication of Torlon PAI ribs, and silicon ribs, for the fabrication of Torlon PAI trenches.

Initially, a silicon wafer was cleaned with 2:1 piranha for 1 hour. After cleaning with piranha, the silicon wafer was rinsed and dried. PR was then spun on the Si wafer and patterned with a previously described mask [13, 76] using photolithography. The mask

pattern includes nine sets of features (waveguide-like structures or trenches, depending on process used). Each set included features of equal width, separated by 125 μm (to allow easy coupling of light when used to fabricate waveguides). The width of subsequent sets increase by 0.5 μm, starting from 1 μm to 6 μm. Two molds were fabricated by using reactive ion etching, one with trenches and one with ribs. The reactive ion etching was performed on an Oxford Instruments device, using a 9:2 sulfur hexafluoride (SF_6) to oxygen (O_2) ratio. This was done under a pressure of 7.5 mtorr and an rf power of 6 W was used. The heights of the ribs and the depth of the trenches depended on the etching time. Each silicon wafer was cleaved into several pieces and etched for different times. Some of heights/depths of the structures obtained (measured using a profilometer) are shown in Table 4.1 below along with the etch time.

Table 4.1: Structure depth and height vs. reactive ion etching time

Etch Time (sec)	Structure Depth/Height
45 – 50	1.5 μm – 1.8 μm
40	1 μm
20	650 nm
11	250 nm
10	110 nm

For forming silicon trenches, after the patterning of the PR by lithography, the patterned silicon wafer was sputtered with 50 nm of chromium (Cr). A Lift off process was then performed using a warm acetone bath, which left the Cr to act as the etch mask in subsequent steps. Silicon was then etched using reactive ion etching, forming the needed trenches with the approximate depth given in Table 4.1. Finally the remaining chromium layer was stripped off using a chromium etchant. A summary of the process is shown in Figure 4.1.

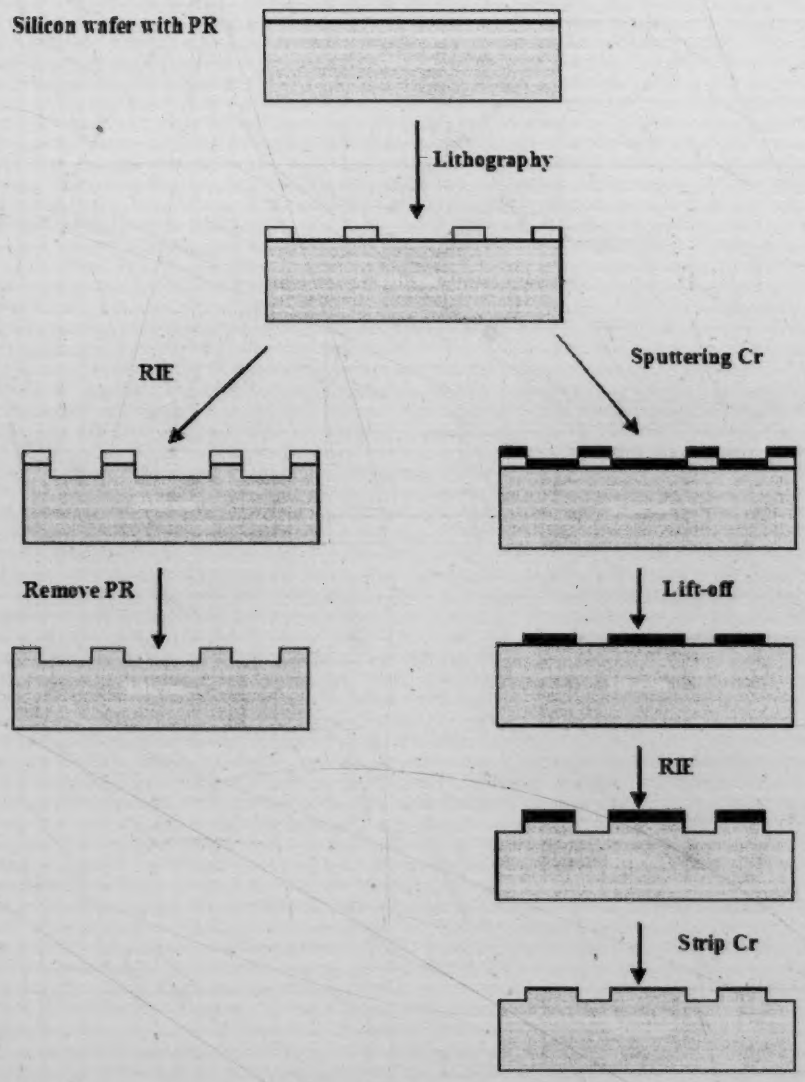

Figure 4.1: Diagram illustrating processing steps used in the fabrication of silicon ribs (left), and silicon trenches (right)

Representative SEM images of the fabricated silicon trenches were then obtained, and are shown in Figure 4.2 and Figure 4.3.

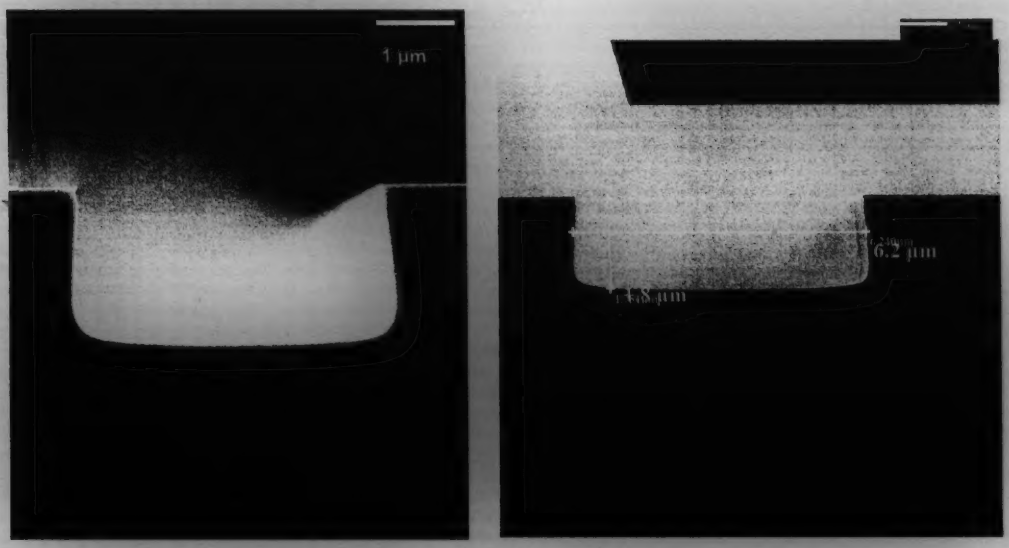

Figure 4.2: 4.2 µm (left) and 6.2 µm (right) wide silicon trenches ~1.8 µm deep (50 s ICP)

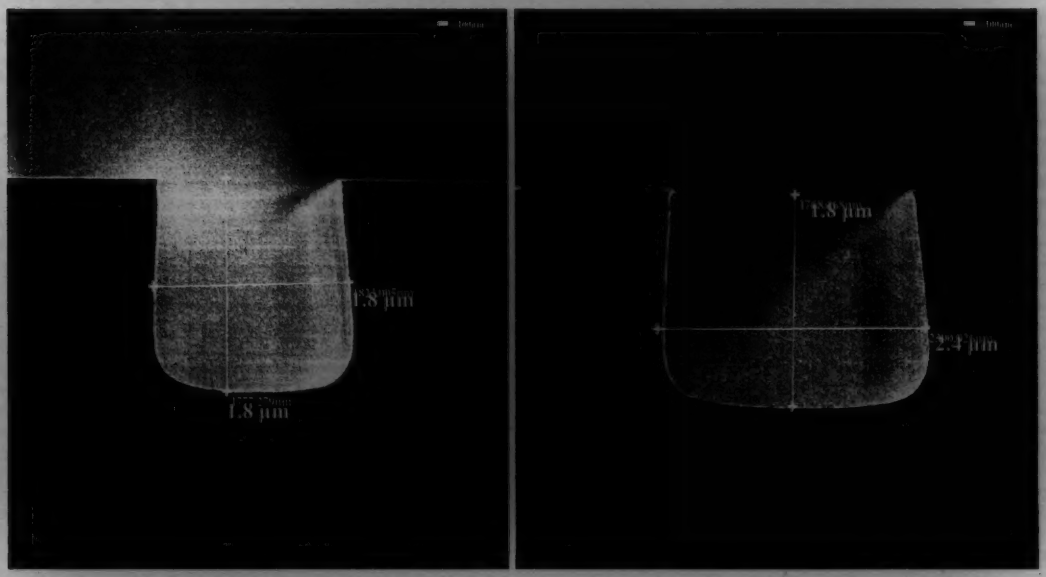

Figure 4.3: 1.8 µm (left) and 2.4 µm (right) wide silicon trenches ~1.8 µm deep (50 s ICP)

It can be seen from the above figures that the fabricated trenches have a small undercut. This is generally undesirable since it can create problems when separating the mold from the polymer during de-embossing.

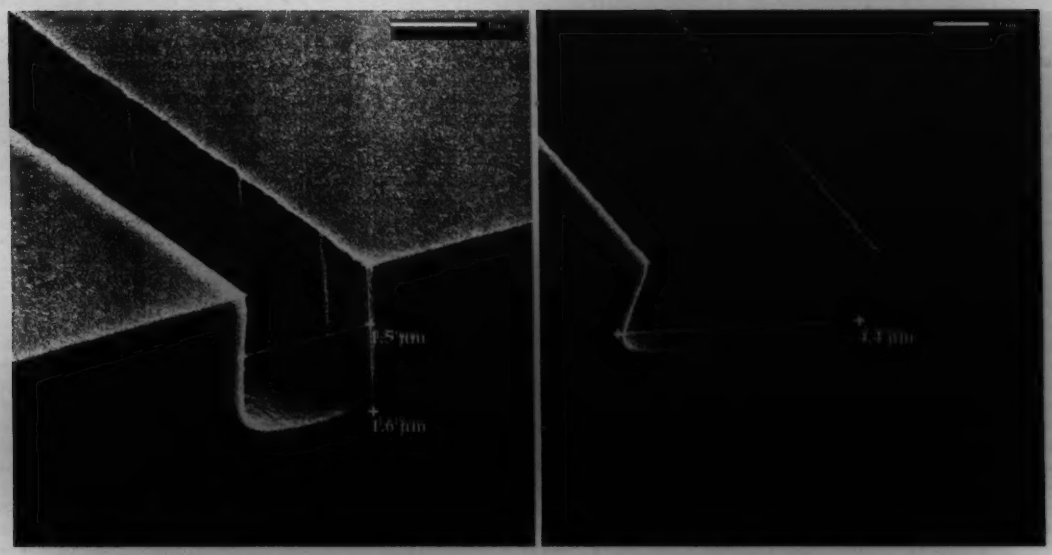

Figure 4.4: Sidewalls of 50 s ICP silicon trenches 1.5 μm (left) and 4.4 μm (right)

As shown in Figure 4.4, the sidewalls are relatively smooth (when compared to the roughness resulting from RIE of a PAI waveguide, see Figure 3.13). The underetching as well as the hook-like shape of the top of the trench (see Figure 4.5) could lead to interlocking between the mold and the polymer. This could cause tearing of the polymer structure, surface distortion, or an increased surface roughness. The surface roughness and structure quality and resolution could be improved by modifying the mold fabrication conditions, or by using a higher resolution fabrication technique. Since this was an initial study of embossing of PAI, the molds fabricated were deemed to be of sufficient quality.

Figure 4.5: Hook-like shape of top edge of 50 s ICP silicon trench

The silicon rib molds were simpler to fabricate as is shown in Figure 4.1. After the mold was patterned with PR, the silicon was etched (as discussed in the beginning of this section) and then the remaining PR was stripped. Figure 4.6 and Figure 4.7, show an SEM of the end-view of some of the rib-like structures fabricated on silicon.

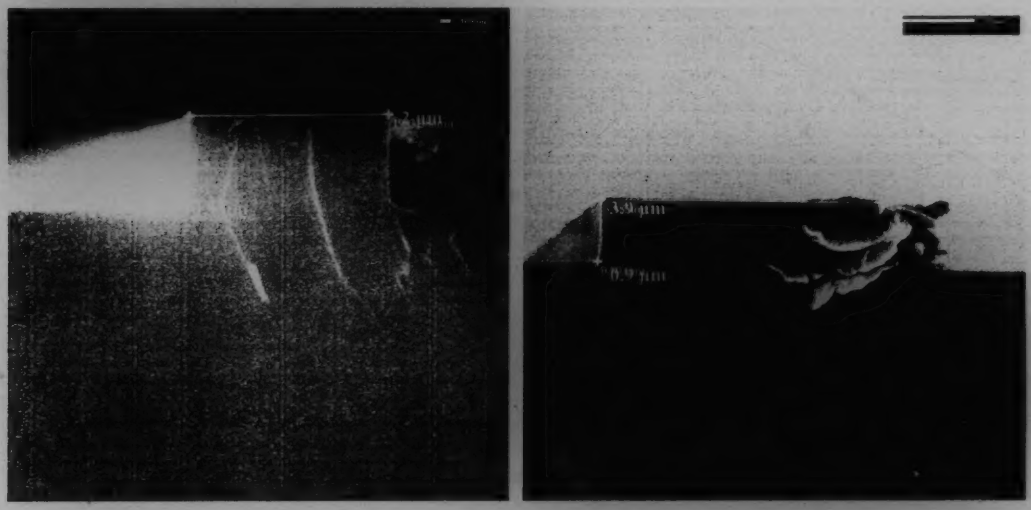

Figure 4.6: 2 μm (left) and 3.9 μm (right) wide silicon rib-like structure ~0.9 μm high (40 s ICP)

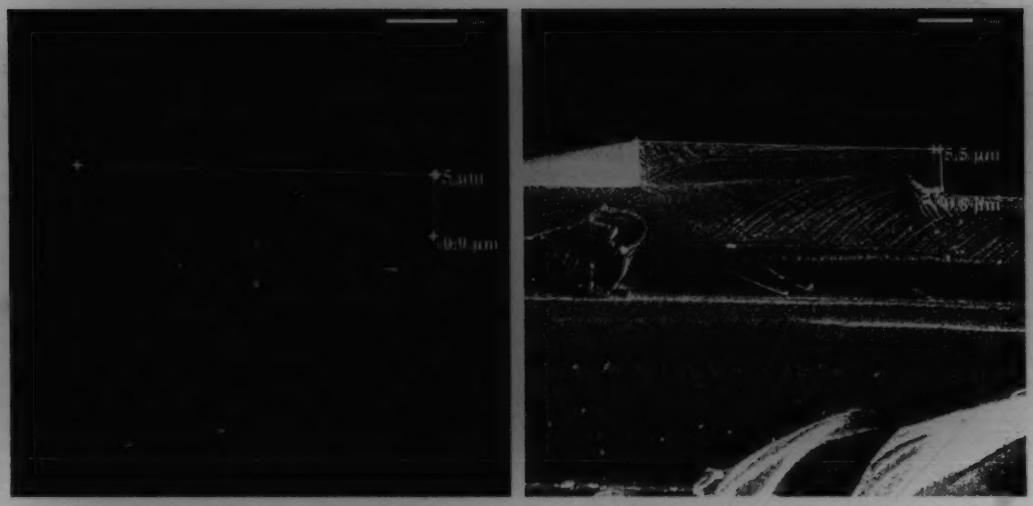

Figure 4.7: 5 μm (left) and 5.5 μm (right) wide silicon rib-like structure 0.9 μm high (40 s ICP)

Figure 4.8: Sidewalls of 40 s ICP silicon rib-like structure

It can be seen in Figure 4.8, however, that the sidewall roughness obtained for the silicon ribs appears greater than that obtained for the silicon trenches (seen in Figure 4.4). Modifying the etching process and conditions could improve the quality of the sidewalls. Since we were more concerned in this study with successfully embossing PAI films, the

quality of the mold were deemed acceptable and no further effort were made to improve it.

After the fabrication of the silicon molds and prior to their use in embossing, they were coated with an ASL. The molds were first re-cleaned with piranha, and then treated with 1,1,2,2 tetrahydro perfluorooctyl trichlorosilane (F6) in order to build a self-assembled anti-sticking monolayer (refer to section 2.4.4.6); the F6 was deposited from the gaseous state. This was done by placing the silicon mold with ~0.2 ml of F6 in a vacuum chamber and leaving them overnight. As was discussed earlier, adhesion between the mold and the polymer is a major challenge in embossing. PAI is known to have strong adhesion to many substrates including silicon. This might cause damage to the patterns on the silicon mold, which would affect the repeatability of the embossing process, or might cause tearing of the Torlon PAI film during demolding. The ASL was used in hopes of reducing the adhesion between the silicon mold and PAI. F6 has been used successfully in many papers, and shown to significantly reduce the resulting adhesion between a silicon mold and the polymer layer [55-57, 59].

4.3 Preliminary Embossing Tests

Initial embossing trials were done to test the flow of Torlon under the application of a force. These tests were done using a poling station (a system originally designed to pole electro-optic polymers) at TRLabs, Edmonton. The poling machine is controlled using Lab View (Poling Station Controller.vi [77]); a screen-shot of the Lab View interface is shown in Figure 4.9. The temperature is measured using a thermocouple, which maintains the temperature within 15°C of the set temperature. The poling machine allows for the heating temperature to be selected, as well as the rate of heating and the hold time. The machine also allows for a voltage to be applied to the polymer (or sample) being heated, for the poling of electro-optic polymers. For the present work, only the heating functionality was used.

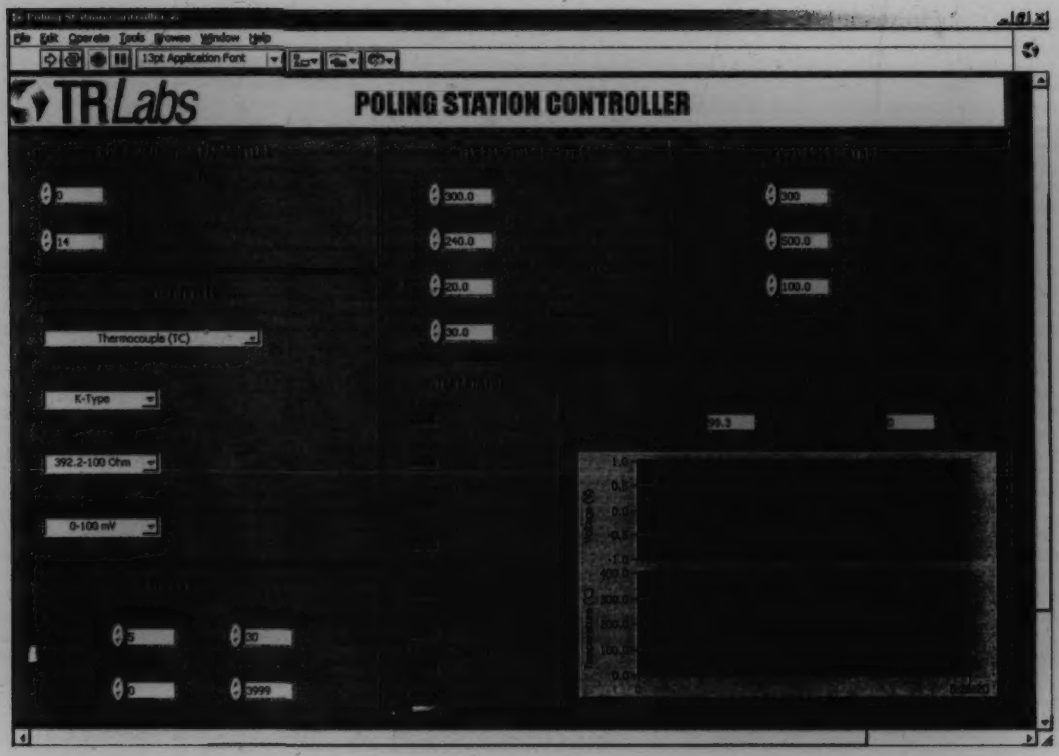

Figure 4.9: Poling Station Controller Interface

Embossing of trenches was attempted first, since such structures can form more easily than ribs due to the smaller distance the polymer needs to flow. Such negative relief structures were reported to have given better results [78]. After preparing the silicon mold (refer to Section 4.2) and Torlon PAI film (refer to Chapter 3), the samples were diced to the required size (this was usually made less than 1 cm x 1 cm, to ensure the application of a larger pressure). Nitrogen was pumped into the station in order to drive out the oxygen to limit the chances of any polymer oxidation at elevated temperatures.

Several means of applying a force between the mold and the polymer were considered. The force could be applied by either clipping the silicon mold to the polymer using a simple metal clip, or by placing weights on top of the sandwiched mold and polymer wafers. Brass weights were first used to apply a pressure of up to approximately 200 kPa. A Torlon sample approximately 2 μm thick was placed in the poling station and heated to

360°C. After the temperature was reached, the cover was removed and the mold along with the weights were placed on the polymer sample. The assembly was left for 4 hours, after which the weights were removed, and the mold and polymer were left to cool to room temperature. After the setup had cooled, the mold and polymer were separated using tweezers. The process resulted in imprints on the polymer. Parts of the mold were not imprinted, so the process was repeated with the time increased to 9 hours, and similar results were obtained. The images obtained by optical microscope can be seen in Figure 4.10 below.

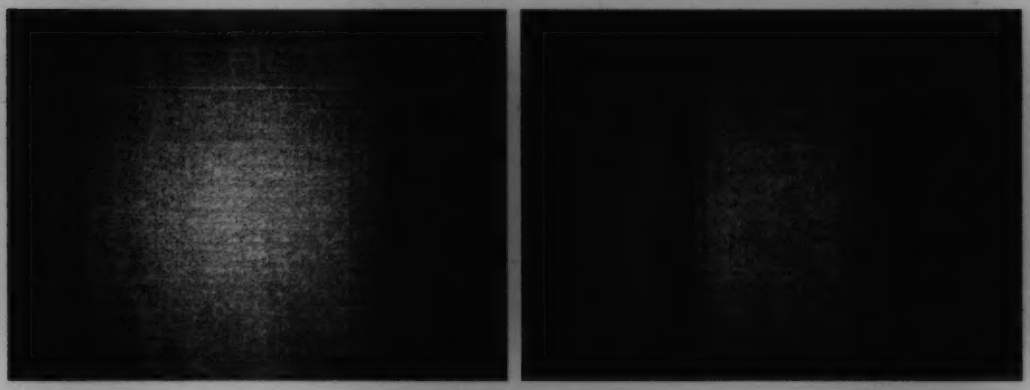

Figure 4.10: Optical Microscope images of embossed Torlon trenches

The embossed trenches were then viewed using SEM, as shown in Figure 4.11. These images give some insight on the flow characteristic of Torlon under pressure. It can be seen that, with the applied pressure, the polymer is pushed out from under the silicon mold and to the side. The incomplete trench formation is attributed to the insufficient force being applied, since doubling the embossing time did not improve the embossed structures significantly. These results, however, showed the possibility of embossing structures on Torlon, and suggested that with the application of proper temperature, pressure, and time, the needed structures could be formed.

Figure 4.11: Incomplete Torlon trenches embossed at 360°C, 200 kPa for 4 hours

Figure 4.12: Incomplete Torlon trenches embossed at 360°C, 200 kPa for 12 hours

Since there were limits on the maximum number of weights that could placed in the poling station, the size of the silicon mold was reduced in order to effectively increase the pressure while keeping the applied force constant. The 50 s ICP (~ 1.7 μm deep) silicon trenches mold, discussed in Section 4.2, was used in order to emboss PAI waveguides. The mold was diced to 0.85 cm x 0.65 cm, and contained sets of 1 μm and 1.5 μm wide trenches. The mold was used to emboss Torlon on BCB sample under nitrogen

environment. Two trials were performed; in the first run, the polymer was heated to 300°C before applying the force for 4 hours. After the process was complete no visible structures could be seen on the polymer. The temperature was raised to 360°C in the subsequent run, and the same weights were used again in order to apply the force for 4 hours. This time, several structures appeared on the polymer. SEM images of the produced structures are shown in Figure 4.13.

Figure 4.13: SEM of embossed Torlon waveguides (360°C for 4 hours)

It can be seen that, when a mold with silicon trenches was used, the polymer did flow upwards to form a waveguide-like structure. It can also be seen that the sidewalls are rougher than that of the 50 s ICP silicon trenches mold (Section 4.2). It is not clear what might have caused the added roughness. A possible reason could be that the silicon mold moved around due to improper balance of the weights mounted on it, thus causing an increased roughness in the sidewalls of the Torlon waveguide. Another reason could be the way the silicon mold was separated from the polymer. The use of tweezers to separate the mold from the polymer at room temperature could have caused an added friction that resulted in the increased roughness. A more controlled experiment was needed to get a better understanding of the process.

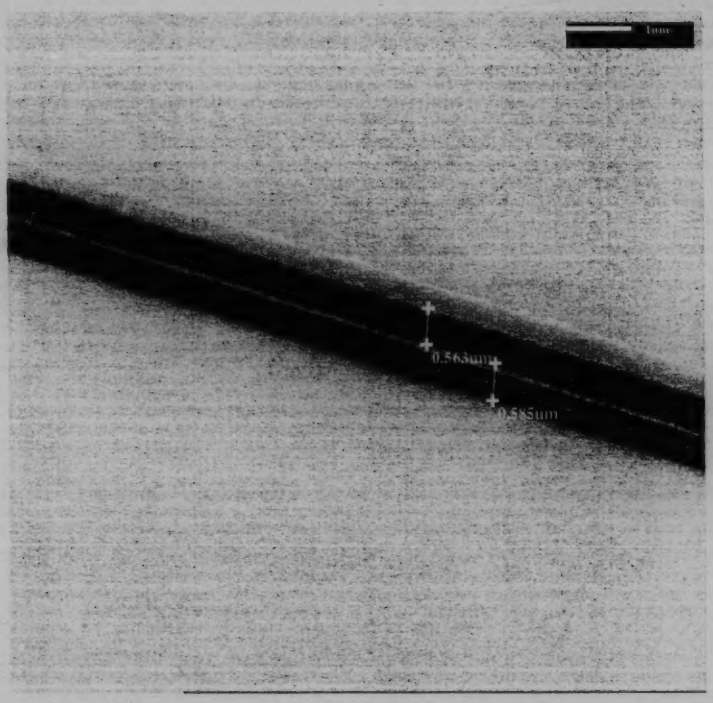

Figure 4.14: Side-view of Torlon embossed waveguides (360°C for 4 hours)

It should be noted that the increase in temperature (by 60°C between the two runs) may not be the sole reason for the different results. Inconsistent results could also be attributed to the unevenness in the force applied with the simple setup used, so that a higher pressure might have been applied at one location (causing the polymer to flow in that place) and small pressure in another (explaining why there were no structures produced at the another location). It was possible that, in the 300°C experiment, the force might have been more evenly distributed causing the pressure not to be high enough at any one location for polymer flow.

For the 360°C experiment, it was noticed that at some locations where waveguides were expected, trench-like structures were formed on the polymer. An example is shown in Figure 4.15. A more comprehensive study of Torlon's flow properties and a simulation of PAI flow at different conditions would need to be done in order to get a better understanding of what caused this behavior. That defect might have been caused by the interaction of oppositely flowing polymer fronts.

Figure 4.15: Side-view of trench-like distortion on embossed Torlon (360°C for 4 hours)

To improve the control over application of the embossing force, a different method of applying the force was used. In this method, a silicon waveguide mold and a 1 cm^2, 5 µm thick polymer sample were placed in contact with each other (at room temperature), between two flat pieces of aluminum. After ensuring that the mold and polymer were centered, a force was applied using two small binder clips (placed on opposite sides). Two pairs of progressively larger binder clips were also placed over the smaller clips. The setup was then placed in the poling station, and heated to 360°C and left for 11 hours. Nitrogen was pumped to drive the oxygen out, but nitrogen flow was subsequently shut down. After the embossing time was over and the setup cooled to room temperature, the polymer was examined. Structures could be seen to be more evenly distributed throughout the polymer layer than was seen in previous results, showing that the force was more evenly distributed. An SEM was performed and the results are shown in Figure 4.16 - Figure 4.17. This run produced deeper mold penetration than was obtained in the runs shown in Figure 4.11 - Figure 4.12. This is most likely due to the larger force that was used, as well as the longer embossing time.

Figure 4.16: Torlon trench embossed by binder-clip based setup

A negative outcome, however, was many of the silicon waveguides in the mold were broken off and stuck to the fabricated Torlon trenches (as seen in Figure 4.17). This was even observed in locations where the silicon mold did not penetrate the polymer, as in Figure 4.18. Several possible causes for the breaking of the silicon mold were identified as follows. The first and most probable reason is, movements that might have occurred during the application of the large force at room temperature (both before and after embossing), might have caused damage to both the silicon and polymer. More damage might be expected in the silicon mold, due to the tall and narrow waveguide structures. A second cause of the damage might have been the separation of the silicon and polymer structures from each other. Since the separation was done, as before, using tweezers, there was no way to guarantee a uniform separation of the mold from the sample. This might have resulted in lateral forces on the waveguide structures in the mold, causing them to break.

Figure 4.17: Broken pieces from silicon waveguide mold, stuck in Torlon trench

Figure 4.18: Silicon mold broken even in locations with minimum penetration

An SEM was taken of the silicon waveguide mold, and the damaged and broken waveguides are easily seen (Figure 4.19).

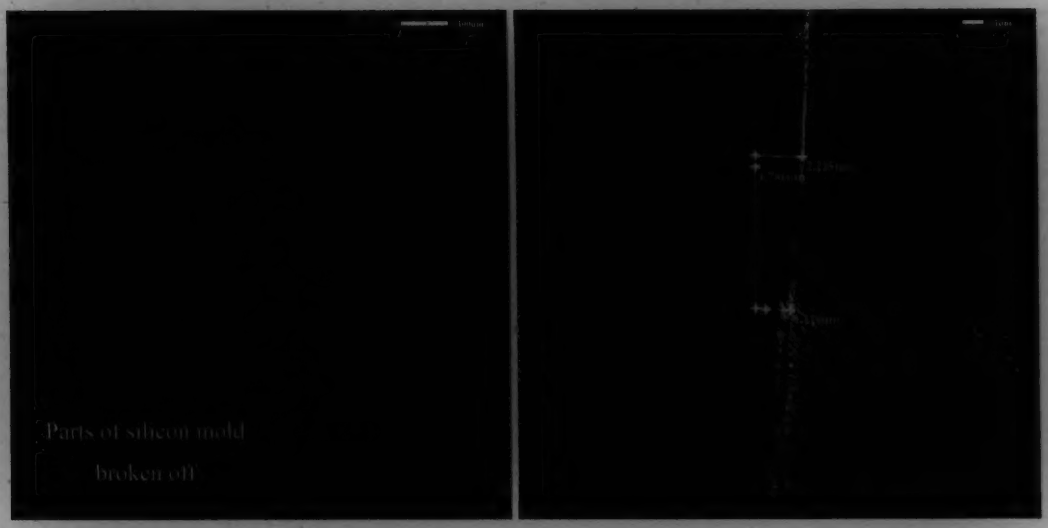

Figure 4.19: SEM of silicon rib mold with parts broken (left), zoomed picture of broken silicon ribs (right)

Different runs were attempted using either weights or binder clips to apply the force. Results obtained suffered from the same problems as described above. Varying the embossing parameters (such as temperature, force applied, or time) did not yield better results, and in some cases, due to the lack of control over the parameters, worse results/structures were obtained. All the results obtained suffered from an incomplete filling, and exhibited locations where no structures appeared. This was mostly due to the insufficiency and unevenness of the force applied. This unevenness can cause the force to be applied only at a certain location, which causes the applied pressure at that location to be much larger then the actual pressure that was measured. This can help explain why features were embossed in some cases when a smaller force was used, but failed to appear in other cases when the force was increased. Another problem faced was that many of the polymer samples that were embossed successfully were stuck to the silicon mold after the embossing process, and attempts to separate them usually led to the breaking of both the polymer and the silicon mold.

These tests, however, demonstrated the ability of fully cured Torlon polymer to flow under a force, when heated close to or above its glass transition temperature. A better setup was needed in order to obtain better results.

4.4 Design and Fabrication of a custom Embossing Station

Due to the limitations of the technique described in Section 4.3, a setup was needed that would allow for the parallel separation of the polymer and mold, and also allow for the application of a greater force. The HEX01 commercial embosser available at the University of Alberta NanoFab was limited to embossing temperatures less than 220°C, which would not allow for embossing of Torlon above its glass transition temperature. This made the development of a custom-made embossing machine important.

Several designs were considered that would use the poling station (described in Section 4.3) for heating purposes. The time would be measured using both a stopwatch and the poling station's timer. For the application of the force the use of compression springs or weights was considered. In the latter case, a pile of weights would be used to apply the needed force. After careful consideration, the spring design was favored due to its compactness and lighter weight. It would also allow for increasing the maximum applied force by simply changing the springs used.

Several things were considered when designing the machine. First, proper springs needed to be chosen, compatible with the desired force. The critical pressure (see Section 2.4.4.2) is that needed to overcome the surface tension of the polymer and is given by:

$$P_{\sigma} = \frac{4 f_s}{D}, \tag{4.1}$$

where f_s is the surface tension at the processing temperature, and D is the diameter of the cavity. Taking the surface tension to be 51.9 dynes/cm (~ 0.0519 N/m) for 587 K (314°C) [26] and a cavity with diameter of 1 μm gives an approximate pressure of 207.2 KPa (the actual critical pressure, based on the relation above, would differ based on the variation in surface tension, from one class of Torlon to another and that caused by the exact temperatures that might be used, as well as the actual dimensions of the mold). It was decided to select springs that would give a pressure of up to 1 MPa on a 1 cm^2 sample. Another consideration was that the embossing unit was to be small enough to fit on top of the poling station, which would be used for heating purposes. The force was to be applied by compressing the springs between two plates, with the top plate fixed in place by a knob, and the lower plate pushed by the springs. Stops were used to control the applied

force, by controlling the compression of the springs. The proposed design is shown in Figure 4.20 (Note: Springs are not shown). An exploded-view shown in Figure 4.21 will be used to explain the setup further.

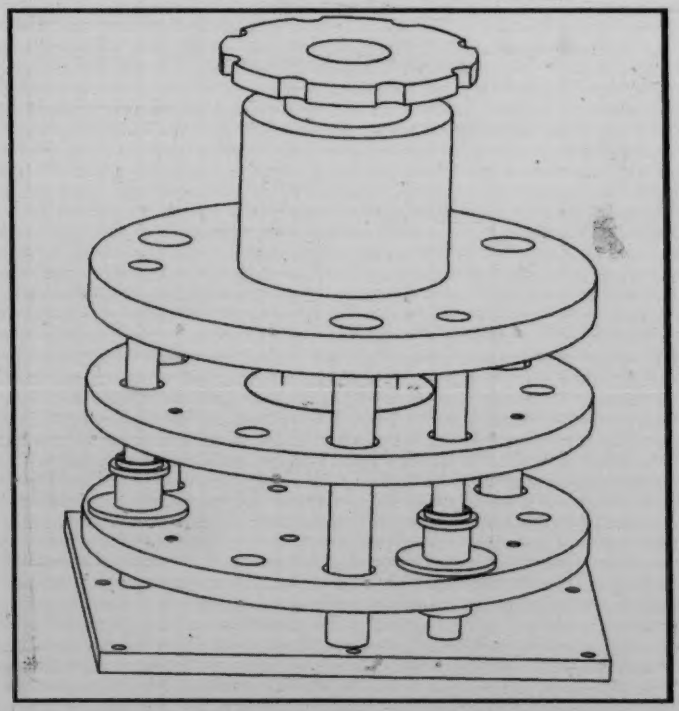

Figure 4.20: 3-dimensional schematic of embossing unit

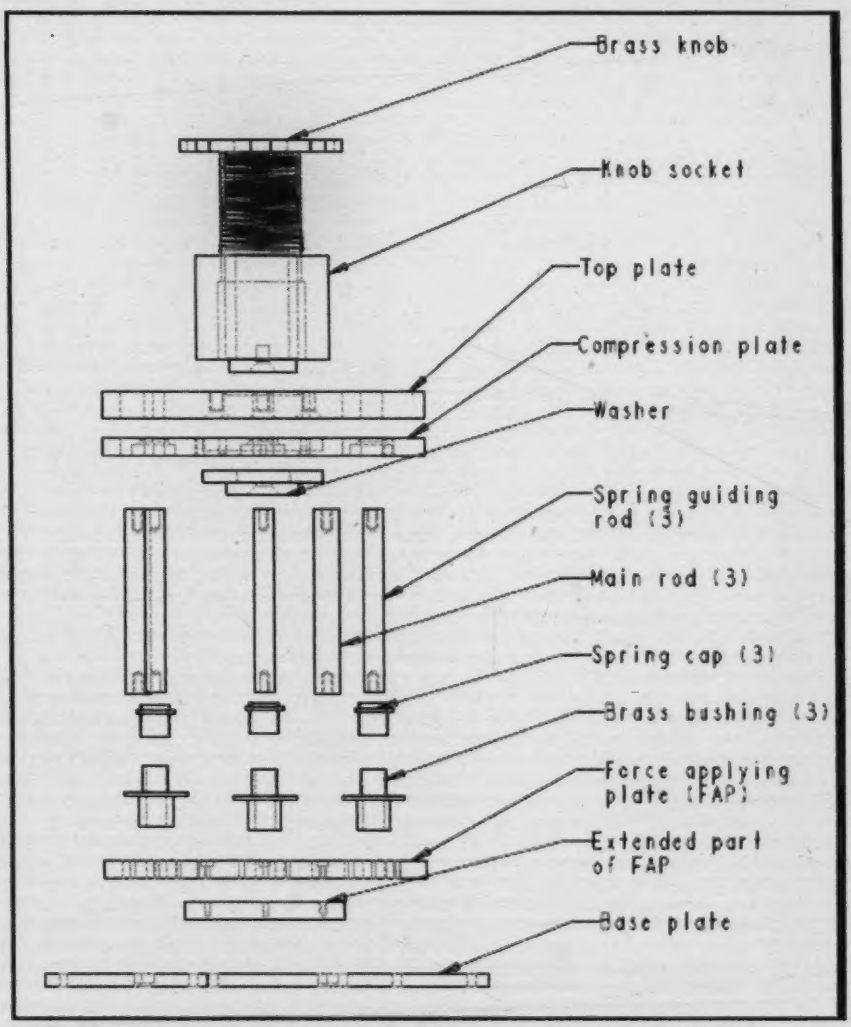

Figure 4.21: Exploded-view of embossing unit schematic

The embossing setup is composed of six rods (three main rods, and three spring guiding rods). The main rods connect the top plate to the base plate, and are used for supporting the embosser. The springs that would be used to apply the force would be placed on the spring guiding rods (they are not shown in the diagram). Three spring guiding rods were chosen for stability reasons, since they would reduce the chances of jamming, and would allow for a more even application of the force. The spring guiding rods are screwed to the top plate, but are made not to touch the base plate. This would reduce any effect the thermal expansion of the base plate would have on the rods. All the rods pass through the

force-applying-plate (FAP), but do not touch the plate. The main rods are given a clearance to avoid any jamming problem that could occur due to expansion of the base, while the spring guiding rods pass through bushings that also have a horizontal clearance, and are used to ensure that the applied force would always be parallel to the base, and thus applied evenly. Spring caps are placed on the bushings to reduce the movement of the springs during compression and relaxation. A knob socket is connected to the top plate. The brass knob is then used to push the compression plate down as it is being turned. A washer is used to connect the bottom of the brass knob to the compression plate, so that the knob pushes the compression plate down without turning it. As the compression plate is pushed downwards, it is guided through the main rods and compresses the springs placed on the spring guiding rods. As the springs are being compressed they push the force applying plate downwards. Once the extended part of the FAP has touched the base plate, further turning of the knob will compress the spring to its maximum position, resulting in the maximum force being applied.

The silicon mold could be connected to the extended part of the FAP using either double sided tape or glue, while the polymer sample could be connected to the base plate. The extended part of the FAP is 'extended' because of the presence of the bushings, as is clear in Figure 4.22 below. It is also made detachable, so that it could be replaced in the future if a different method was conceived for attaching the mold. Finally, three extra springs (not shown), connected between the compression plate and the force applying plate were added to pull the force applying plate up when the applied force was released, simultaneously with the compression plate being pulled up.

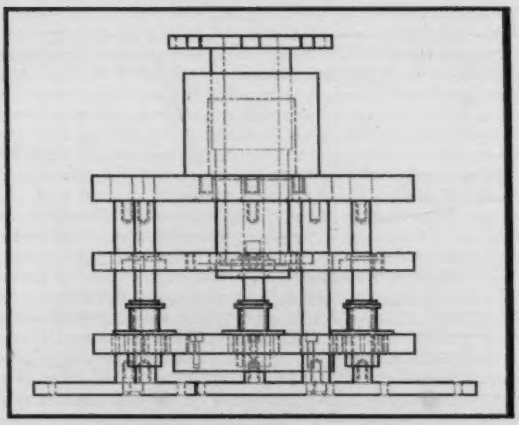

Figure 4.22: Front view schematic of embosser unit

The embosser unit was built and modified by the Mechanical Machine shop at the University of Alberta. A picture of the embosser unit is shown in Figure 4.23.

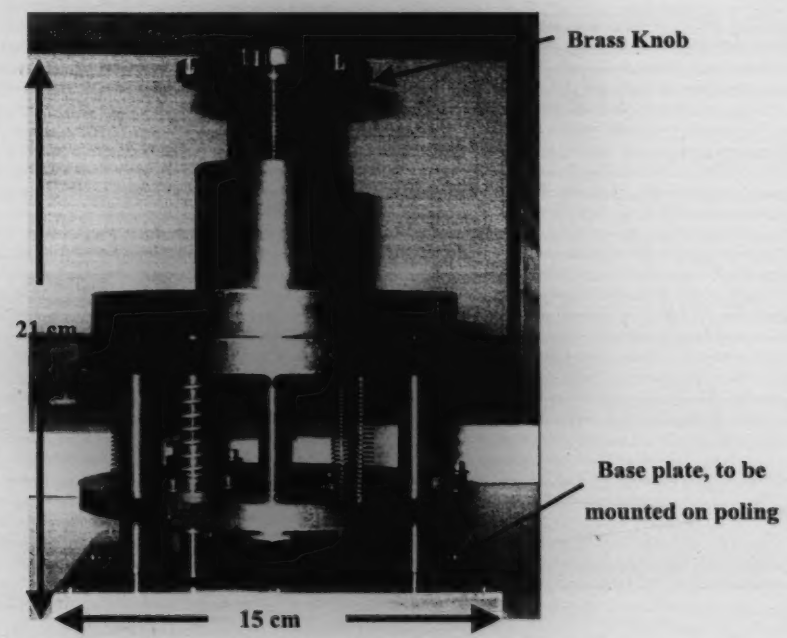

Figure 4.23: Photograph of embosser force applying unit

The holes on the base plate are used for mounting it on the poling station. The pull-up springs and the force applying springs can also be seen. The force applying springs can apply a total force equivalent to that of 36 lbs (~ 16 kg), which gave a pressure of 1.6 MPa on 1 cm^2 sample.

Figure 4.24 below gives a closer view of the rods and the springs. As can be seen, the guiding rods do not to touch the base-plate. This decreases the heating effect of the rods, and thus minimizes the heating of the springs, thereby allowing them to maintain their strength. The brass bushings are place on the force-applying plates to allow the rods to slide through the plate. The bushings are tightened using shoulder screws, which allow the bushings to move around horizontally to accommodate for any expansion in the rods of the plate. Extra holes were drilled on the force applying plate to allow for varying the maximum force applied in the future. They can be seen more clearly in Figure 4.25.

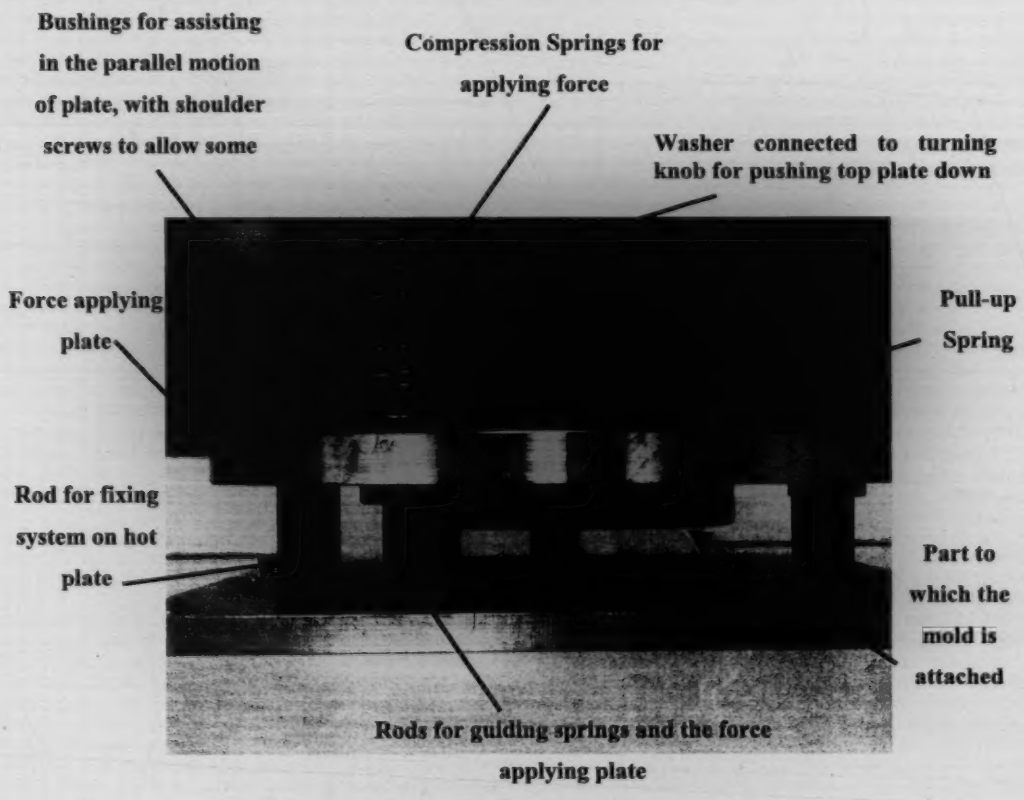
Bushings for assisting in the parallel motion of plate, with shoulder screws to allow some
Compression Springs for applying force
Washer connected to turning knob for pushing top plate down
Force applying plate
Pull-up Spring
Rod for fixing system on hot plate
Part to which the mold is attached
Rods for guiding springs and the force applying plate

Figure 4.24: Close Up of Embossing Machine

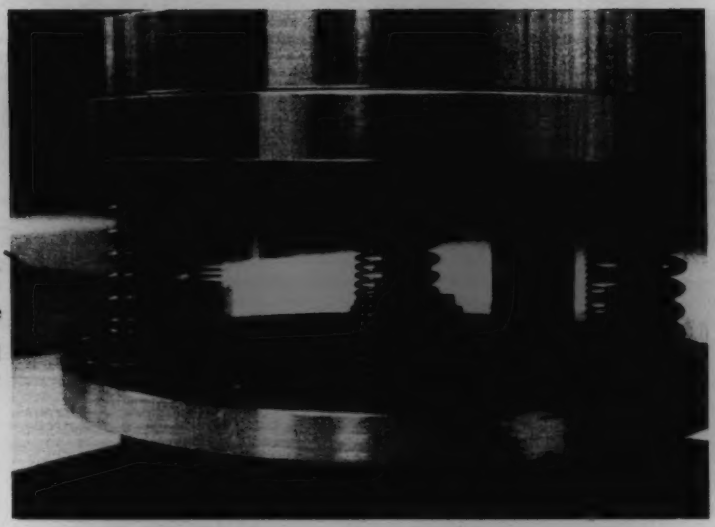

Figure 4.25: Another view of the springs

Figure 4.26 to Figure 4.31, show pictures of the steps in mounting the embossing unit onto the poling station and of the embossing unit at different stages during the embossing process. Finally, Figure 4.32 shows a full look at the embosser. The cover was built such that the poling station could be sealed with the embossing unit attached, in order to allow for embossing under a nitrogen environment.

Figure 4.26: Poling station where the embossing device was mounted

Figure 4.27: Device mounted on Poling Station

Figure 4.28: Extended part of force-applying plate before force is applied

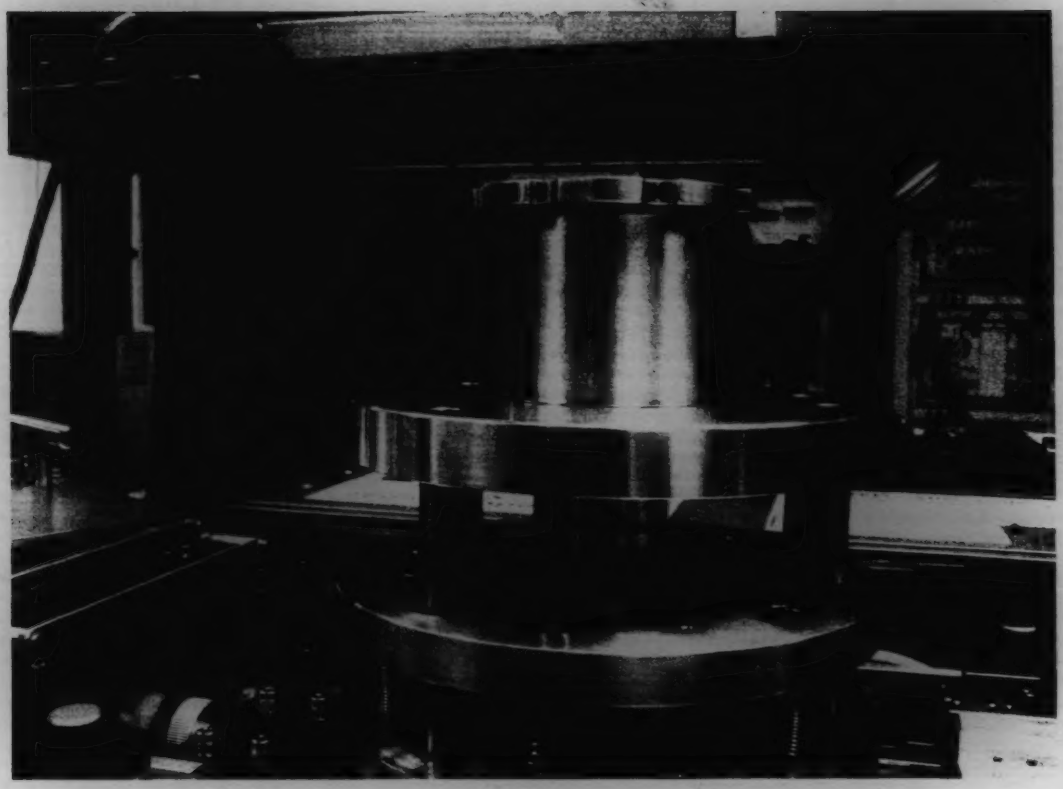

Figure 4.29: Top knob applying force fully

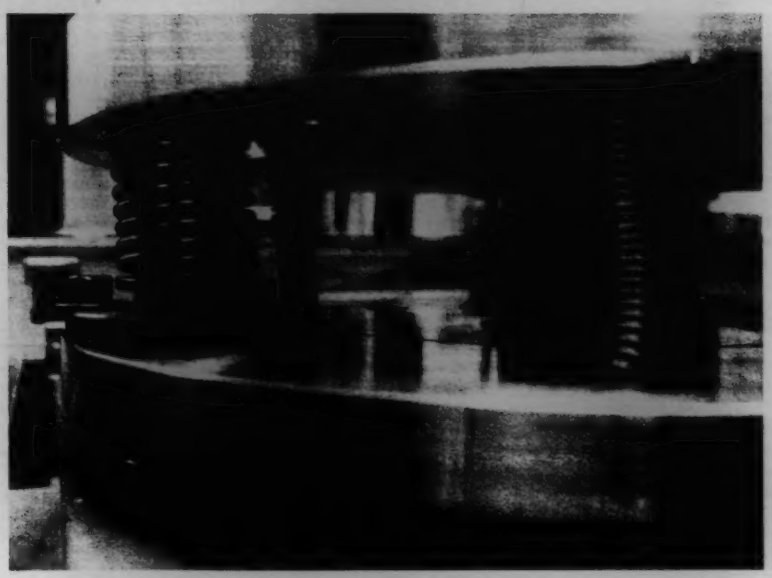

Figure 4.30: Compression springs in the fully compressed state, such that the applied force is maximum

Figure 4.31: Extended part of force applying plate with highest force applied

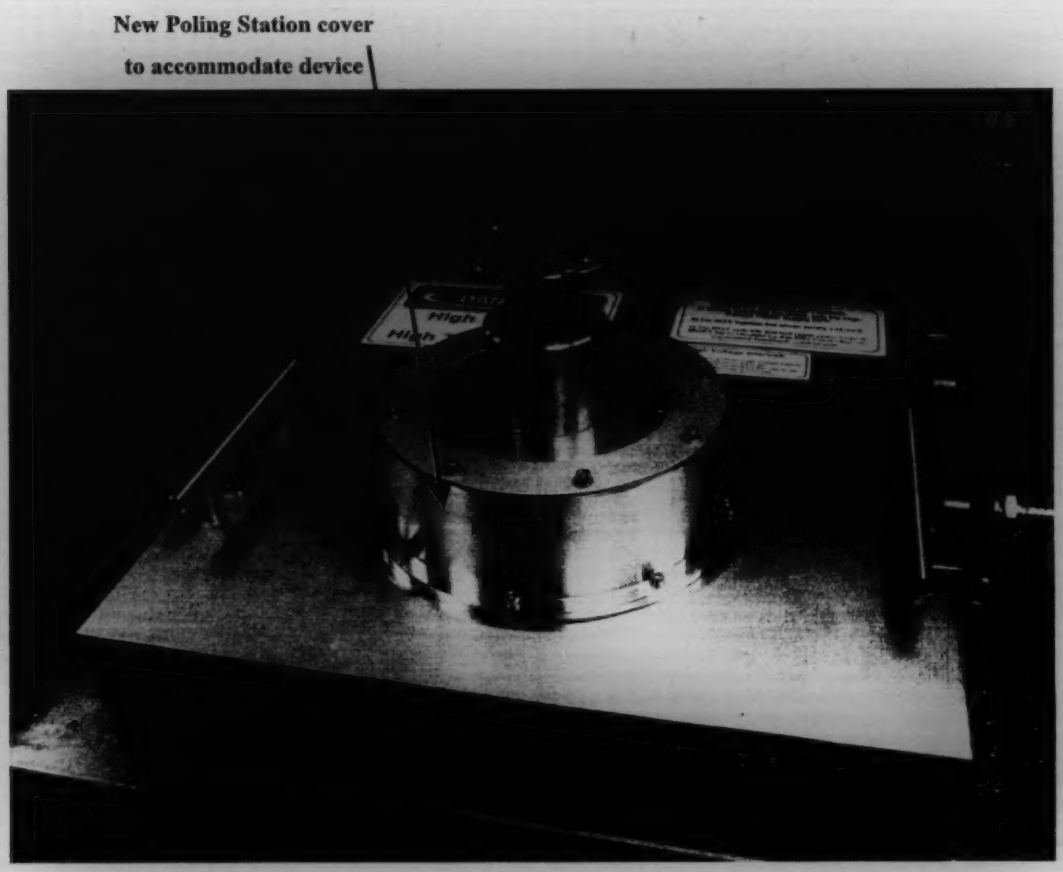

Figure 4.32: The complete embossing setup including: the force applying unit, the poling station, and the cover

The home-made embossing device had several limitations, but it was intended to provide adequate functionality for experimental work. One limitation is it does not allow for the heating of the mold and polymer plates simultaneously. The lower plate is directly heated, and the upper plate is heated through convection. This could lead to a thermal shock when the samples are brought into contact, causing an added strain in the polymer. This effect, however, can be minimized by placing a small contact force before heating the embossing station i.e., bringing the silicon mold in contact with the polymer before the system is heated. The machine also provides no cooling capability, other than through convection. This would usually cause the cooling time to be long, but this was not expected to be a major issue for the experimental work.

Two methods were used to attach the silicon mold and the polymer to opposite plates. The first method employed 4965 (Tesa) double sided tape. However, the double-sided tape suffered from many problems such as not being able to withstand temperatures over 180°C. The tape thickness was specified to be 8 mils (~0.2 mm). Since the features on the mold are in the micrometer range, the tape thickness was considered not thin enough to ensure that the mold and polymer layers are parallel to each other during the embossing process. This could lead to several imprinting non-uniformities. Thickness variation in the tape would cause uneven application of embossing forces across the sample. Several problems also occurred when trying to separate the polymer sample from the tape.

The second method employed Permatex High-Temp silicone to attach the samples to their appropriate plates. Silicone can withstand temperatures of up to approximately 350°C, keeps the silicon and the polymer attached to their plates during the embossing process, and allows for easy removal of the samples from the plates (after embossing) through the application of a small force. Although this method produced the best results, it was important that the silicone layer is as thin as possible, to ensure that the mold and polymer are parallel to each other. A thick, uneven silicone layer led to breaking of the silicon mold and the polymer sample in some cases. Figure 4.33 shows a silicon mold attached to the extended part of the FAP using silicone.

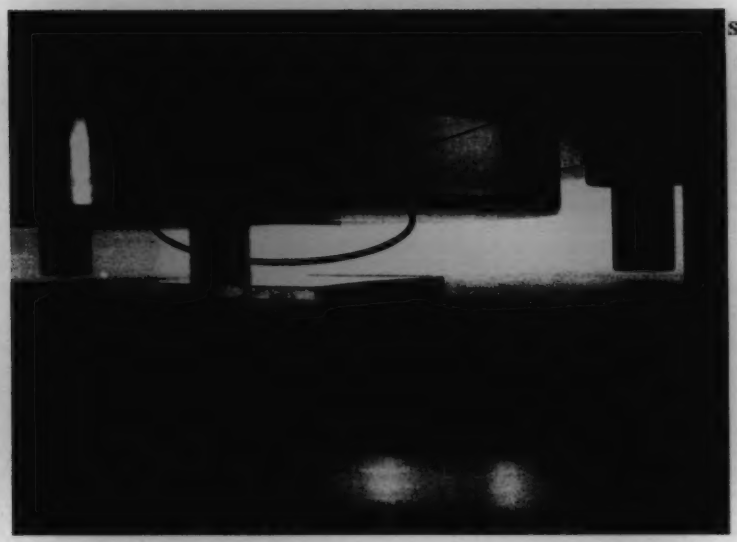

Figure 4.33: Silicon mold attached to embosser plate using Silicone adhesive

With the home-made embosser, the embossing process was typically composed of the following steps.

Step 1: Embossing machine setup: This step included attaching the mold and the polymer sample to opposite plates, covering the embossing station, turning on the nitrogen flow, and ramping the hot plate up to some desired temperature.

Step 2: After the embossing temperature is reached, the force was applied by manually turning the brass knob to compress the springs. Typically, the maximum force was applied for some desired period of time.

Step 3: After the embossing time had passed, the power to the hot plate was turned off and the system would start to cool to room temperature. After the de-embossing temperature was reached, the applied force was released by manually turning the brass knob.

Step 4: The system was left to cool to room temperature. Cooling could be sped up by flowing nitrogen through the system.

Step 5: Once the system had cooled to an appropriate temperature, the polymer sample was removed and inspected.

Step 6: Lubricant was applied to the rod and to the threads of the knob, if needed, in order to avoid any jamming that might occur. The silicon mold and polymer sample were

attached to opposite plates for the next embossing attempt. This process has the disadvantage that it does not allow for fast loading and unloading of the sample, but this was not a major issue for experimentation purposes.

Initial embossing attempts did not produce the results that were expected. After an examination of the system, using an external thermometer, it was discovered that the actual temperature reached by the hot plate was different from the temperature indicated in the software interface. The setup was heated to 360°C for two hours, and the temperature at the top of the base plate was measured and recorded using a *Fluke* Digital Thermometer. This was compared to the displayed temperature, and the results are shown in Table 4.2.

Table 4.2: Difference between the actual and displayed temperature in the embossing station.

Time (h:mm:ss)	Reading °C	Measured °C
13:40	280	131
20:00	370	200
45:00	355	260
1:10:00	354	270
1:57:40	348	278.8

It is important to note that the final temperature displayed by the software interface, fluctuated between 345°C and 375°C, while the temperature measured by the thermometer increased throughout the heating time, but did not reach the set temperature. The temperature measurement was repeated several times, but the temperature recorded at the top of the base plate never surpassed 300°C (maximum reached was 297°C when left for 5 hours). The reason for the difference between the displayed and measured temperature is that the displayed temperature actually shows the temperature measured by a thermocouple located at the bottom of the hot plate (close to the actual heater), which is different then that at the top of the base plate (where the sample is placed for embossing).

Since the glass transition temperature of Torlon is reported to be around 272°C [67], this implies that the embossing runs described earlier were completed at a temperature very close to the glass transition temperature of Torlon. This means that the forced applied

was likely not high enough to get a complete filling at this temperature. In order to obtain good results with this setup, a higher pressure, a longer embossing time, and/or a new heating mechanism would be needed. The results described below, however, show that there is potential to fully emboss structures in fully-cured Torlon with use of the appropriate temperature.

As noted in the datasheet of Torlon AI-10 [67], the properties of the films are improved through heat treatment up to approximately 325°C. These properties include molecular weight (which is increased by full curing), presence of solvent (which is reduced), and the glass transition temperature (which is increased). Embossing of a partially cured sample might therefore assist the embossing process [30, 79, 80], since partially cured films have lower T_g. The embossed structures can then be fully cured after the embossing process. Soft baked (SB) Torlon films were prepared (Section 3.1), with the concentration of the initial solution changed to 30 g of PAI dissolved in 75 ml of DMAC (to allow for a thicker film). The SB film was then embossed used a 1.5 cm x 1.5 cm silicon waveguide mold. The embossing temperature was set to 360°C, and the hold time to 200 minutes. The temperature was monitored and the summary is given in Table 4.3 below, followed by the temperature profile seen in Figure 4.34.

Table 4.3: Embossing of SB Torlon at 360°C for 200 min. T_{read} refers to the temperature read in the poling station's software interface, while T_{TC} gives the temperature measured with the thermometer.

Time	T_{read}	T_{TC}	Event
0:00:00	25.6°C	24.6°C	Start
0:23:00	368°C	265°C	Apply Force
0:57:00	347°C	259°C	
2:00:00	361°C	258°C	
3:07:00	366°C	265°C	
3:24:00	370°C	262.8°C	
3:37:00	315°C	250°C	Ramp Down
3:54:00	214°C	176°C	Separate + leave to cool

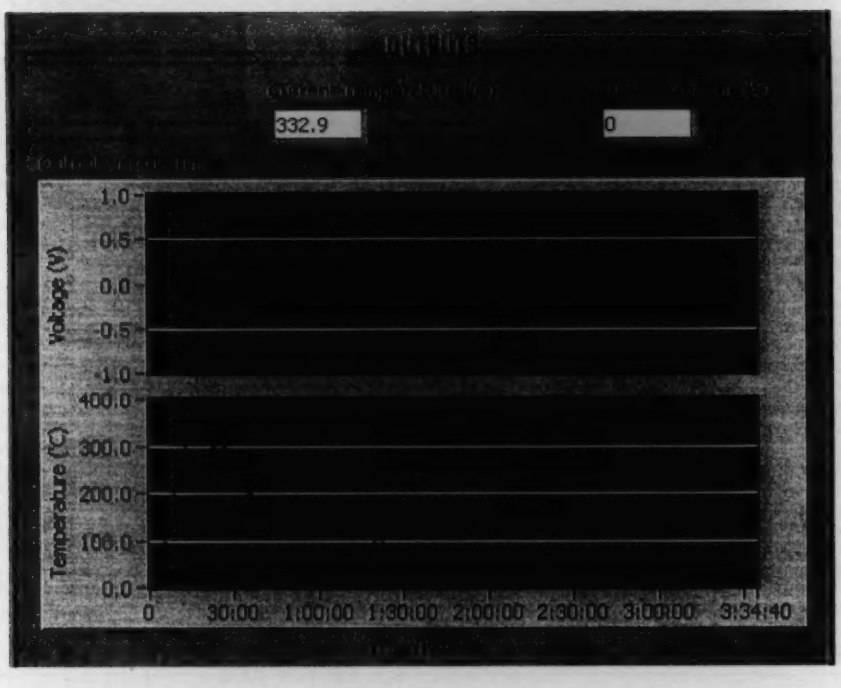

Figure 4.34: Poling Station Profile for Embossing Torlon trenches for 200min

The process parameters are summarized in Table 4.4:

Table 4.4: Summary of the embossing parameters.

Force Applied:	~160 N (with pressure ~ 0.71 MPa)
Duration force applied (t_{hold})	2:59:00
Total time (with heat + cool)	5:27:00
Actual embossing temperature	265°C
Actual de-embossing temperature	176°C

Embossing of the partially cured sample as described resulted in structures that were visible to the naked eye. From examining the PAI polymer under an optical microscope, improvements could be seen over the results described in Section 4.3. Some typical structures are shown in Figure 4.35.

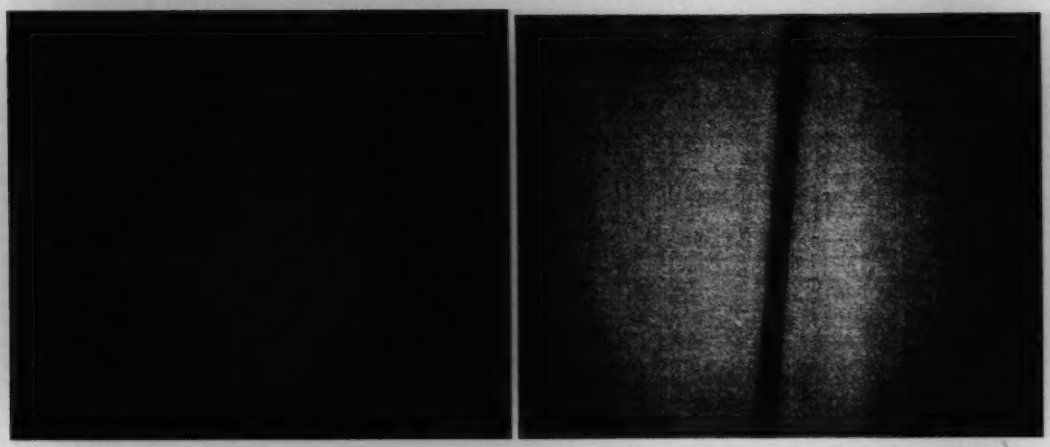

Figure 4.35: Optical microscope view of PAI embossed trenches

From SEM images (Figure 4.36), it could be seen that the trenches produced were deeper than those obtained from embossing fully cured PAI films. While the results were improved, they were still not entirely satisfactory since they still did not fully replicate the structure of the mold (with more vertical sidewalls being expected, for example). Several additional runs were performed, but they gave similar results. Better results were expected if a greater temperature is used or a greater pressure is applied.

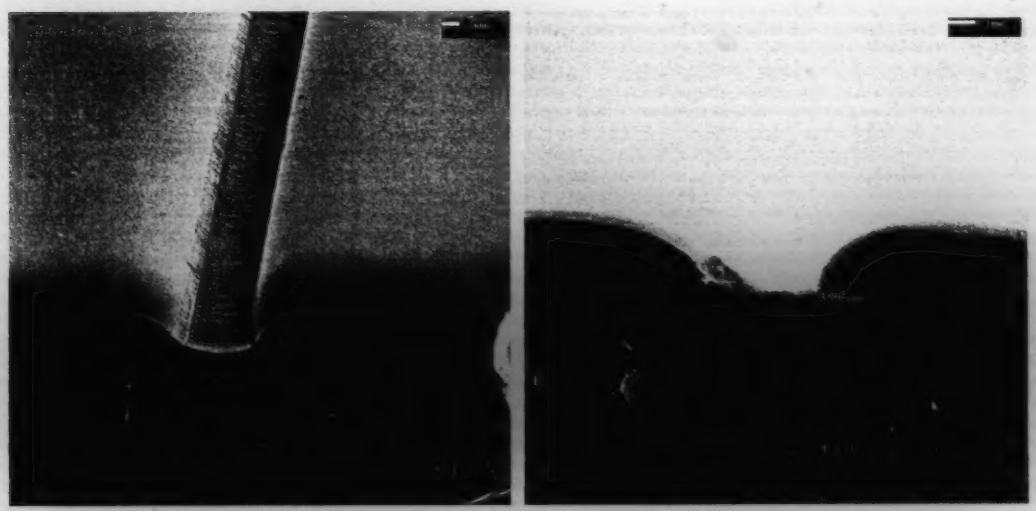

Figure 4.36: PAI embossed trenches.

4.5 *Results obtained by placing the home-made embossing unit in an oven*

In order to emboss at higher temperature, the home-made embossing unit was placed in an oven at the U of A Mechanical Engineering Laboratory (Hotpack Supermatec Oven). This oven could reliably reach a temperature of about 350°C. This allowed for the embossing of Torlon at a temperature higher than possible with the poling station. A small contact force would be placed first, and the embossing unit would then be placed inside the oven. After the temperature (measured using a thermocouple) passed 260°C, the full force was applied. After the embossing time had passed, the oven was shut down and left to cool. The force was typically released when the temperature dropped below 100°C. The setup used is shown in Figure 4.37 - Figure 4.44. The pressure was doubled by placing three extra springs on the main rods (as can be seen in Figure 4.42).

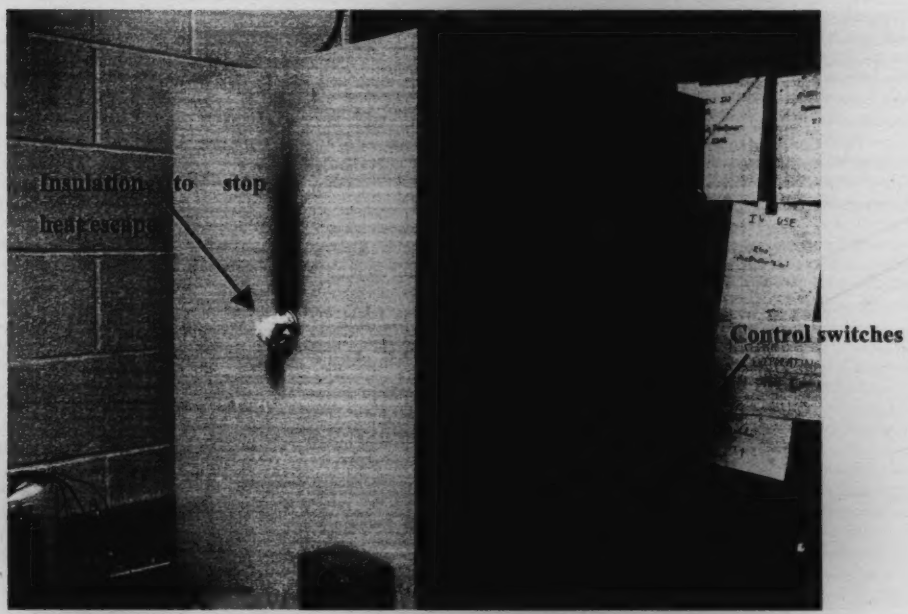

Figure 4.37: Overview of the oven.

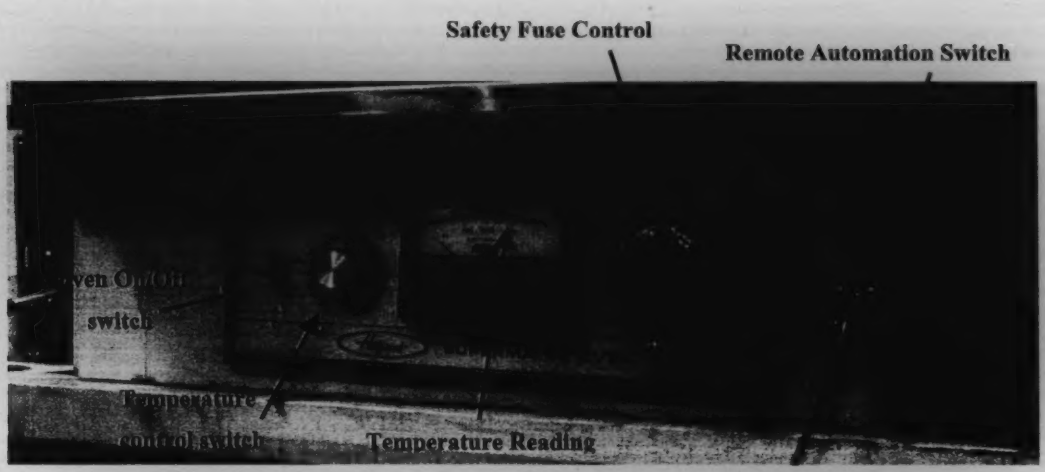

Figure 4.38: Control Switches

Figure 4.39: Temperature Reading (left), Switch and Temperature Control (right)

Figure 4.40: Inside of the Oven

Figure 4.41: Embossing Machine placed in the oven

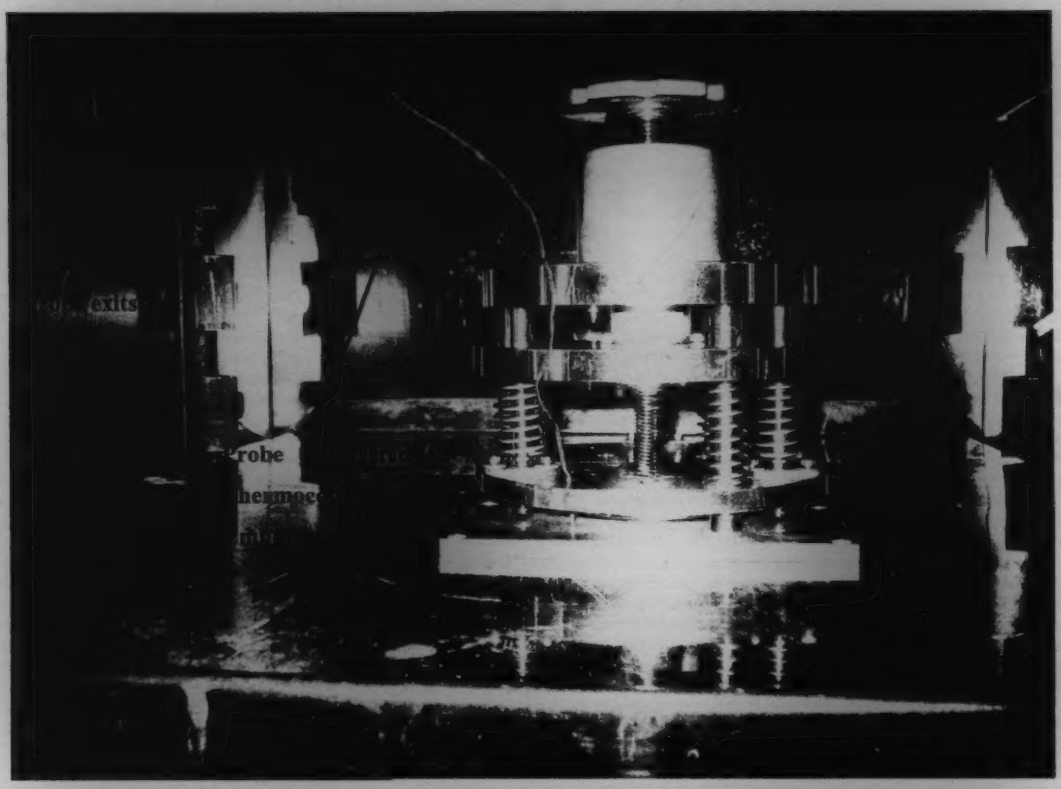

Figure 4.42: Probe connected to embossing machine

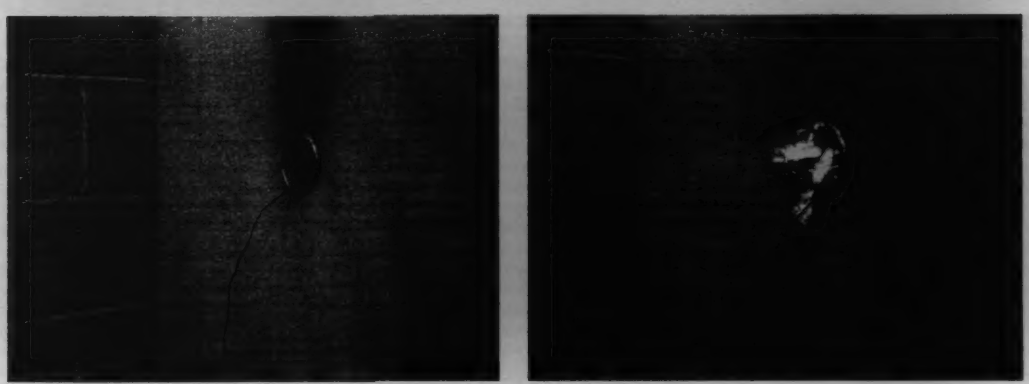

Figure 4.43: Probe opening covered with insulation to avoid heat escape

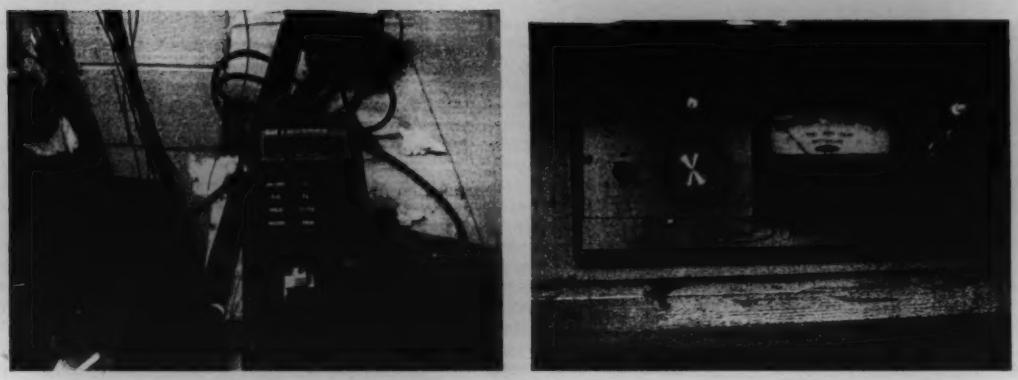

Figure 4.44: Thermocouple (left), Oven turned on (right)

Several embossing attempts were completed, and results were obtained for both fully and partially cured PAI films. In either case, the results were superior to those obtained with the poling station. Figure 4.45 shows that the bottom of the PAI trench has conformed well to the silicon waveguide. A PAI film (prepared with 30 g of PAI and 60 ml of DMAC) was spun on a BCB polymer undercladding on a silicon wafer, and cured at 200°C for 2 hr. It was then embossed using a silicon rib mold at a pressure of ~2.6 MPa for 5 hours, with an embossing temperature of about 330°C.

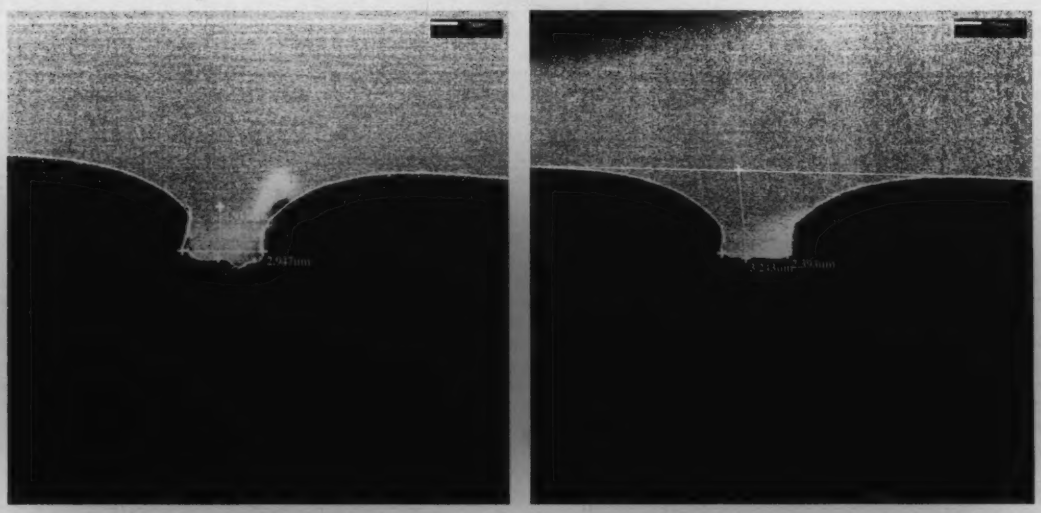

Figure 4.45: Embossed trenches in a PAI film that was cured at 200°C for 2 hours. The embossing pressure, temperature, and time were 2.6 MPa, 328°C, and 5 hours, respectively.

Some results suffered from the breakage of the silicon mold, as is shown in Figure 4.46. This breakage might have been caused by reasons similar to those discussed in Section 4.3.

Figure 4.46: Part of a silicon waveguide mold broken and attached to the PAI trench

Attempts to emboss waveguides on PAI with this setup did not give fully satisfactory results; the results were similar to those described in Sections 4.34.4. One possible way to get better results would be to apply a greater force. Since this would require the replacement of the springs in the embosser unit, a different method was preferred. The home-made embosser was used to emboss SB PAI films at a temperature of 200°C in the oven. The results obtained were inspected by SEM and were similar to previously obtained results (see Figure 4.47 below). The purpose of this run was to explore the possibility of embossing partially cured PAI films at a temperature below 220°C, which is the maximum temperature that can be reached by the Jenoptik HEX01 Embosser available at the Nanofabrication facility at the University of Alberta. The advantage of using this commercial embosser is the possibility to apply forces as high as 20 kN, as opposed to the 320 N reachable by the home-made embosser unit described above.

Figure 4.47: SB PAI trenches embossed at 200°C for 4 hours.

The heating of the embossing unit as a whole, as opposed to just the base plate (as was done when using the poling station), caused some damage to the embossing unit. Lubricant had to be placed on the threads of the knob after every embossing run, or it was found that the knob would get stuck.

4.6 Embossing using a Commercial Embosser

It has been reported that the molecular structure that gives Torlon PAI its high temperature properties makes the fully cured polymer too viscous for some conventional processing techniques [81]. Thus, Torlon is supplied at a relatively low molecular weight in order to facilitate processing [35, 36]. This is why parts fabricated by injection molding need to be cured in order in order to achieve high molecular weight and optimum thermal and mechanical properties. The tests and experiments described in Sections 4.3 - 4.5 showed the potential of embossing soft baked PAI films under conditions that were insufficient for embossing fully cured PAI films. In spite of the limitations of the home-made embossing setup, partially successful embossing runs were completed. Structures were formed by embossing with a force as low as 160 N and at a temperature less than 200°C. These conditions were not sufficient to allow the silicon

mold to totally penetrate the polymer film. However, these tests showed the possibility of using the commercial embossing unit available at the University of Alberta NanoFab (which can reach a maximum temperature of 220°C and can apply a maximum force of up to 20 kN).

Embossing trials were subsequently carried out in the NanoFab at the University of Alberta. These trials employed the HEX01 hot embosser from JENOPTIK Mikrotechnik, shown in Figure 4.48. As mentioned, this machine allows the application of a force as high as 20 kN at a temperature of up to 220°C (with a stability of ±2 K). The typical embossing time is usually set to 5 min. The chamber can be heated from 60°C to 180°C in less than 7 minutes, and cooled by heat conducting oil (this oil is cooled in a reservoir by heat exchange with cooling water) in a similar time. The machine allows for embossing under vacuum; pressure less than 1 mbar can be achieved in less than one minute. The machine also allows for the embossing of a 180 mm substrate, and has a substrate holder designed for samples of this size. However, since it was desired to work with smaller samples, the silicone adhesive described in Section 4.4 was also used here.

Figure 4.48: Jenoptik HEX01 hot embosser

Software routines (macros) must be defined as input to the Jenoptik embosser, in order to set the parameters of the process (refer to Appendix A). Before the embossing process, a standard preparation macro is run in order to stabilize the embossing machine, and bring it to a temperature of 80°C (this is done to reduce the heating and cooling times and to minimize any thermally induced stresses in the material [50]). In a typical embossing run, the Torlon PAI polymer and the silicon mold were diced and mounted on opposite heating plates in the embosser. Another predefined macro that controls the embossing temperature, pressure, and time is then initiated. The embossing chamber is then evacuated before bringing the Si mold in contact with the PAI polymer. This would ensure that no air would be trapped between the mold and sample during the embossing process. After the chamber has been evacuated, the mold and the polymer move towards each other to the point of mutual contact, and a small contact force is applied before heating the samples. This avoids any 'thermal shocks', or other temperature effects that might occur. Once in position, the samples are heated to the set embossing temperature. An embossing temperature of 180°C was typically used. After the top and the bottom heating chucks, to which the silicon mold and polymer are attached, have reached the set temperature, the specified force is applied for the set time. Following this, the temperature is brought down to 80°C, the force released, the samples separated, and the chamber is brought to atmospheric pressure. In some cases, the separation was done close to the embossing temperature. This was noticed not to affect the imprint quality since the only deformation force present is gravity (as discussed in Section 2.3).

Several embossing runs were completed and the results obtained showed considerable improvement over all of the previously described results. Figure 4.49 shows some embossed PAI waveguides. A PAI thin film (prepared by dissolving 25 g of AI-10 Torlon in 100 ml of DMAC, see Section 3.1) was spun coated on BCB and soft baked at 80°C for 3 minutes. A 4 cm^2 sample was diced and embossed at 180°C with a force of 6 kN being applied for 5 minutes. The whole embossing process (from loading the samples to completion of the process) took less than 20 minutes. This helps demonstrate the potential for high throughput with an embossing process. Production of similar waveguides by an etching process would take a much longer time, due to the lithographic patterning and etching steps required in that case.

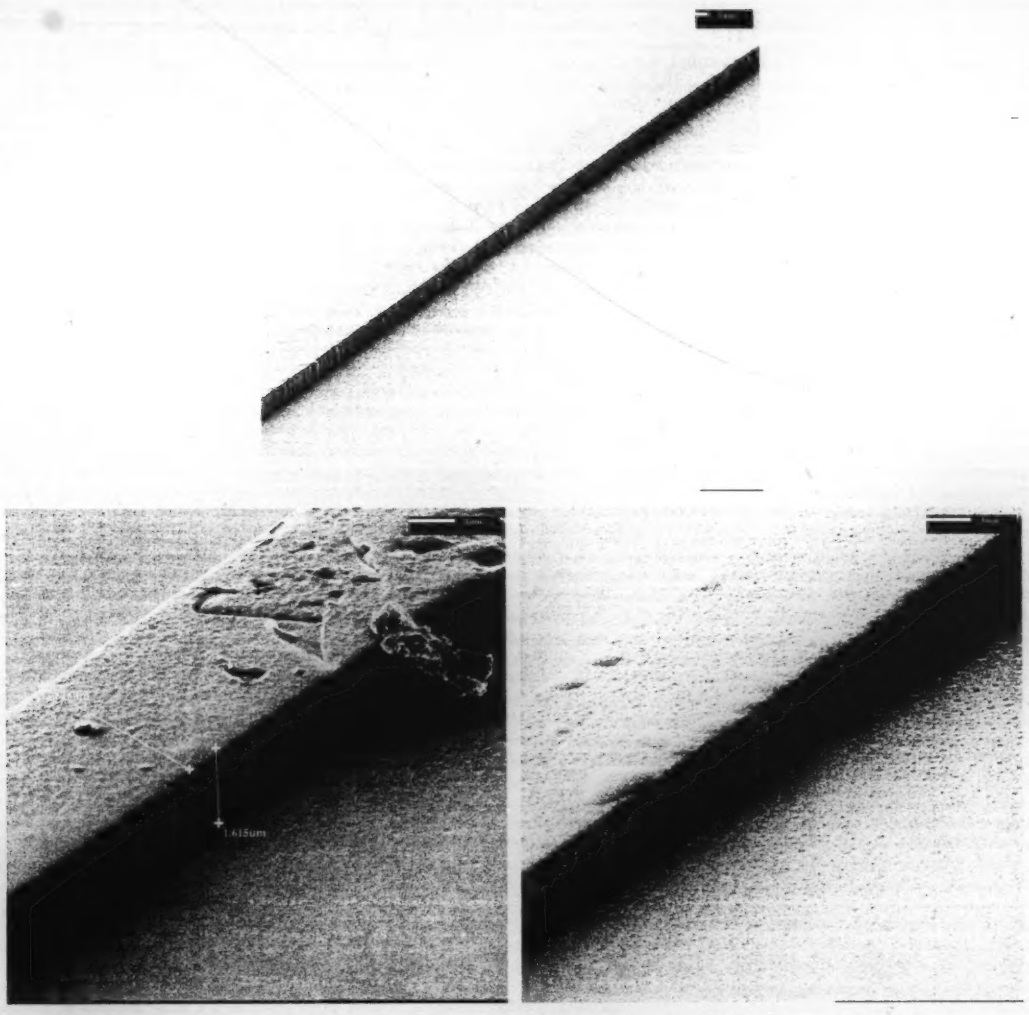

Figure 4.49: Overview of embossed PAI waveguide (top), with close-up view at different locations along the guide (bottom)

The surface roughness is comparable to that obtained through reactive ion etching (see Section 3.1), and is attributed mainly to the surface roughness already present in the silicon mold. A lower surface roughness is attainable through the use of a mold fabricated by a higher resolution technique. The damage that can be seen on the top of the waveguide is possibly due to unwanted particles already present on the silicon mold. It might also have been caused by tearing of some parts of the PAI during separation of the mold and sample, due to incomplete coverage by the silane anti-sticking layer. Proper

cleaning of the silicon mold and improved application of the silane layer is expected to improve the results. The presence of bubble-like structures is likely caused by traces of the solvent present in the partially cured PAI film. Residual solvent might be evaporated during the embossing process (which occurs at high temperatures and low pressure), resulting in the bubbles visible. These bubbles might be eliminated by proper reflow of the Torlon PAI sample after the embossing process.

PAI trenches with vertical edges were also realized; the verticality was much improved compared to the trenches described in Sections 4.3 to 4.5. Figure 4.50 shows SEM images of some embossed trenches that were produced with a force of 3 kN applied for 5 minutes at 180°C.

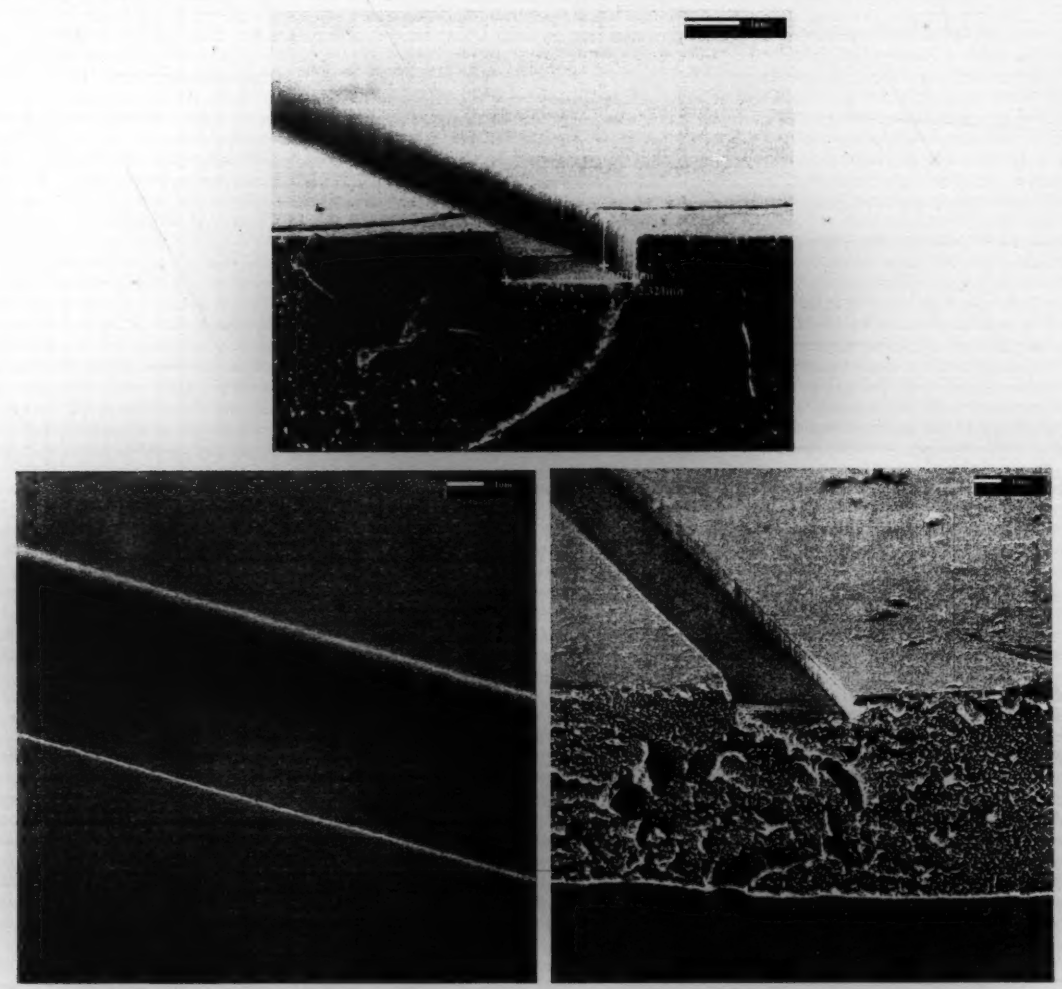

Figure 4.50: Embossed PAI trenches at 3001N and 180°C

The embossing process successfully imprinted other features, such as circular markers and numbers that were present on the silicon mold. This can be seen in Figure 4.51, and shows great promise for embossing of more complex features in PAI.

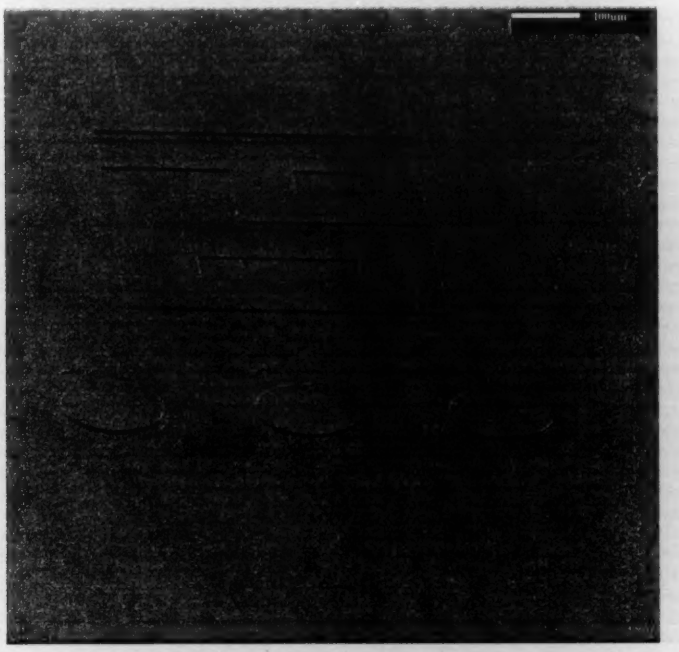

Figure 4.51: Embossed numerical and circular markers on PAI film.

Several promising waveguides and trenches with sidewall roughness better than those obtained using reactive ion etching technique were produced. This work represents the first study of embossing Torlon PAI, and complements other recent studies on the embossing of partially cured, high T_g polymers [30, 79, 80].

It was found that care must be taken when applying the silicone adhesive. The use of an improper amount can lead to unevenness of the force, which would usually lead to the breaking of both the silicon mold and the PAI sample. Lack of knowledge of how the properties of PAI film vary with baking created a limitation on the control of the embossed results. Results that were obtained with the embossing parameters described are also dependent on the Torlon PAI film thickness and curing conditions. In order to

achieve full control over the process, additional information is needed about how the viscosity and glass transition temperature of PAI vary with curing conditions. Finally, while the waveguides obtained show lower surface roughness in SEM images, loss measurements are yet to be completed and are needed to give a quantitative assessment of the quality of the embossed structures.

Chapter 5 Conclusion & Future Work

The main objective of this work was to characterize and study polyamide-imide (PAI) waveguides, and to study and analyze the possibility of fabricating structures on PAI using the hot embossing lithography. Although a full characterization of the embossing process was not completed, the results obtained show great promise for embossing and nanoimprint lithography of PAI.

In summary, **the results described in this thesis will hopefully be a driving factor for continuing research on Torlon PAI polymer and hot embossing lithography.**

The following sections discuss some of the key conclusions derived from this work, and provide suggestions for future work.

5.1 Polyamide-imide waveguides

With a refractive index of about 1.66, PAI has the prospect of being used for the fabrication of high index contrast waveguides. Its glass transition temperature of about 280°C makes it one of the few polymers that can perform in applications where a high thermal stability is needed. Previous work [32, 37] involved a study of the processing conditions of PAI films and waveguides. In this research, some loss measurements were completed, and they agreed with previously obtained results.

Thermal reflow was used to reduce the sidewall roughness in PAI waveguides. The waveguides were reflowed under different conditions and it was found that the reduction in sidewall roughness is related to reflow temperature and time. Reflow is expected to significantly reduce the losses in PAI waveguides, which are partly caused by surface roughness. Light was coupled through the reflowed waveguides, which shows that the process did not damage the waveguides. Further experiments and runs are needed to get a complete understanding of the relationship between the reflow temperature and time, and the resulting reduction in roughness. Also it is important to complete a quantitative assessment and test on the reflow process by measuring the optical losses vs the applied temperature or time.

The transmission spectrum of PAI waveguides were then measured using a spectrum analyzer, and compared to previous results obtained by measuring the absorption

spectrum of PAI thin films. The results seemed to agree, and the resulting peaks were matched to values of vibrational overtones in the literature. This would give us an understanding of the composition of PAI polymer, which is important for knowing the causes of losses in PAI waveguides. Additional runs need to be completed with waveguides of varying dimensions in order to confirm the results obtained.

Further work on characterization of PAI should include tests that ensure that the waveguides fulfill the requirements developed for telecommunication network devices [1]. One of the important tests that needs to be completed is the thermal stability test, where the PAI waveguide is placed in an environmental chamber at an elevated temperature for a prolonged period of time. The thermal stability is then verified by monitoring the refractive index or loss during the high temperature storage [1, 14, 28, 29].

5.2 Embossing

Embossing of waveguides on polyamide-imide polymer is intended to allow for the fabrication of high performance waveguides (polyamide-imide) using a high throughput technique. Although the process has not been fully characterized, several satisfactory results were obtained by embossing partially cured Torlon PAI films. The results obtained show the great promise of using this technique for the rapid production of waveguides with low surface roughness in just one step.

Due to the limitations in the equipment used for embossing, embossing of fully cured samples did not give complete results. It is proposed that future work on embossing of PAI should be focused on the issues described in the following sub-sections.

5.2.1 Viscosity and other thermal properties

Detailed information about Torlon's flow and other viscoelastic properties is essential in order to choose the optimum pressure and processing temperature for the hot embossing process [46, 78]. Knowledge of the variation in viscosity with temperature, for example, would allow us to determine at which temperature Torlon PAI would have the maximum flow. Some studies have reported that the melt viscosity of polyamide-imide would decrease until a certain temperature and then would increase. This increase in viscosity

when the temperature is increased over a certain limit is caused by chain extensions in the polymer resulting in the decrease of flow with further temperature increase [81].

Different techniques have been used for the measurement of viscosity, depending on the temperature range of interest (below, around, or above the glass transition temperature). Typical techniques for measuring viscosity and other rheological properties of PAI include the rotation disk viscometer [52], rheometrics Dynamic Spectrometer (RDS) [33], thermo-gravimetric analysis, differential scanning calorimetric analysis [33], as well as various other techniques [51].

The viscosity of polymers varies not only with the temperature, but also with the molecular weight [2]. Even though no numerical values are currently reported for the molecular weight of Torlon, several papers have reported techniques on how to measure the molecular weight of thermoplastic polymers. It is known however that Torlon will cure and increase in molecular weight with temperature, time and residual solvent, as was mentioned earlier. It will also start to cross-link above 250°C [35]. Thus knowledge of the molecular weight of Torlon and how it relates to viscosity will be useful. Knowledge of the glass transition temperature and how it varies with curing will also be very beneficial especially if we wish to continue to explore embossing of PAI below the reported glass transition temperature.

5.2.2 Embossing above Tg and Process Control

Several interesting and satisfactory results have been obtained by embossing Torlon PAI polymer at a temperature below its known glass transition temperature. This technique helps avoid several problems that might arise when embossing at elevated temperature, such as increased film stress that can be caused due to the elevated thermal cycles. However, while continuing experimentation with partially cured PAI polymer samples is very interesting, it would also be important to explore embossing at temperatures above Tg.

Embossing a polymer above its glass transition temperature would allow the polymer to fill the cavities of the mold in a shorter time. Due to the reduced viscosity at high temperature, the polymer can flow easier, which would reduce any voids that might occur. Based on several reports, the ideal embossing temperature is between 80°C and 100°C

above the glass transition temperature [78]. Thus for PAI, the ideal temperature would be between 370°C [35] and 377°C (650°F, which was reported as the temperature where maximum spiral flow of one class of Torlon occurs [81]). A study of viscosity is needed as mentioned above, in order to determine the optimal temperature for embossing cured PAI films.

It was reported that using non-isothermal heating of the mold and polymer produced better results in many cases [57, 59]. This is yet to be tested, but is expected to decrease the dependence of the replication accuracy on the processing conditions [59], which would be very useful when moving into mass production.

Issues such as the process control should also be considered, since they affect the final product accuracy and variation [43]. Thus a study of the variability of embossed features fabricated with nominally identical embossing condition would be useful for establishing the repeatability of the embossing process [42]. This study is needed in order to understand the origins of variations and to develop means for their minimization, which is very important if this technique is to be used for full-scale production. Different criteria that can be used for quality assessment have already been discussed in section 2.3.8.7.

Several results obtained in this research showed local inhomogeneity that was attributed to the imperfect alignment between the mold and the sample. This led to an uneven distribution of pressure during imprinting. The unevenness could have been caused by the presence of dust particles, the uneven or excess placement of silicone adhesive, or the influence of the edges of the stamp and polymer pieces [82]. Ways to limit this should be studied and care should be taken when preparing the silicon stamp to ensure it is totally clean. Although the silicone method was found to be very effective, great care must also be taken when applying adhesives.

5.2.3 Reflow and using PAI as a mold

Torlon PAI waveguides fabricated by hot embossing exhibited a lower sidewall roughness (by visual inspection of SEM images) than those fabricated by a reactive ion etching process. The resulting sidewall roughness could be reduced further through the thermal reflow of the embossed samples. Thermal reflow of embossed polymer has been

reported and it was found that the roughness transferred to the polymer from the mold was significantly reduced [2].

Also of interest for future work, the embossed and reflowed Torlon waveguide could be used as the mold during further embossing of soft baked Torlon samples. The embossing process could be performed at a temperature high enough to allow the partially cured film to flow, but lower than the glass transition temperature of the fully cured mold in order to avoid the flowing and distortion of the mold (since it would be too viscous to flow). This would allow the high throughput fabrication of PAI waveguides with very low sidewall roughness. An ASL can be deposited on the Torlon mold to ensure it does not adhere with the Torlon film to be embossed. In the case where peeling off still occurs, a thin layer of SiO_2 can be deposited on the Torlon mold before the application of the ASL layer [30]. The Torlon mold, having been fully cured, would be much harder than the soft baked PAI film. It is reported that polymers (used as the mold in embossing) with a compression modulus of 2 MPa limit the achievable resolution to >100 nm, while those with a modulus of 9 MPa can achieve a resolution of 50 nm. This demonstrates the need of an even harder mold to enable embossing of structures at a small scale [83]. PAI Torlon is known to have a very high compression modulus of 5.3 GPa [36], which should allow for the successful embossing [83] of very high resolution structures unachievable with other polymer molds. Such a high modulus is needed to ensure that the mold retains its structure after the embossing process. Obviously, PAI Torlon might also be used in the future to emboss other polymers. The hardness of the PAI Torlon structure to be used as the mold is also important [2, 84] and can be measured using a Nanoindenter [16].

Such an implementation might reduce the surface roughness of the embossed waveguides. This is because the Torlon PAI mold would have a lower surface roughness than the silicon mold, due to the effect of thermal reflow. New structures embossed with this mold would consequentially have a lower surface roughness. Distortion and stresses would also be reduced, since the mold and the polymer, being both from PAI Torlon, would have the same thermal expansion coefficient.

5.2.4 Variation of the embossing tool

During the embossing runs performed, it was noticed that the stamp was filled at certain locations faster than at others. While this could simply have been caused by the unevenness in the pressure discussed earlier, it can also be caused by the geometry and structure distribution of the mold. Several studies considered the effect that the mold design and distribution of structures have on the completion of the embossing process [46, 85]. Several papers concentrated on improving the filling of the mold and the flow of the polymer through optimization of the stamp design [86] and of the structure distribution on the mold [2]. For example, it was discovered that, when embossing small features, best results were obtained with periodic mold patterns [78]. Future embossing trials on more complex structures and optical devices, such as a Torlon PAI microring resonator, would need to take these issues into account.

5.2.5 Simulations

Simulations would be needed to capture the physics of the polymer flow for differing mold dimensions and embossing conditions. This would allow the tailoring of tool geometry and embossing conditions, rather then relying on trial-and-error experimentation [86]. It might also allow the desired results to be obtained more quickly, and save experimental time. The Torlon PAI flow could be simulated by using finite element method (FEM) using the MARC program [87], or other commercially available simulation programs. The simulation results can later be compared to experimental results in order to test the theory. This would help in determining the exact parameters for a completed embossing process, which can sometimes be very difficult to determine by experiment alone.

5.2.6 Uses for the embossing station built

The desktop embossing machine that was built could become very useful with some modifications. One simple modification would be to add a handle to the knob. This would allow us to apply and retract the force without the need of gloves (due to the elevated

temperature of the knob). The machine also suffered degradations due to the heating and cooling cycles. This could be solved through the use of more compatible materials in the machine, such as making the majority of the parts from stainless steel. This would reduce the effects that the difference in the thermal expansion coefficients between the different materials used (brass, aluminum, and stainless steel) has on the machine. A hot plate could also be added, so that no external heat source would be required.

This home-made machine might enable the embossing of non-standard materials, which cannot be used in the embossing machine available at the university (due to toxicity and other issues). The machine also offers more flexibility when compared to the commercially available embossing machine.

Bibliography

[1] H. Ma, A. K. Y. Jen, and L. R. Dalton, "Polymer-based optical waveguides: Materials, processing, and devices," *Advanced Materials,* vol. 14, pp. 1339-1365, Oct 2 2002.

[2] L. J. Guo, "Recent progress in nanoimprint technology and its applications," *Journal of Physics D-Applied Physics,* vol. 37, pp. R123-R141, Jun 7 2004.

[3] A. F. Benner, H. F. Jordan, and V. P. Heuring, "Digital Optical Computing with Optically Switched Directional-Couplers," *Optical Engineering,* vol. 30, pp. 1936-1941, Dec 1991.

[4] V. P. Gladkii, V. A. Nikitin, V. P. Prokhorov, and N. A. Yakovenko, "Waveguide optoelectronic components for devices used in functional processing of digital information.," *Kvantovaya Elektronika,* vol. 22, pp. 1027-1033, Oct 1995.

[5] M. Lawrence, "Lithium-Niobate Integrated-Optics," *Reports on Progress in Physics,* vol. 56, pp. 363-429, Mar 1993.

[6] I. B. Sohn, M. S. Lee, J. S. Woo, S. M. Lee, and J. Y. Chung, "Fabrication of photonic devices directly written within glass using a femtosecond laser," *Optics Express,* vol. 13, pp. 4224-4229, May 30 2005.

[7] S. Takahashi, "Fibers for Optical Communications," *Advanced Materials,* vol. 5, pp. 187-191, Mar 1993.

[8] J. L. Pan, J. E. Mcmanis, T. Osadchy, L. Grober, J. M. Woodall, and P. J. Kindlmann, "Gallium arsenide deep-level optical emitter for fibre optics," *Nature Materials,* vol. 2, pp. 375-378, Jun 2003.

[9] L. Eldada, "Polymer integrated optics: Promise vs. practicality," San Jose, CA, United States, 2002, pp. 11-22.

[10] A. T. Fiory and N. M. Ravindra, "Light emission from silicon: Some perspectives and applications," *Journal of Electronic Materials,* vol. 32, pp. 1043-1051, Oct 2003.

[11] H. Wong, "Recent developments in silicon optoelectronic devices," *Microelectronics Reliability,* vol. 42, pp. 317-326, Mar 2002.

[12] J. K. S. Poon, Y. Y. Huang, G. T. Paloczi, and A. Yariv, "Soft lithography replica molding of critically coupled polymer microring resonators," *Ieee Photonics Technology Letters,* vol. 16, pp. 2496-2498, Nov 2004.

[13] Y. Y. Huang, G. T. Paloczi, A. Yariv, C. Zhang, and L. R. Dalton, "Fabrication and replication of polymer integrated optical devices using electron-beam lithography and soft lithography," *Journal of Physical Chemistry B,* vol. 108, pp. 8606-8613, Jun 24 2004.

[14] T. Watanabe, N. Ooba, S. Hayashida, T. Kurihara, and S. Imamura, "Polymeric optical waveguide circuits formed using silicone resin," *Journal of Lightwave Technology,* vol. 16, pp. 1049-1055, Jun 1998.

[15] J. Jiang, C. L. Callender, C. Blanchetiere, S. Jacob, J. P. Noad, J. F. Ding, Y. H. Qi, and M. Day, "Optimizing fluorinated poly(arylene ether)s for optical waveguide applications," *Optical Materials,* vol. 28, pp. 189-194, Feb 2006.

[16] W. H. Wong, J. Zhou, and E. Y. B. Pun, "Low-loss polymeric optical waveguides using electron-beam direct writing," *Applied Physics Letters,* vol. 78, pp. 2110-2112, Apr 9 2001.

[17] C. Y. Chao and L. J. Guo, "Polymer microring resonators fabricated by nanoimprint technique," *Journal of Vacuum Science & Technology B,* vol. 20, pp. 2862-2866, Nov-Dec 2002.

[18] R. Moosburger, G. Fischbeck, C. Kostrzewa, and K. Petermann, "Digital optical switch based on 'oversized' polymer rib waveguides," *Electronics Letters,* vol. 32, pp. 544-545, Mar 14 1996.

[19] B. Michel, A. Bernard, A. Bietsch, E. Delamarche, M. Geissler, D. Juncker, H. Kind, J. P. Renault, H. Rothuizen, H. Schmid, P. SchmidtWinkel, R. Stutz, and H. Wolf, "Printing meets lithography: Soft approaches to high-resolution patterning (vol 45, pg 697, 2001)," *Ibm Journal of Research and Development,* vol. 45, pp. 870-870, Nov 2001.

[20] H. A. Biebuyck, N. B. Larsen, E. Delamarche, and B. Michel, "Lithography beyond light: Microcontact printing with monolayer resists," *Ibm Journal of Research and Development,* vol. 41, pp. 159-170, Jan-Mar 1997.

[21] C. Y. Chao and L. J. Guo, "Thermal-flow technique for reducing surface roughness and controlling gap size in polymer microring resonators," *Applied Physics Letters,* vol. 84, pp. 2479-2481, Apr 5 2004.

[22] Z. Y. Zhang, G. Z. Xiao, and C. P. Grover, "Volume relaxation in polymers and its effect on waveguide applications," *Applied Optics,* vol. 43, pp. 2325-2331, Apr 10 2004.

[23] J. T. Kim, C. G. Choi, and H. K. Sung, "Polymer planar-lightwave-circuit type variable optical attenuator fabricated by hot embossing process," *Etri Journal,* vol. 27, pp. 122-125, Feb 2005.

[24] M. Zhou, "Low-loss polymeric materials for passive waveguide components in fiber optical telecommunication," *Optical Engineering,* vol. 41, pp. 1631-1643, Jul 2002.

[25] J. Jiang, C. L. Callender, C. Blanchetiere, J. R. Noad, S. G. Chen, J. Ballato, and D. W. Smith, "Property-tailorable PFCB-containing polymers for wavelength division devices," *Journal of Lightwave Technology,* vol. 24, pp. 3227-3234, Aug 2006.

[26] E. P. Ivanova, M. Papiernik, A. Oliveira, I. Sbarski, T. Smekal, P. Grodzinski, and D. V. Nicolau, "Feasibility of using carboxylic-rich polymeric surfaces for the covalent binding of oligonucleotides for microPCR applications," *Smart Materials & Structures,* vol. 11, pp. 783-791, Oct 2002.

[27] N. Yurt, K. Mune, R. Naito, T. Fukuoka, A. Mochizuki, K. Matsumoto, G. Meredith, N. Peyghambarian, and G. E. Jabbour, "Fabrication and characterization of low-loss optical waveguides using a novel photosensitive polyimide," *Journal of Lightwave Technology,* vol. 23, pp. 1291-1294, Mar 2005.

[28] J. W. Kang, J. P. Kim, J. S. Lee, and J. J. Kim, "Structure-property relationship of fluorinated co-poly(arylene ether sulfide)s and co-poly(arylene ether sulfone)s for low-loss and low-birefringence waveguide devices," *Journal of Lightwave Technology,* vol. 23, pp. 364-373, Jan 2005.

[29] T. Matsuura, S. Ando, S. Matsui, S. Sasaki, and F. Yamamoto, "Heat-resistant singlemode optical waveguides using fluorinated polyimides," *Electronics Letters,* vol. 29, pp. 2107-2109, 1993.

[30] B. Cui, Y. Cortot, and T. Veres, "Polyimide nanostructures fabricated by nanoimprint lithography and its applications," *Microelectronic Engineering,* vol. 83, pp. 906-909, Apr-Sep 2006.

[31] T. Takasaki, Y. Kuwana, T. Takahashi, and S. Hayashida, "Synthesis and optical properties of polyimides," *Journal of Polymer Science Part a-Polymer Chemistry,* vol. 38, pp. 4832-4838, 2000.

[32] R. M. Bryce, H. T. Nguyen, P. Nakeeran, T. Clement, C. J. Haugen, R. R. Tykwinski, R. G. DeCorby, and J. N. McMullin, "Polyamide-imide polymer thin films for integrated optics," *Thin Solid Films,* vol. 458, pp. 233-236, Jun 30 2004.

[33] M. H. Y. Kil-Yeong Choi, "Synthesis and characterization of N-alkylated polyamide-imides." vol. 222, 1994, pp. 103-109.

[34] P. G. Kelleher, "Report on the state of the art. Injection molding of fiber reinforced thermoplastics. Part I. Materials and processes," *Advances in Polymer Technology,* vol. 10, pp. 219-230, 1990.

[35] "Injection Molding Guide ". vol. 2006: Solvay Advanced Polymers.

[36] "4301 Product Data." vol. 2006: Solvay Advanced Polymers, 2002.

[37] R. M. Bryce, "Photonic Devices in Chalcogenide Glass," in *Electrical and Computer Engineering*. vol. M.Sc. Edmonton: University of Alberta, September 2003.

[38] M. M. Pai, "Microphotonic device fabrication in silver photodoped chalcogenide glasses and polymers " in *Electrical and Computer Engineering*. vol. M.Sc. Edmonton: University of Alberta, 2006.

[39] S. O. Kasap, *Optoelectronics and photonics : principles and practices*. Upper Saddle River, NJ: Prentice Hall, 2001.

[40] W. Groh, "Overtone Absorption in Macromolecules for Polymer Optical Fibers," *Makromolekulare Chemie-Macromolecular Chemistry and Physics,* vol. 189, pp. 2861-2874, Dec 1988.

[41] S. Y. Chou and P. R. Krauss, "Imprint lithography with sub-10 nm feature size and high throughput," *Microelectronic Engineering,* vol. 35, pp. 237-240, Feb 1997.

[42] D. E. Hardt, B. Ganesan, M. Dirckx, G. Shoji, K. Thaker, and W. Qi, "Process Variability in Micro-Embossing," *Singapore MIT Alliance Programme in Innovation in Manufacturing Systems and Technology,* January 2005.

[43] D. E. Hardt, B. Ganesan, W. Qi, M. Dirckx, and A. K. Rzepniewski, "Process Control in Micro-Embossing: A Review," *Singapore MIT Alliance Programme in Innovation in Manufacturing Systems and Technology,* January 2004.

[44] W. Jordan, "Using embossing to create a fiber reinforced honeycomb composite," *Journal of Engineering Materials and Technology-Transactions of the Asme,* vol. 127, pp. 257-262, Apr 2005.

[45] Q. F. Xia, C. Keimel, H. X. Ge, Z. N. Yu, W. Wu, and S. Y. Chou, "Ultrafast patterning of nanostructures in polymers using laser assisted nanoimprint lithography," *Applied Physics Letters,* vol. 83, pp. 4417-4419, Nov 24 2003.

[46] L. J. Heyderman, H. Schift, C. David, J. Gobrecht, and T. Schweizer, "Flow behaviour of thin polymer films used for hot embossing lithography," *Microelectronic Engineering,* vol. 54, pp. 229-245, Dec 2000.

[47] M. Heckele, "Hot embossing - A flexible and successful replication technology for polymer MEMS," San Jose, CA., United States, 2004, pp. 108-117.

[48] X. J. Shen, L. W. Pan, and L. W. Lin, "Microplastic embossing process: experimental and theoretical characterizations," *Sensors and Actuators a-Physical,* vol. 97-8, pp. 428-433, Apr 1 2002.

[49] L. Lin, Y. T. Cheng, and C. J. Chiu, "Comparative study of hot embossed micro structures fabricated by laboratory and commercial environments," *Microsystem Technologies,* vol. 4, pp. 113-116, May 1998.

[50] H. Becker and U. Heim, "Hot embossing as a method for the fabrication of polymer high aspect ratio structures," *Sensors and Actuators a-Physical,* vol. 83, pp. 130-135, May 22 2000.

[51] Y. J. Juang, L. J. Lee, and K. W. Koelling, "Hot embossing in microfabrication. Part II: Rheological characterization and process analysis," *Polymer Engineering and Science,* vol. 42, pp. 551-566, Mar 2002.

[52] H. Kobayashi, H. Takahashi, and Y. Hiki, "Viscosity measurement of organic glasses below and above glass transition temperature," *Journal of Non-Crystalline Solids,* vol. 290, pp. 32-40, Sep 2001.

[53] S. Matsui, Y. Igaku, H. Ishigaki, J. Fujita, M. Ishida, Y. Ochiai, H. Namatsu, and M. Komuro, "Room-temperature nanoimprint and nanotransfer printing using hydrogen silsequioxane," *Journal of Vacuum Science & Technology B,* vol. 21, pp. 688-692, Mar-Apr 2003.

[54] N. Roos, H. Schulz, L. Bendfeldt, M. Fink, K. Pfeiffer, and H. C. Scheer, "First and second generation purely thermoset stamps for hot embossing," *Microelectronic Engineering,* vol. 61-2, pp. 399-405, Jul 2002.

[55] N. Roos, H. Schulz, M. Fink, K. Pfeiffer, F. Osenberg, and H. C. Scheer, "Performance of 4" wafer-scale thermoset working stamps in hot embossing lithography," Santa Clara, CA, USA, 2002, pp. 232-9.

[56] N. Roos, M. Wissen, T. Glinsner, and H.-C. Scheer, "Impact of vacuum environment on the hot embossing process," Santa Clara, CA, United States, 2003, pp. 211-218.

[57] N. Roos, T. Luxbacher, T. Glinsner, K. Pfeiffer, H. Schulz, and H. C. Scheer, "Nanoimprint lithography with a commercial 4 inch bond system for hot embossing," Santa Clara, CA, 2001, pp. 427-435.

[58] L. J. Lee, M. J. Madou, K. W. Koelling, S. Daunert, L. Siyi, K. Chee Guan, J. Yi-Je, L. Yumin, and Y. Liyong, "Design and fabrication of CD-like microfluidic platforms for diagnostics: polymer-based microfabrication," *Biomedical Microdevices,* vol. 3, pp. 339-51, 2001.

[59] Y. J. Juang, L. J. Lee, and K. W. Koelling, "Hot embossing in microfabrication. Part I: Experimental," *Polymer Engineering and Science,* vol. 42, pp. 539-550, Mar 2002.

[60] H. Schift, L. J. Heyderman, M. A. D. Maur, and J. Gobrecht, "Pattern formation in hot embossing of thin polymer films," *Nanotechnology,* vol. 12, pp. 173-177, Jun 2001.

[61] H. C. Scheer, T. Glinsner, M. Wissen, and R. Pelzer, "Nanostructuring of polymers by hot embossing lithography," Santa Clara, CA, United States, 2004, pp. 203-208.

[62] S. Matsui, Y. Igaku, H. Ishigaki, J. Fujita, M. Ishida, Y. Ochiai, M. Komuro, and H. Hiroshima, "Room temperature replication in spin on glass by nanoimprint technology," *Journal of Vacuum Science & Technology B,* vol. 19, pp. 2801-2805, Nov-Dec 2001.

[63] J. Narasimhan and I. Papautsky, "Polymer embossing tools for rapid prototyping of plastic microfluidic devices," *Journal of Micromechanics and Microengineering,* vol. 14, pp. 96-103, Jan 2004.

[64] S. Y. Chou, P. R. Krauss, and P. J. Renstrom, "Nanoimprint lithography," *Journal of Vacuum Science & Technology B: Microelectronics Processing and Phenomena,* vol. 14, p. 4129, 1996.

[65] G. B. Lee, S. H. Chen, G. R. Huang, W. C. Sung, and Y. H. Lin, "Microfabricated plastic chips by hot embossing methods and their applications for DNA separation and detection," *Sensors and Actuators B-Chemical,* vol. 75, pp. 142-148, Apr 30 2001.

[66] R. G. DeCorby, N. Ponnampalam, M. M. Pai, H. T. Nguyen, P. K. Dwivedi, T. J. Clement, C. J. Haugen, J. N. McMullin, and S. O. Kasap, "High index contrast waveguides in chalcogenide glass and polymer," *Ieee Journal of Selected Topics in Quantum Electronics,* vol. 11, pp. 539-546, Mar-Apr 2005.

[67] "TORLON AI Powders for Coatings." vol. 2006: Solvay Advanced Polymers.

[68] R. Reuter, H. Franke, and C. Feger, "Evaluating Polyimides as Lightguide Materials," *Applied Optics,* vol. 27, pp. 4565-4571, Nov 1 1988.

[69] Y. A. Vlasov and S. J. McNab, "Losses in single-mode silicon-on-insulator strip waveguides and bends," *Optics Express,* vol. 12, pp. 1622-1631, 2004.

[70] G. P. Robertson, M. D. Guiver, M. Yoshikawa, and S. Brownstein, "Structural determination of Torlon [registered trademark] 4000T polyamide-imide by NMR spectroscopy," *Polymer,* vol. 45, pp. 1111-1117, 2004.

[71] I. Mcculloch and H. Yoon, "Fluorinated Nlo Polymers with Improved Optical Transparency in the near-Infrared," *Journal of Polymer Science Part a-Polymer Chemistry,* vol. 33, pp. 1177-1183, May 1995.

[72] Y. Takezawa, N. Taketani, S. Tanno, and S. Ohara, "Light-Absorption Due to Higher Harmonics of Molecular Vibrations in Transparent Amorphous Polymers for Plastic Optical Fibers," *Journal of Polymer Science Part B-Polymer Physics,* vol. 30, pp. 879-885, Jul 1992.

[73] R. Yoshimura, M. Hikita, S. Tomaru, and S. Imamura, "Low-loss polymeric optical waveguides fabricated with deuterated polyfluoromethacrylate," *Journal of Lightwave Technology,* vol. 16, pp. 1030-1037, Jun 1998.

[74] A. Leinse, M. B. J. Diemeer, and A. Driessen, "Scattering loss reduction in polymer waveguides by reflowing," *Electronics Letters,* vol. 40, pp. 992-993, Aug 5 2004.

[75] C. Y. Chao and L. J. Guo, "Reduction of surface scattering loss in polymer microrings using thermal-reflow technique," *Ieee Photonics Technology Letters,* vol. 16, pp. 1498-1500, Jun 2004.

[76] T. J. Clement, "Studies on the Potential for Optical Amplification in Erbium-doped Silicon Monoxide," in *Electrical and Computer Engineering*. vol. M.Sc. Edmonton: University of Alberta, 2006.

[77] D. Clegg, "Electro-Optic Polymer Poling Unit Manual (Model: MZ Poling Jig-01)," Edmonton: TRLabs, 2001, p. 37.

[78] H. C. Scheer, H. Schulz, T. Hoffmann, and C. M. S. Torres, "Problems of the nanoimprinting technique for nanometer scale pattern definition," *Journal of Vacuum Science & Technology B,* vol. 16, pp. 3917-3921, Nov-Dec 1998.

[79] C. Gourgon, J. H. Tortai, F. Lazzarino, C. Perret, G. Micouin, O. Joubert, and S. Landis, "Influence of residual solvent in polymers patterned by nanoimprint lithography," *Journal of Vacuum Science & Technology B,* vol. 22, pp. 602-606, Mar-Apr 2004.

[80] I. T. Pai, I. C. Leu, and M. H. Hon, "Nanostructures prepared on polyimide films by nanoimprinting with the assistance of residual solvent," *Journal of Micromechanics and Microengineering,* vol. 16, pp. 2192-2196, Oct 2006.

[81] L. D. Spaulding, "Molding Tricky Amide-Imide Polymers," *Plastics Engineering,* vol. 38, pp. 25-28, 1982.

[82] F. Gottschalch, T. Hoffmann, C. M. S. Torres, H. Schulz, and H. C. Scheer, "Polymer issues in nanoimprinting technique," *Solid-State Electronics,* vol. 43, pp. 1079-1083, Jun 1999.

[83] C. Goh, K. M. Coakley, and M. D. McGehee, "Nanostructuring titania by embossing with polymer molds made from anodic alumina templates," *Nano Letters,* vol. 5, pp. 1545-1549, Aug 2005.

[84] H. Schmid and B. Michel, "Siloxane polymers for high-resolution, high-accuracy soft lithography," *Macromolecules,* vol. 33, pp. 3042-3049, Apr 18 2000.

[85] C. M. Sotomayor Torres, *Alternative lithography : unleashing the potentials of nanotechnology*. New York: Kluwer Academic/Plenum, 2003.

[86] H. D. Rowland, A. C. Sun, P. R. Schunk, and W. P. King, "Impact of polymer film thickness and cavity size on polymer flow during embossing: toward process design rules for nanoimprint lithography," *Journal of Micromechanics and Microengineering,* vol. 15, pp. 2414-2425, Dec 2005.

[87] Y. Hirai, M. Fujiwara, T. Okuno, Y. Tanaka, M. Endo, S. Irie, K. Nakagawa, and M. Sasago, "Study of the resist deformation in nanoimprint lithography," *Journal of Vacuum Science & Technology B,* vol. 19, pp. 2811-2815, Nov-Dec 2001.

Appendix A: HEX01 Macros

This chapter provides some of the software routines that were written and used for embossing purposes, when using the Jenoptik Hex01 embosser, along with a brief description of it.

A.1 Standard Preparation Macro

The standard preparation macro is run when the embosser is turned on. This macro helps stabilize the embossing machine and brings the machine to an elevated temperature.

StdPreparation.mcr:

Initialize ForceControl(true/false=0)
Close Chamber( )
Heating(Top=60.0°C,Bottom=60.0°C)
Wait Time(Time=300.00s)
Heating(Top=165.0°C,Bottom=153.0°C)
Evacuate Chamber( )
Temperature >=(Temperature=123.0deg,Channel=12)
Heating(Top=120.0°C,Bottom=125.0°C)
Wait Time(Time=300.00s)
Cooling(Top=80.0deg,Bottom=80.0deg)
Temperature <=(Temperature=119.0deg,Channel=12)
Open Chamber fast( )
Unlock door( )
Temper(Top=85.0deg,Bottom=85.0deg)

A.2 Silicone Adhesion Macro

This optional macro was written and used to ensure that silicone adhesive that was applied is as thin as possible. This macro, run before the actual embossing macro, applies a force of 200 N for 1 minute. The time and force can be easily varied as needed.

Silicone Adhesion.mcr

Initialize ForceControl(true/false=0)
Close Chamber( )
Evacuate Chamber( )
Position relative(Position=-9.00000mm,Velocity=50.00000mm/min,MaxForce=1000N)
Touch Force(Force=100N)
Wait Time(Time=60.00s)
Open Chamber fast( )
Unlock door( )

A.3 Typical Embossing Macro

This macro is the one that controls the embossing process. The embossing commands can easily be varied to apply different embossing conditions. Similarly, the order of the commands can be changed to accommodate for different process flow (refer to 2.3.5). This macro also plots and records the embossing parameters. In this macro, the embossing process is done at a temperature of 180°C for 5 minutes, using a force of 6 kN.

embossing 180C.mcr:

Initialize ForceControl(true/false=0)
Open File Protocol(New,View,Print=0(0,1,2))
Open File Measure( )
Close Chamber( )
Evacuate Chamber( ).
Show Chart Window(Show/Hide=11/0)
Position relative(Position=-9.00000mm,Velocity=50.00000mm/min,MaxForce=1000N)
Touch Force(Force=151N)
Heating(Top=220.0°C,Bottom=190.0°C)
Temperature >=(Temperature=180.0deg,Channel=12)
Heating(Top=180.0°C,Bottom=180.0°C)
Force - Force controled(Force=6000N,Velocity=1.00000mm/min)
Wait Time(Time=300.00s)
Cooling(Top=20.0deg,Bottom=70.0deg)
Temperature <=(Temperature=90.0deg,Channel=12)
Temper(Top=80.0deg,Bottom=80.0deg)
Open Chamber fast( )
Unlock door( )
Close File Measure( )
Show Chart Window(Show/Hide=01/0)
Open File Protocol(New,View,Print=1(0,1,2))